Sediment bypassing at Ameland inlet

And the role of an ebb-tidal delta nourishment

Paula Lambregts

TU Delft
Deltares
Enabling Delta Life
Rijkswaterstaat
Ministerie van Infrastructuur en Waterstaat

Sediment bypassing at Ameland inlet

And the role of an ebb-tidal delta nourishment

by

Paula Lambregts

In partial fulfilment of the requirements for the degree of

Master of Science
In Applied Earth Science

at the Delft University of Technology (TU Delft)
to be defended publicly on Monday June 28, 2021 at 12:00

Thesis Committee

Prof. dr. ir. Z.B. Wang	Delft University of Technology & Deltares
Dr. ir. B.C. van Prooijen	Delft University of Technology
Dr. J.E.A. Storms	Delft University of Technology
Dr. ir. E.P.L. Elias	Deltares
Ir. S.G. Pearson	Delft University of Technology & Deltares
MSc. Stefan Pluis	Rijkswaterstaat

Summary

This thesis investigates sediment bypassing under natural conditions and under the influence of a nourishment. The Ameland inlet is used as study area, where a 5.5 million m^3 pilot nourishment is placed on the ebb-tidal delta between March 2018 and February 2019. Improved understanding of sediment bypassing processes is essential in making well-founded decisions in policy-making and maintenance of the Dutch sandy coastal system.

The aim of this thesis is twofold. The first objective is to set up conceptual models describing the ebb-tidal delta dynamics at the scale of the ebb-tidal delta through a detailed analysis of the Ameland ebb-tidal delta between 2005 and 2020. The second objective is to determine the role of the pilot nourishment within the context of these sediment bypassing processes, both in terms of the development of the nourishment itself and the influence it has on transport pathways in its vicinity.

As part of the Kustgenese 2.0 campaign, (half-)yearly bathymetric surveys have been collected at the Ameland ebb-tidal delta, and combined with older bathymetric datasets, this creates an extensive and high-frequency dataset. The nourishment area is surveyed even more frequently: every 3 months before, during and after construction. This dataset provides a unique opportunity for an in-depth analysis of the morphodynamic changes occurring on the Ameland ebb-tidal delta between 2005 and 2020.

The available bathymetries are analysed in two steps. First, the bathymetries themselves are analysed by tracking individual features, looking at sedimentation erosion patterns, analysing transects and performing volumetric analyses. This extends the work synthesised by Elias et al. (2020) which includes the bathymetries from 2005 to 2019. Secondly, sediment transports and pathways are computed using the Delft3D FM and SedTRAILS models. These transport pathways link tide- and wave-driven transports to the morphodynamic changes observed in the bathymetries.

Analysis of the bathymetric surveys gives detailed insights into the development of a series of ebb-shields on the western side of the ebb-tidal delta, which form an essential part of the sediment bypassing cycle. Small-scale instabilities develop into ebb-chute and shield systems which eventually influence the sediment bypassing processes at the scale of the ebb-tidal delta. The growth of these ebb-shields is driven by ebb flows which displace sediment seaward through the chute. When the ebb-shields are sufficiently shallow and wave sheltering by the ebb-delta front is limited, waves drive the clockwise rotation of the ebb-shields. This leads to the constriction and migration of the Akkepollegat, resulting in a gradual switch of the main ebb channel where the most landward ebb-chute becomes the new main ebb-channel from 2019 onwards. As the ebb-shields develop, transport pathways along the outer edges of the ebb-shields increasingly connect the western side of the ebb-tidal delta to the major wave-driven transport pathway passing along the ebb-delta front. In 2017, the ebb-delta front forms a direct connection with the Ameland coast through the attachment of the Bornrif Bankje. These insights are brought together in a series of conceptual models of which the most recent is shown in Figure 1.

The effects of the nourishment on sediment bypassing processes are limited and the nourishment acts mainly as a passive source of sediment. Following construction, most of the sediment remains at the nourishment location. A first largely wave-driven response is observed in which sediment from the nourishment is transported eastward along the outer edge of the second ebb-shield, and from there to the major transport pathway along the ebb-

delta front. This results in the smoothing of the nourishment along the outer edge of the second ebb-shield, after which its shape is more in equilibrium with the surrounding morphology. After this initial wave-driven response, a second tide-dominated response takes over and is expected to remain dominant in the long-term. Shore-parallel tidal currents transport sediment from the nourishment towards the east. Sediment originating in the northern part of the nourishment is transported along the outer edge of the second ebb-shield like in the first response. Sediment originating further south is transported eastward into the second ebb-chute. Here, ebb flows transport the sediment to the outer edge of the ebb-shield to re-join the pathway followed by sediment passing directly along the outer edge. The first and second response are labelled (1) and (2) respectively in Figure 1.

In both the first and second response, sediment from the nourishment follows transport pathways which already exist prior to the placement of the nourishment, with no clear changes to the existing pathways. The same is true for transport pathways in the vicinity of the nourishment. Although a morphodynamic model run is needed for verification, this suggests that the nourishment has no significant effect on the natural sediment bypassing processes. Transport pathways show that sediment from the nourishment will eventually end up on the Ameland coast and is unlikely to feed either the Terschelling coast or the Ameland tidal basin under average conditions. An exception is if the nourished sediment attaches to the northwest Ameland coast close to the Borndiep as part of large shoal. In this case, a part of the shoal will likely be transported into the basin, as was also the case for the Bornrif Strandhaak.

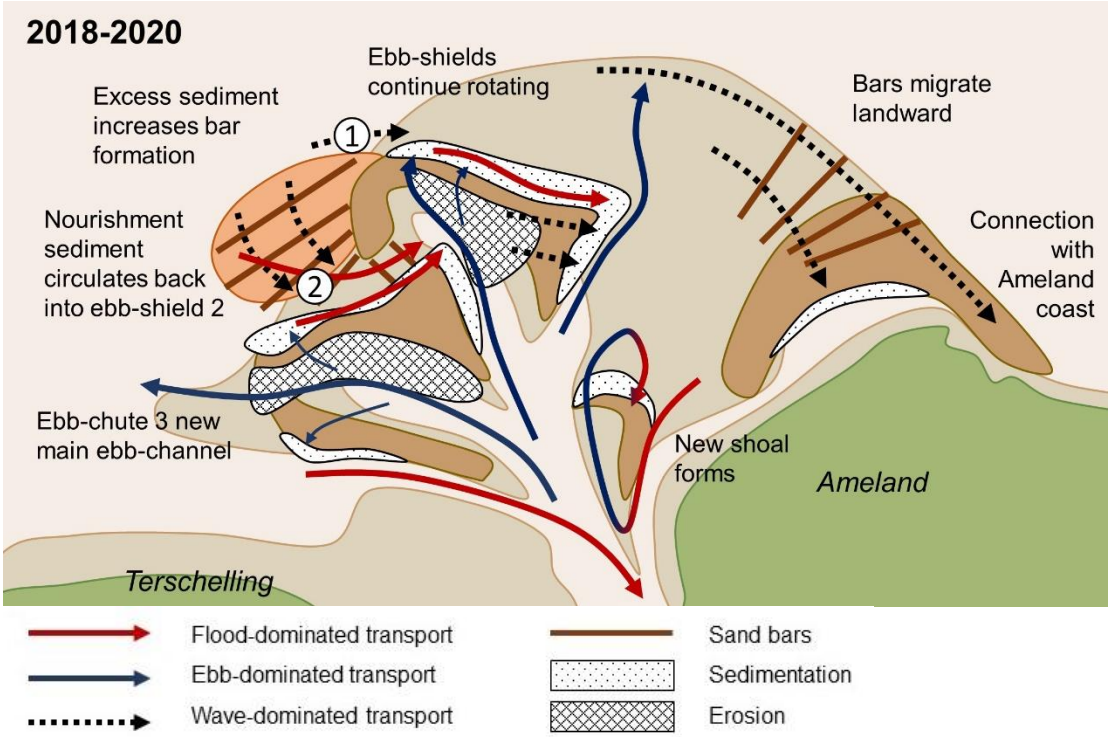

Figure 1 – Conceptual model illustrating sediment bypassing behaviour after the construction of the nourishment, from 2018 until 2020. The diagram includes residual transports (arrows) and areas of sedimentation and erosion (shaded areas). The first and second response are labelled with 1 and 2.

The final product of this thesis is a series of conceptual models describing in detail the ebb-tidal delta dynamics which play a role in sediment bypassing at the Ameland inlet between 2005 and 2020. The development of ebb-shields on the Kofmansplaat is shown to play an extremely important role in forming transport connections towards the eastern side of the

ebb-tidal delta and in forcing a switch of the main ebb-channel. Results also show that the influence of the pilot nourishment on sediment bypassing processes is limited, adding volume to the system but not altering the existing transport pathways. This is valuable knowledge for the future sustainable coastal management of Ameland inlet, which can also be extended to other inlets.

Contents

	Summary	**2**
1	**Introduction**	**8**
1.1	Context	8
1.2	Study area	9
1.3	Research questions	11
1.4	Thesis outline	11
2	**Literature review**	**13**
2.1	General principles of ebb tidal deltas	13
2.1.1	Tidal inlet systems	13
2.1.2	Hydrodynamics	14
2.1.3	Sediment bypassing	15
2.2	Synthesis of sediment bypassing studies at Ameland inlet	16
2.2.1	Long-term behaviour	17
2.2.2	Meso-scale processes	19
2.2.3	Ebb-tidal delta dynamics between 1926 and 2002	21
3	**Methodology**	**26**
3.1	Data availability	26
3.2	Modelling approach	27
3.2.1	Basics of Delft3D FM	28
3.2.2	SedTRAILS	28
3.3	Model setup	30
3.3.1	Delft3D FM	30
3.3.2	SedTRAILS	34
3.4	Model simulations	36
3.5	Limits of the followed modelling approach	36
4	**Data analysis – Natural inlet dynamics**	**38**
4.1	Morphodynamics of Ameland inlet	38
4.2	Tidal channel behaviour	40
4.2.1	Akkepollegat	40
4.2.2	Westgat	41
4.2.3	Outer channel switching	42
4.3	Behaviour of ebb-shields and -chutes	44
4.3.1	Development of ebb-shields and chutes	44
4.3.2	Growth of an ebb-shield	46
4.3.3	Transition from growth to migratory phase	48
4.3.4	A hypsometric perspective on ebb-shield development	48
4.4	Baseline and dynamic sediment volumes	50

5 Data analysis – Nourishment area 52

5.1 Nourishment construction 52

5.2 Post-construction 52
5.2.1 Bathymetric analysis 52
5.2.2 Volumetric analysis 54
5.2.3 Cross-sectional analysis 55

6 Modelling study 60

6.1 Natural ebb-tidal delta dynamics 60
6.1.1 Transport patterns at ebb-tidal delta scale 60
6.1.2 Ebb-shield dynamics 64

6.2 Post-nourishment behaviour 66
6.2.1 Isolating the effect of the nourishment 66
6.2.2 Transport patterns at ebb-tidal delta scale 67
6.2.3 Transport pathways from the nourishment 69

6.3 Evolution of ebb-tidal delta dynamics from 2005 to 2020 70

7 Synthesis and discussion 72

7.1 Conceptual models 72
7.1.1 Natural sediment bypassing 72
7.1.2 Sediment bypassing under the influence of a nourishment (ca. 2018-2020) 76

7.2 Implications for the ebb-tidal delta dynamics 77
7.2.1 Natural dynamics 77
7.2.2 Thoughts on the pilot nourishment 80

7.3 An outlook to future change 81
7.3.1 Development of the Boschplaat 81
7.3.2 Shoal attachments 82

7.4 Novelty 83

7.5 Recommendations 84

8 Conclusions 86

8.1 Natural sediment bypassing processes 86

8.2 Sediment bypassing under the influence of a nourishment 87

9 References 90

A Bathymetries 94

A.1 Ebb-tidal delta 94

A.2 Nourishment 104

B Additional modelling results 108

B.1 Wave-driven transport along the Bornrif 108

B.2 Discharge through the Westgat 109

C Connectivity 110

C.1 Working principles 110

C.2 Connectivity analysis 113
C.2.1 Shortest transport pathways 115
C.2.2 Modularity 115
C.3 A reflection on the current approach to connectivity 117
C.4 Experimenting with connectivity 117
C.4.1 Using sediment communities as units for connectivity 117
C.4.2 The role of residence time in connectivity 120
C.4.3 Connectivity based on transitions between polygons 120

1 Introduction

1.1 Context

A large part of the Dutch coast, the barrier islands in the Wadden Sea included, would be eroding if the deficit in the total sediment budget was not compensated for through nourishments. The Wadden Sea acts as a sediment sink to the Dutch coastal system (Stive et al., 1990), and many natural sediment sources that are responsible for the formation of the coast throughout the Holocene have been depleted (Beets et al., 1994; Beets & Van Der Spek, 2000). This resulted in the construction of for instance, groynes and sea walls to keep sediment in place and provide protection from floods. Because of these human interventions, the coast can no longer respond naturally at a geological scale by landward barrier and coastline retreat (Elias et al., 2012). As a result, the Netherlands is constantly combatting erosion and drowning of land.

In 1990 the Netherlands adopted a new coastal policy called 'dynamic preservation' in which sand deficit and coastline erosion is compensated by means of sand nourishments to keep the coastline (dynamically) in place (*1e Kustnota*, 1990). In addition, this policy was extended in 2001 by increasing the annual nourishment volume for the coastal foundation to keep up with sea level rise (*3e Kustnota*, 2000). Hence, the Netherlands has progressed from a coastal defence strategy centred around hard measures (Lintsen, 2002), to a strategy where soft measures are the norm (de Vriend et al., 2014; Van Der Brugge et al., 2005). This new policy demands increased understanding of the coastal dynamics. Where the knowledge about sediment transport along a linear coast is extensive, tidal inlet systems are more complex and much remains to be learnt. Ebb-tidal deltas have two important functions within the coastal system that make them of interest for coastal defence: first they are a source and transport path for sand to the back-barrier basins and the coastline, and second they play a role in the breaking of large waves. A decreasing volume of the ebb-tidal deltas in the Wadden Sea would endanger these functions.

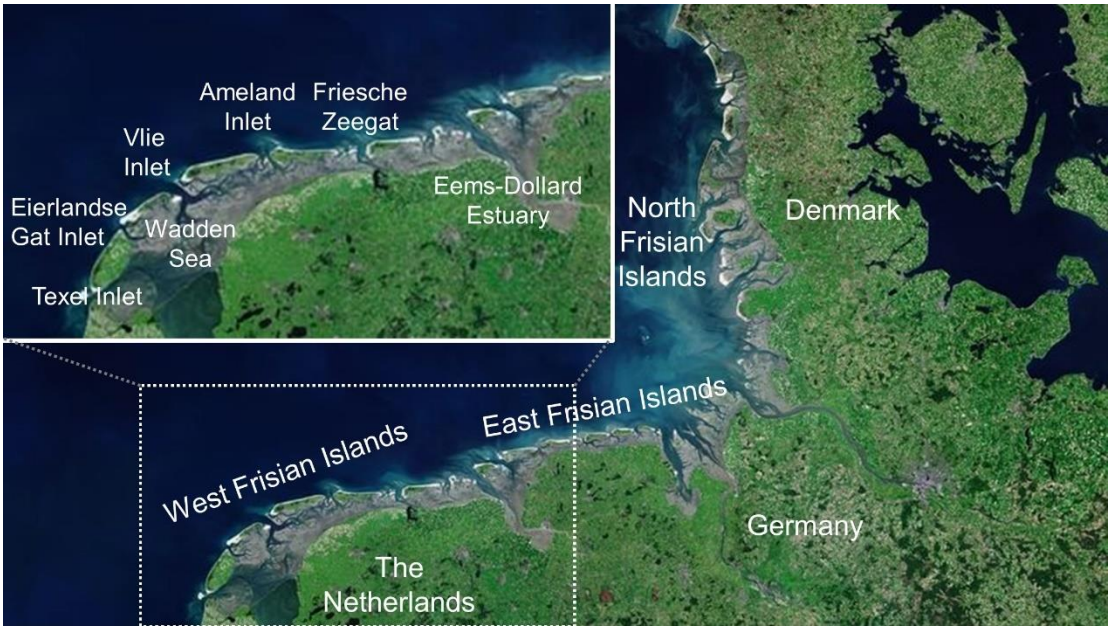

Figure 1.1 – Overview of the islands and inlets that form the Wadden Sea along the Dutch, German and Danish coast (based on a picture from www.waddensea-secretariat.org). The top panel shows the inlets in the Dutch Wadden Sea.

This thesis aims to improve the understanding of sediment bypassing processes at tidal inlets, and specifically of the Ameland inlet (Figure 1.1). Sediment bypassing describes the transfer of sediment from the updrift to the downdrift barrier island across the tidal inlet. Downdrift and updrift refer to the direction of net longshore transport, which is from south to north along the major part of the Holland coast and western part of the Wadden Sea coast, and from west to east along the eastern Wadden Sea islands. The sequence of events involved in sediment bypassing at Ameland inlet has been described in detail (Elias et al., 2019). Observations suggest that such a cycle can be initiated by small-scale shoal instabilities on the ebb-tidal delta, which then lead to the formation of an ebb-chute and -shield system (Elias et al., 2019; Elias, Pearson, et al., 2020). However, the trigger for a new sediment bypassing cycle is not fully understood. Within the framework of the dynamic preservation policy and the Kustgenese 2.0 research program, improved understanding of these sediment bypassing processes is valuable knowledge for strategic placement of nourishments in the future (Elias et al., 2019). Moreover, ebb-tidal delta nourishments can be an addition or an alternative to the current practice of beach nourishments, which are being used to maintain the coastline on the tip of the barrier islands. For instance, when ebb-tidal delta nourishments can be used to increase the frequency and volume of shoal attachments.

Research being performed in and around Ameland inlet is part of a much larger project, namely Kustgenese 2.0, which is largely funded by the Dutch government (Rijkswaterstaat, 2021). The aim is to generate knowledge to be able to make well-founded decisions in policy-making and maintenance of the Dutch sandy coastal system after 2020. Part of this project is the pilot-nourishment placed on the outer edge of the ebb-tidal delta of the Ameland inlet. This first ever ebb-tidal delta nourishment should give insight into how the morphodynamics of the ebb-tidal delta respond to the nourishment. The impact of the pilot nourishment on these processes is investigated within this thesis project.

1.2 Study area

The Wadden Sea consists of a series of 33 tidal inlet systems spanning 500km along the northern part of the Netherlands (West Frisian Islands) and the North Sea coast of Germany and Denmark (East Frisian Islands and North Frisian Islands) (Figure 1.1). This makes it the world's largest uninterrupted system of tidal flats and barrier islands. These barrier islands separate the North Sea from the shallower tidal basins and the hinterland. This system of salt marshes, tidal flats, tidal gullies, barrier islands, and ebb-tidal deltas has developed over the past 7000 years (Elias, Pearson, et al., 2020). Interaction between waves, tides, wind and sea-level rise determine the ever-changing morphology.

Ameland inlet lies between the island of Terschelling (to the west) and Ameland (to the east), which are part of the chain of barrier islands enclosing the Dutch Wadden Sea. The basin has an area of roughly 270km^2 of which approximately 60% consists of intertidal shoals (Elias et al., 2019). Borndiep is the main ebb-channel. The present-day Frisian coastline formed around 1600AD with damming of the Middelzee for which Ameland inlet formed the outlet in the past. With a tidal range of 2.15m and an average significant wave height of around 1.4m (Elias et al., 2019; Elias, Pearson, et al., 2020), the Ameland inlet is classified as mixed-energy (Hayes & FitzGerald, 2013). The drumstick-shaped island and large stable inlet are characteristic of this category (Hayes, 1979; Hayes & FitzGerald, 2013).

Morphology of Ameland inlet and ebb-tidal delta

With morphodynamic changes taking place continuously, it is difficult to maintain a consistent definition for morphologic features. For the purpose of this study, the morphologic features present on the Ameland ebb-tidal delta are defined as shown in the overview in Figure 1.2. In the description that follows, the numbers in square brackets […] refer to the numbers in Figure 1.2.

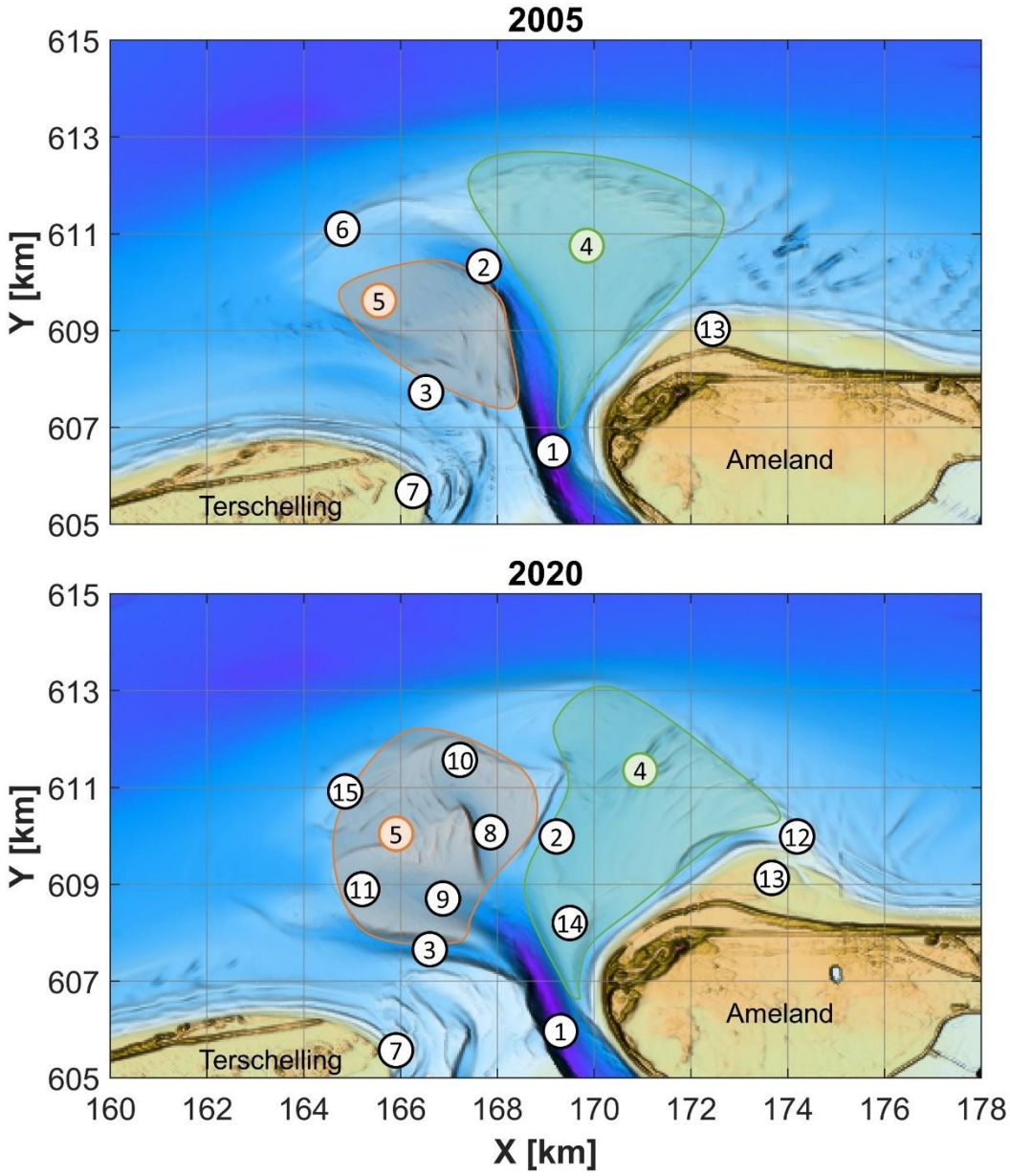

Figure 1.2 – Overview of the morphologic features on the Ameland ebb-tidal delta based on the 2005 and 2020 bathymetries.

In the tidal inlet, a deep main ebb-channel known as Borndiep [1] exists along the west coast of Ameland. Between the tip of Terschelling (Boschplaat [7]) and the Borndiep there is a shallow platform dissected by a series of smaller channels. Above this shallower area lies the Westgat [3] which is the main flood channel. The main ebb-channel on the ebb-tidal delta is initially the Akkepollegat [2]. The area west of the Akkepollegat is defined as the Kofmansplaat [5], the platform where the ebb-shields later form. The northwest margin of the

ebb-delta front is shallower than the rest of the western ebb-tidal delta and is known as the Kofmansbult [6]. On the Kofmansplaat, a series of ebb-chutes [8,9] and ebb-shields [10,11] form, and by 2020 ebb-chute 3 [9] has taken over as main ebb-channel. Ebb-shield and chute 1 also form on the Kofmansplaat but are not visible in Figure 1.2 because this shield forms in 2006 and is swallowed by the second ebb-shield in 2014. The pilot nourishment [15] is placed seaward of the second ebb-shield [10]. East of the Akkepollegat is the Bornrif platform [4]. Along its eastern margin, connected to the Ameland coast in 2020, are the remnants of the Bornrif Bankje [12]. Closer to the inlet are the remnants of an earlier shoal attachment, the Bornrif Strandhaak [13]. In the 2020 bathymetry, a newly forming shoal is visible on the southern tip of the Bornrif [14].

1.3 Research questions

In the present-day morphodynamics of the Ameland ebb-tidal delta, sediment bypassing takes place through main ebb-channel switching. Through mapping of the transport pathways and how they evolve with a changing bathymetry, the first objective is to set up a conceptual model describing the morphological behaviour at ebb-tidal delta scale. The second objective is then to predict the influence of the pilot nourishment on the ebb-tidal delta of Ameland inlet by applying this conceptual model.

To develop the conceptual model, we aim to answer the following research question:

> *How does sediment bypassing work in the ebb-tidal delta of the Ameland inlet under natural circumstances and under the influence of an ebb-tidal delta nourishment?*

This research question will be answered in two steps, first by investigating the natural processes and then including the effects of the pilot ebb-tidal delta nourishment. The sub-questions for natural processes are:

- *Which morphological processes are wave-, tide- or wind-driven?*
- *Which of the three modes of sediment bypassing as defined by Herrling & Winter (2018) occur on the Ameland ebb-tidal delta? These are flow bypassing and bar welding, sediment recirculation and ebb-delta periphery bypassing.*

Improved understanding of the natural processes will form a starting point for understanding the impact of interventions. The sub-questions related to the (pilot) ebb-tidal delta nourishment are:

- *How is the pilot nourishment developing?*
- *Is the morphological response of the ebb-tidal delta dominated by storms or day-to-day processes?*
- *How does the pilot nourishment affect the naturally occurring sediment transport mechanisms on the ebb-tidal delta at the scale of channel and shoals?*
- *How are sediment bypassing processes influenced by the pilot nourishment on an ebb-tidal delta scale, either actively by directly influencing the process of shoal attachments, or passively by increasing sediment volume?*
- *How is sediment from the nourishment linked to other areas in the Ameland inlet?*
- *How can the location of a nourishment be optimised based on a specific goal?*

1.4 Thesis outline

To answer these questions, a detailed analysis of the bathymetric data between 2005 and 2020 is performed at the scale of the ebb-tidal delta and at the scale of individual features. Based on this analysis a series of conceptual models is setup. These conceptual models are

further refined through a modelling study in which the same bathymetries are used to visualise sediment transport patterns. To determine what the influence of the ebb-tidal delta nourishment is on the sediment bypassing processes, the more frequent surveys of the nourishment area are also analysed in detail and included in the model study. The structure of the report reflects this approach.

First, Chapter 2 gives an overview of the relevant literature. This includes general principles on ebb-tidal deltas as well as previous research which is specific to the Ameland inlet. This is followed by Chapter 3 which describes the methodology. It describes the bathymetric data available and introduces the Delft3D FM and SedTRAILS models.

This is followed by two chapters with the results of the data analysis, and a third chapter with results from the modelling study. Chapter 4 discusses the natural ebb-tidal delta dynamics, also zooming in on individual features such as the ebb-shield and the main channels. Chapter 5 continues with an analysis of the ebb-tidal delta nourishment based on the nourishment bathymetries, several transects and a volumetric analysis. Chapter 6 includes the results of the modelling study for both the natural ebb-delta dynamics and the ebb-tidal delta nourishment, building on the ideas in the data analysis section.

Chapter 7 synthesises the results from the data analysis and modelling studies in a series of conceptual models which describe the morphodynamic behaviour on the ebb-tidal delta both before and after the construction of the nourishment. This is followed by a discussion on the implications of the results for the ebb-tidal delta dynamics, again split into a section on the natural dynamics and a section on the role of the ebb-tidal delta nourishment. Finally, there is an outlook to future changes and recommendations for future research. Concluding remarks are found in Chapter 8.

2 Literature review

2.1 General principles of ebb tidal deltas

2.1.1 Tidal inlet systems

The formation of a barrier coast and inlet system is dominated by hydrodynamic forcing of tidal currents and wind waves, as they determine the direction of sediment transport and the regions of erosion and deposition (De Swart & Zimmerman, 2009). Such a system typically consists of several morphological units as illustrated in Figure 2.1. Together the barrier islands, tidal inlets, ebb-tidal deltas and tidal basins with their channels and tidal flats form a sediment-sharing system (Wang et al., 2018) and strive to maintain an equilibrium between the different morphological elements. This means that a change within one of the elements can induce exchange of sediment until a new equilibrium is reached (Stive & Wang, 2003).

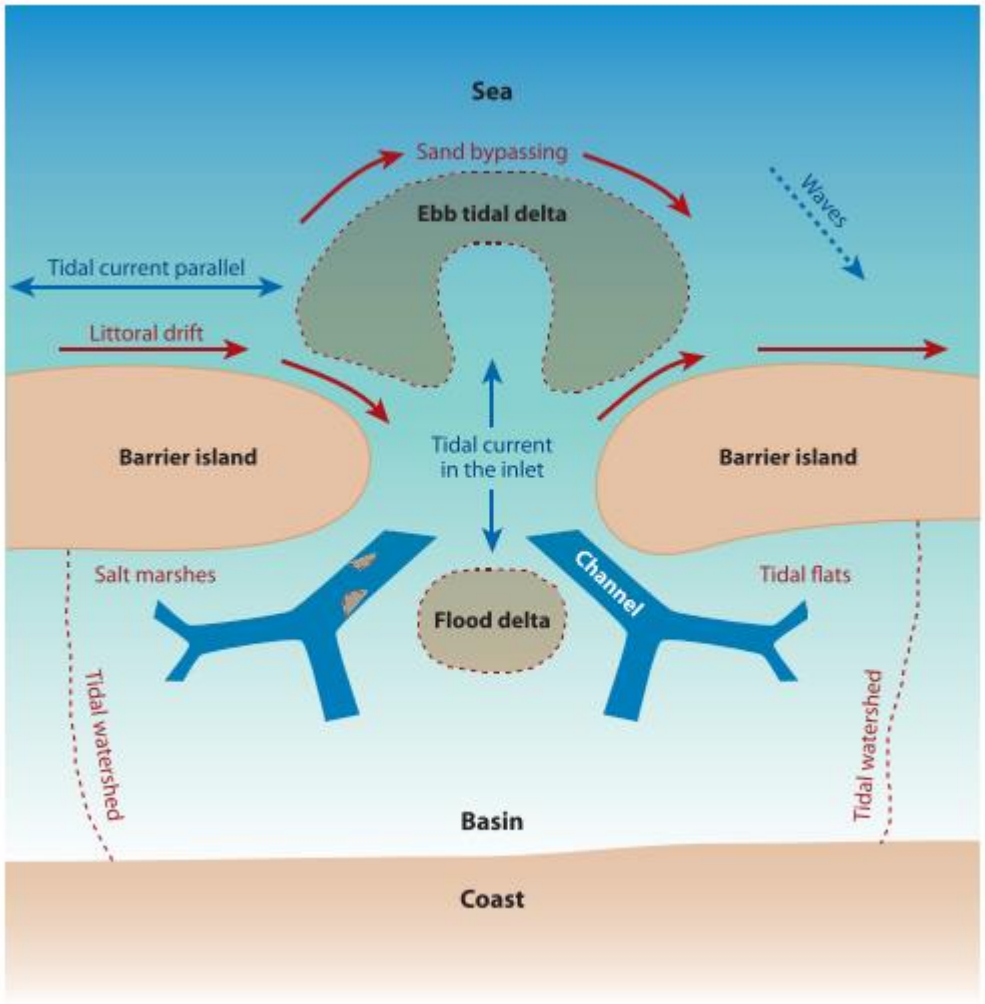

Figure 2.1 - The morphological units forming a barrier coast (De Swart & Zimmerman, 2009).

Tidal inlets are characterised by certain morphological features depending on the relative dominance of tidal and wave energy in shaping the system. Mixed-energy (tide-dominant) barrier coasts as found in the Wadden Sea typically feature abundant tidal inlets, large ebb-tidal deltas and drumstick-shaped barrier islands (Hayes, 1979).

The geometry of the tidal basin in combination with the tidal range determines the tidal prism (Davis & Hayes, 1984), which in turn determines the size of the inlet. Ebb-currents accelerate in the narrow inlet gorge, and above a critical velocity will pick up sediment from the sea bed, resulting in a sediment-laden current. Upon entering the open sea, the tidal flow disperses and as the flow velocities drop below a threshold value the sand is deposited (Elias, Pearson, et al., 2020). An ebb-tidal delta forms in which large volumes of sand can be stored (Dean & Walton, 1975). Seaward transport by tidal currents is countered by landward transport due to wave shoaling and breaking. The morphology of the ebb-tidal delta itself is determined by the balance between these wave and tidal processes. Wave-dominated ebb-tidal deltas are relatively small because waves push the sediment landward through wave shoaling and breaking. On the other hand, tide-dominated ebb-tidal deltas extend further offshore. Similar behaviour can also be observed at smaller scales for ebb-chute and -shield systems.

2.1.2 Hydrodynamics

Hydrodynamics are important for the sediment transport which causes the morphological changes described. For tidal inlets waves, tides and wind are the primary drivers.

Tides

When discussing the contribution of tides to sediment transport, the definition from Sha (1989) is used. Shore-parallel tidal currents refer to flow velocities which are due to the propagation of the tide along the coast. These are generally flood-dominated over the Ameland ebb-tidal delta. Inlet tidal currents refer to currents which are due to water flowing into and out of the tidal basin. They are onshore-offshore directed. On the Ameland ebb-tidal delta, these are generally ebb-dominated.

The onshore-offshore tidal currents through the inlets interact with the shore-parallel tidal currents. Immediately updrift of the inlet, the shore-parallel tidal currents are reinforced by onshore-offshore tidal currents through the inlet. This results in stronger currents in both directions. Downdrift of the inlet, the tidal currents through the inlet counteract the shore-parallel tidal currents resulting in relatively weak tidal currents (Sha, 1989). The phase difference between the tides in the basin and at open sea determine the ebb-channel orientation for inlets with a larger tidal prism, because tidal transports then dominate over wave-induced longshore transports. This is also the case for Ameland inlet where the main ebb-channel is directed updrift (towards the west).

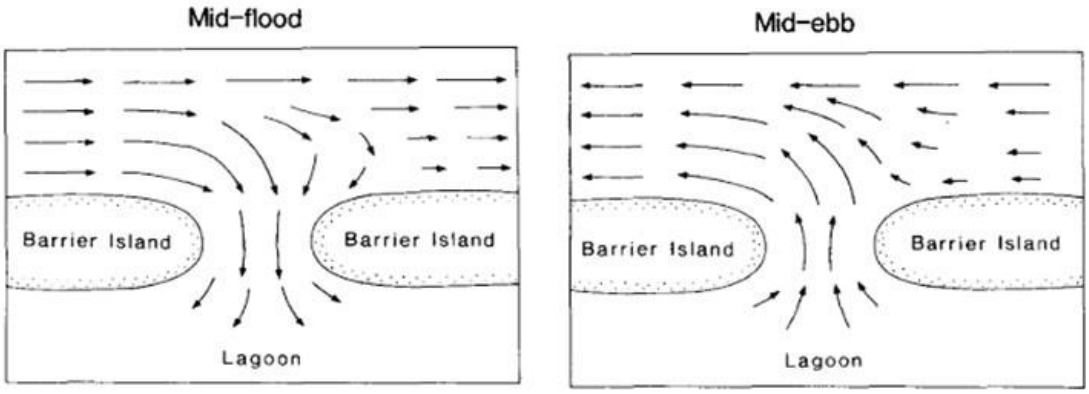

Figure 2.2 – Schematic diagram showing the interaction between shore-parallel tidal currents and inlet tidal currents at an inlet during ebb and flood (Sha, 1989).

Waves

Waves contribute to sediment transport through wave shoaling as the wave travels into a shallower area, wave breaking when a limiting water depth is reached for a given wave height, wave-driven currents and stirring up of sediment.

2.1.3 Sediment bypassing

Sediment bypassing is defined as the process through which sediment is transported from the updrift to the downdrift island across a tidal inlet (FitzGerald, 1982). One of the first attempts to classify different mechanisms of sediment bypassing in mixed-energy inlets was done by Bruun & Gerritsen, (1959):

1) Through wave induced transport along the periphery of the ebb-tidal delta
2) Through transport of sand in channels by tidal currents
3) By the migration of tidal channels and sand bars

They related the mechanism of sediment bypassing to the ratio between longshore sediment transport (wave-driven) and tidal discharge under spring tidal conditions.

One of the problems in identifying an active mechanism within an inlet is that only processes involving bar migration and shifting of channels and shoals are visible in bathymetric data. Other mechanisms can only be deduced through process-based modelling. In some cases, bar migration and attachment does not necessarily lead to sediment bypassing, because sediment recirculation dominates (Elias et al., 2006; Son et al., 2011). This brings into question the general applicability of the conceptual models as described by Bruun & Gerritsen (1959) and FitzGerald (1982). To address this, Herrling & Winter (2018) include sediment recirculation in the sediment bypassing processes as one of three principal mechanisms:

1) Flow bypassing and bar welding
2) Sediment recirculation
3) Ebb-delta periphery bypassing

These processes are illustrated in Figure 2.3 and will be explained in more detail below.

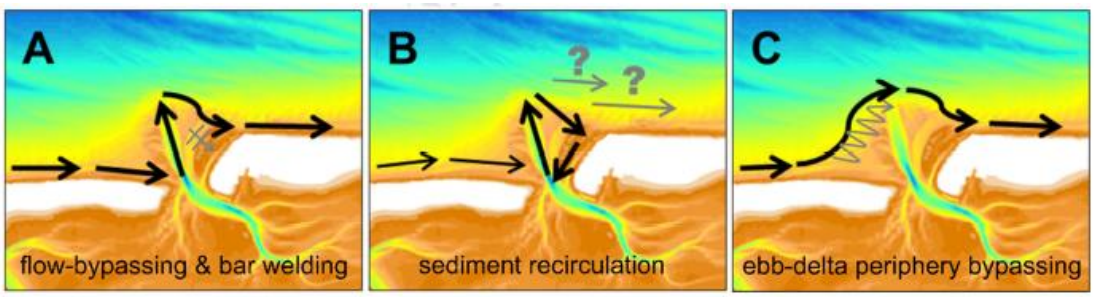

Figure 2.3 - Sediment bypassing processes as classified in three principal mechanisms by Herrling & Winter (2018).

Flow bypassing and bar welding

This mechanism includes both sediment bypassing through transport of sand in channels by tidal currents and by the migration of tidal channels and sandbars as described by Bruun & Gerritsen (1959). In both cases, sediment is delivered to the inlet throat through longshore transport, where the ebb-dominant channel flow transports the sediment to the ebb-tidal delta (Herrling & Winter, 2018). From here-on bypassing occurs either continuously through wave- and tide-driven transport or through the formation and migration of bar complexes. As discussed previously, the former mechanism cannot be identified from bathymetric data. The formation and migration of bar complexes occurs through stable inlet processes or ebb-tidal delta breaching (FitzGerald, 1982). Stable inlet processes have both a stable inlet throat and a stable main channel with swash bars forming and migrating landward on both sides of the

channel. Ebb-tidal delta breaching is characterised by a stable inlet throat with an ebb channel that migrates. Preferential deposition on the updrift side of the channel results in downdrift migration of the channel, which becomes increasingly hydraulically inefficient. Eventually the ebb-delta is breached forming a new channel, and the old channel gradually fills with sediment.

Sediment recirculation
At both Texel inlet (Elias et al., 2006) and Otzum ebb-tidal delta (Son et al., 2011) evidence is found for recirculation of sediment over the downdrift ebb-delta shoal. This is largely based on sedimentary structures, grain size distributions and process-based modelling. Rather than bypassing the inlet, sediment is continually recirculated through the combined action of currents and waves (Son et al., 2011).

Ebb-delta periphery bypassing
This is a wave-driven transport which occurs along the outer edge of the ebb-tidal delta. Sediment is transferred from the updrift to the downdrift beach through migrating sand bars which periodically detach from the updrift beach.

Furthermore, Herrling & Winter (2018) suggest that the sediment bypassing processes active at a particular tidal inlet are not purely dictated by the wave and tidal conditions (Bruun & Gerritsen, 1959) but that multiple mechanisms can be active simultaneously and can be attributed to specific grainsizes. Notable is that flow bypassing is found to be active for all sand fractions (Herrling & Winter, 2018).

Cyclicity
Given that bar attachments are a recurring event with a number of stages leading up to this, sediment bypassing is often described as being cyclic. Examples are the work of Oost (1995) on the Pinkegat, and Israel & Dunsbergen (1999) on Ameland tidal inlet. These build forth on the conceptual models for sediment bypassing described amongst others by Bruun & Gerritsen (1959) and FitzGerald (1984). Cyclic behaviour is convenient as it makes a system predictable. However, researchers such as Elias et al. (2019), Herrling & Winter (2018) and Son et al (2011) now question the validity of this claim, based on detailed analysis of the bathymetric data available.

A cyclic conceptual model implies that sediment bypassing is a deterministic process, meaning that subsequent events have a causal relationship. However, this sequence is arguably initiated by a local small-scale instability (Elias et al., 2019; Elias, Pearson, et al., 2020). These instabilities sometimes develop into an ebb-shield and -chute system, marking the start of a new sediment bypassing cycle, while at other times they do not. This trigger does not have a clear cause, making it a stochastic response. Only once the ebb-shield and -chute system has formed, does the remainder of the sediment bypassing cycle become largely predictable and thus deterministic.

2.2 Synthesis of sediment bypassing studies at Ameland inlet

The Ameland inlet is part of a sediment-sharing system of tidal inlet, tidal basin and barrier islands (Elias, Pearson, et al., 2020; Wang et al., 2018). One of the mechanisms for sediment-sharing is sediment bypassing which is the transfer of sediment from the updrift (Terschelling) to the downdrift (Ameland) island (Elias et al., 2019). Attachments of sand bars to the downdrift coast are observed. However, these bars can result from processes acting on different timescales. The scale cascade concept (see Figure 2.4) is used to understand and distinguish between processes important at different spatial and temporal scales (Cowell et al., 2003; Stive et al., 1990). Each level is a system which shares sediment internally.

Smaller scale processes affect the coastal behaviour at intermediate levels, and larger scale processes form the boundaries.

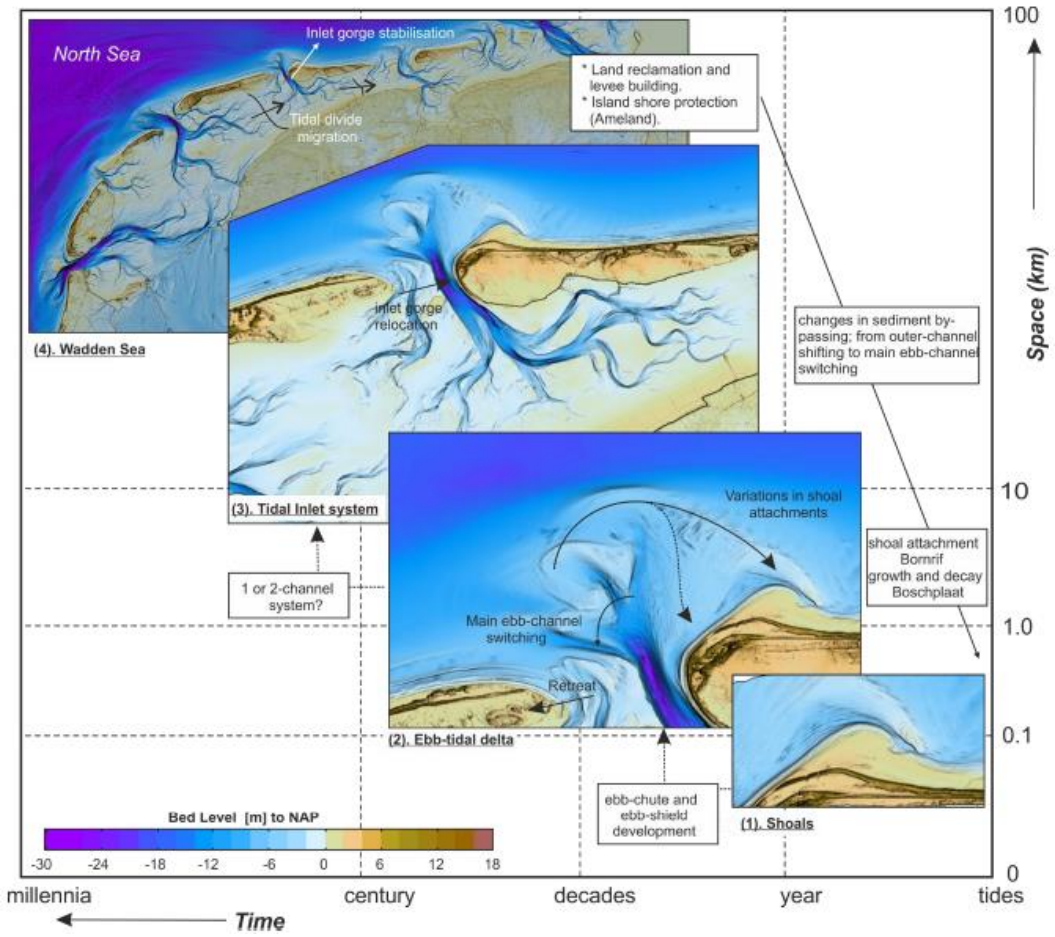

Figure 2.4 - Scale cascade with the morphodynamics relevant at different scales in the Ameland tidal inlet as illustrated in Elias et al. (2019).

For the purpose of this research, the processes occurring at meso-scale are most relevant. This is the scale at which typical morphological elements on the ebb-tidal delta such as channels and shoals form and migrate, and includes sediment bypassing. The associated temporal scale is years to decades and the spatial scale is kilometres. Processes occurring in neighbouring scales affect the behaviour at the meso-scale. These are the scales of the tidal inlet system at the larger scale, and of individual channels and shoals at the smaller scales. Changes at the scale of the entire Wadden Sea are less relevant for ebb-tidal delta scale developments. In the following paragraphs, the long-term changes and the effect they have on the present-day morphology will be described, as well as the current understanding of the small scale morphodynamics.

2.2.1 Long-term behaviour

In this section, the long-term and large-scale behaviour relevant for the Ameland tidal inlet will be discussed, because they form the context for the processes active at smaller time scales. This includes both human interventions through land reclamation or coastal protection, but also sea level rise.

First, we will look at the major human interventions and their effects in the past 500 years. The last major land reclamations in the Ameland tidal basin occurred around 1600 CE with

the closing of the Middelzee, forming the present-day coastline. This changed the basin from a hydrodynamically long basin to a short basin (Elias et al., 2019). Combined with the disappearance of a connection with the Zuiderzee, this caused a significant decrease in the tidal prism of the Ameland inlet, and as a result siltation of second major channel which existed until the early 18th century (the Coggediep). This delayed the arrival of the flood tide and led to an eastward shift of the tidal watersheds, which have since then accreted to intertidal level, separating the Borndiep tidal basin from neighbouring basins (Van der Spek, 1995). The response of the Borndiep channel to the shifting tidal watersheds was to rotate from a north-south to a northwest-southeast orientation, migrating towards the southwestern tip of Ameland. Starting in 1926, the main channel eroded the tip Ameland and has been fixed in place with hard coastal protection measures and nourishments (Elias, Pearson, et al., 2020).

The moment when the Borndiep channel was fixed in place by human interventions also marks a change in morphodynamic behaviour. Before 1926, sediment bypassing across the ebb-tidal delta occurred through outer channel shifting (Figure 2.5). The main ebb-channel remained in place, but the outer part known as the Akkepollegat periodically changed orientation. Post-1926, sediment bypassing occurred through main ebb-channel switching whereby the Westgat and the Akkepollegat alternately grow and decay (Elias et al., 2019).

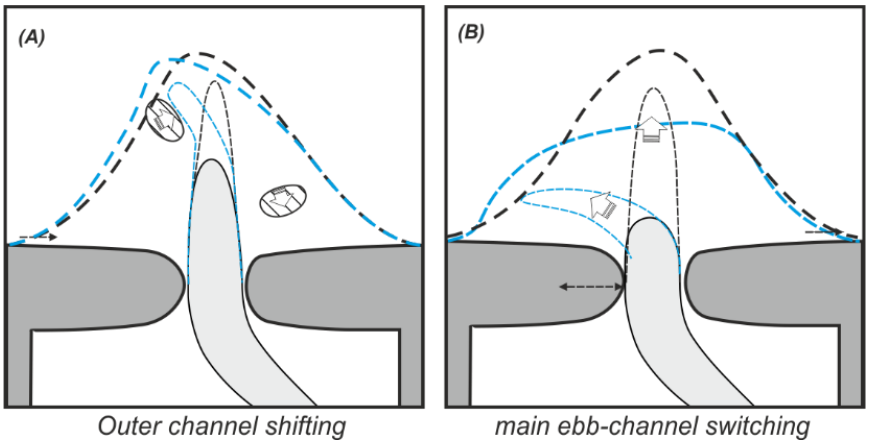

Figure 2.5 – Conceptual description of the sediment bypassing models at Ameland inlet: (a) outer channel shifting and (b) main ebb-channel switching (Elias, Pearson, et al., 2020).

Although human interventions such as the closing of the Middelzee and the fixing in place of the Borndiep have been the dominant forcing in the past centuries, natural forcings – most importantly sea level rise – also play a role in the long-term evolution of the tidal basin. Until the basin dimensions were fixed through the construction of dikes and closure dams, sea level rise (SLR) had been the primary driver in the formation of the present-day Wadden Sea over the past 7000 years. Here the balance between accommodation space and sediment supply is leading, determining whether the barrier – basin system will drown or fill and whether the coast will prograde or retreat (Wang et al., 2018). Now with the basin dimension largely fixed in place, the natural response to a deficit in the sediment budget – the roll-over mechanism of landward barrier and coastline retreat – is prevented. As a result, the system will have to find a different way to respond to sea level rise.

Notable is that in recent years (1935-2005) the accretion rates within the Wadden Sea have been higher than the mean sea level rise of about 2.0 mm a^{-1} (Wang et al., 2018). Present-day sediment import is mainly due to the damming of the Zuiderzee and the Lauwerszee and only partially due to sea level rise. Accretion rates are highest in the Texel and Vlie inlets (both 4.69 mm a^{-1}) and the Frisian inlet (6.66 mm a^{-1}), which were strongly impacted by the

respective closures of the Zuiderzee and the Lauwerszee. The impact of these closures on the Ameland basin is limited and this basin shows the lowest accretion rates (2.52 mm a^{-1}). Irrespective of the cause, the source of imported sediment is the ebb-tidal deltas and North Sea coasts of the barrier islands, there being no alluvial sediment input (Wang et al., 2018). This explains the structural coastline retreat and erosion of the outer deltas (Stive et al., 1990). This is less extreme in the eastern Wadden where the sediment demand is lower and import volume is accommodation-limited rather than transport limited. This means that there is little accommodation space and as a result less sediment import. In the near future (until 2030), the effects of sea level rise are expected to be limited, and in the long-term this will depend on the SLR scenario (Wang et al., 2018).

Considering the long-term behaviour discussed above, Ameland can be described as relatively undisturbed as no major ongoing human interferences or interventions in the past directly impact the present-day natural processes of the ebb-tidal delta (Elias et al., 2019). The main channel (Borndiep) has shifted once and is now fixed in place through hard coastal protection measures and frequent nourishments (Elias et al., 2019). Moreover, the ongoing SLR is expected to have a limited effect on the processes governing sediment bypassing, and the ongoing effects of the damming of the Zuiderzee and Lauwerszee are limited for the Ameland tidal basin. This means that within the boundaries established through human interferences in the past, natural processes are free to reshape the shoals and channels within the Ameland ebb-tidal delta (Elias et al., 2012). Because their impact is expected to be limited, the long-term behaviour discussed in this section, will not be included in the scope of this research.

2.2.2 Meso-scale processes

The meso-scale processes are the processes active at the scale of the ebb-tidal delta. These processes which govern sediment bypassing are active at much smaller scales, O(0.1 – 10km). As discussed above, since 1926 the morphodynamic regime of the Ameland ebb-tidal delta has changed from outer channel switching to main ebb-channel switching. This means that the Akkepollegat and Westgat remain in place but alternately grow and decay (Elias et al., 2019). When the Akkepollegat is dominant, sediment is delivered to the northern part of the ebb-tidal delta and the Bornrif. Alternatively, when the Westgat is dominant, the sediments deposits shelter the Terschelling coast from waves (Elias, Pearson, et al., 2020).

The sediment bypassing behaviour shows repetitive patterns in time, but recent studies conclude that the cyclic predictability at Ameland inlet is limited (Elias et al., 2019; Elias, Pearson, et al., 2020). This contradicts earlier studies which claim that a cycle of 50-60 years exists at Ameland inlet (Israel & Dunsbergen, 1999). Elias et al. (2019) shows that the sediment bypassing sequence is triggered by a local shoal instability. Only when this develops into a full-size ebb-chute and -shield system is the remainder of the sequence predictable. This makes the trigger stochastic and only the remainder of the sediment bypassing sequence deterministic. Elias et al. (2019) argues that the process occurs in similar areas but is never the same and that the time span from the morphodynamic regime starting in 1926 until present is too short to identify something as a cycle of 50-60 years. A possible implication is that we are dealing with a chaotic system, a system which is in principle deterministic but highly sensitive to small perturbations and initial conditions. Stochastic forcing such as storms makes these perturbations likely.

The stages of a sediment bypassing cycle triggered by a shoal instability are described in Figure 2.6 (Elias, Pearson, et al., 2020). This study also suggests that the ebb-tidal delta is more dynamic than current conceptual models. The apparently stochastic nature of these instabilities raises additional questions. Why does one ebb-chute and -shield system fully develop and start a sediment bypassing sequence while the other does not? Such a question

may be answered with improved understanding of the processes and pathways involved. Next to the processes described in the different stages, a secondary active sediment bypassing process is also identified. Small scale swash bars migrate along the ebb-delta periphery, transporting sand towards Ameland (Elias et al., 2019), a mechanism also identified by Herrling & Winter (2018) and described in section 2.1.3.

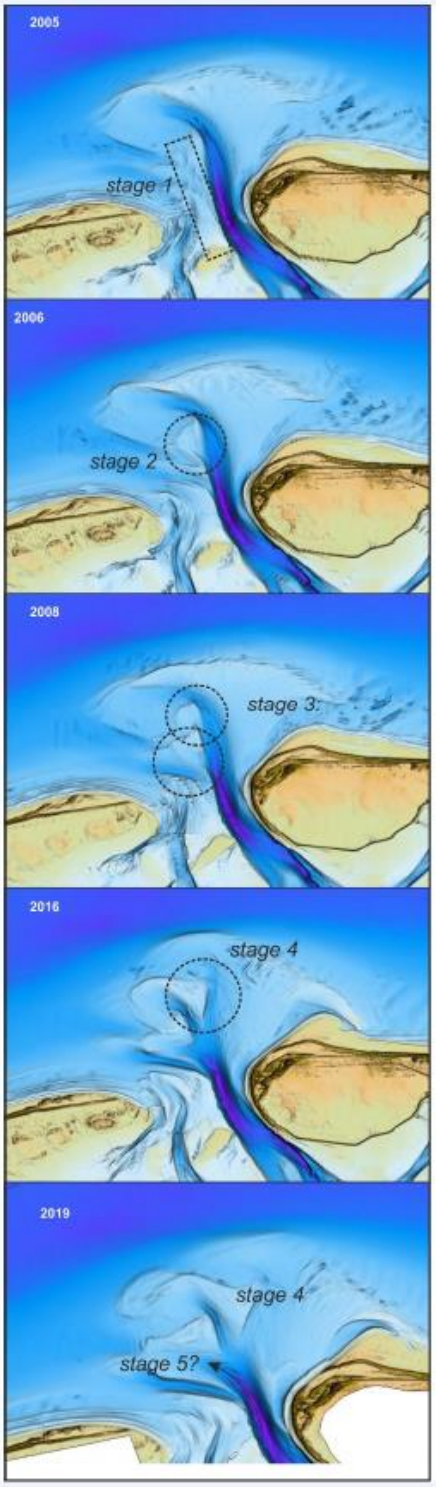

Stage 1; Sediment accumulation along the (central) main channel: Abundant sediment delivered from the updrift coast and through erosion of the western margin of the ebb-tidal delta, is transported into the inlet, and eventually accumulates in an elongate bar flanking the main ebb-delta channel (see 2005).

Stage 2; Morphodynamic instabilities form on this elongate bar: These instabilities result in small ebb-chute like features (2005-2006).

Stage 3; Ebb-chute and shield formation of the shoal instabilities: The instabilities rapidly grow and expand into ebb-chute and shield systems (2006-2014), which start to dictate the ebb-shoal morphology.

Stage 4; Channel – shoal interactions: As the ebb-shield grows in height and size, wave-dominant transports become increasingly important. As a result, the ebb-chute and shield systems migrate downdrift (to the east) and thereby constrain the flow in the former main channel Akkepollegat, (2014-2019). The recent 2019 bathymetries show a near-abandoned main ebb channel (Akkepollegat) and initial growth of a new channel to the south. The deeper part of Borndiep connects to the ebb-chute channel. This suggests that another channel switch is imminent (step 5).

Figure 2.6 - The five stages of development of a sediment bypassing cycle as described by Elias et al, 2020.

Development of ebb-chute and -shield systems play an important role in the sediment bypassing process as described here. These features build out seaward due to the tidally driven sediment supply passing through the chute (Elias, Pearson, et al., 2020). Surges may also be a significant driver of the extension the ebb-shield (Elias, Pearson, et al., 2020). If this is so then storm conditions may play an important role in the development (or not) of an ebb shield. The rotation and eastward migration of the ebb shield is wave-driven and occurs mainly under high energy conditions – changes are much bigger under winter than under summer conditions. These combined forcings result in the ebb shields having an asymmetric shape with the bulk of the sediment on the downdrift side (Elias, Pearson, et al., 2020). If multiple shields are active simultaneously, they may influence each other's development through wave sheltering.

Effects of an ebb-tidal delta nourishment

The second part of this research focuses on the interaction of an ebb-tidal delta nourishment with the sediment bypassing processes. A pilot nourishment was placed seaward of the second ebb-shield between March 2018 and February 2019. Contrary to the initial design, it was placed slightly offshore leaving a small trough between the nourishment and the ebb-shield. Observations during the construction of the nourishment show that little occurs during calm conditions. However, considerable changes do occur during storm events (Van Rhijn, 2019). Increased erosion of the nourishment during rougher winter conditions continues in the months after the completion of the nourishment (Elias, Pearson, et al., 2020). This suggests that waves and not open-sea tides are the primary driver for the redistribution of sediments. Even so, the bulk of sediment remains at the original nourishment site and the strong initial response may be due to the non-equilibrium morphology rather than a recurring response to storm events (Elias, Pearson, et al., 2020). Furthermore, the nourishment did not visibly alter the morphodynamic behaviour of the ebb-tidal delta and the ebb-chute and -shield systems have retained their previously observed behaviour.

Sediment balance of the ebb-tidal delta

As is also the case for other ebb-tidal deltas along the Wadden Sea, the Ameland ebb-tidal delta is showing signs of erosion. Correcting for the sand volumes added through the nourishments, the ebb-tidal delta would have experienced a net loss of 2.7 million m^3 between 2005 and 2016. As is the case for many coastal processes, the gross changes (~200 million m^3) are orders of magnitude larger than net volumetric changes. In the case of the Ameland inlet, dynamics of channels and shoals dominate over exchange with the coast. The large gross volume changes in the Ameland ebb-tidal delta again underline how dynamic the system is but also indicate a possible resilience to nourishments as these volumes are only a fraction of the total changes taking place (Elias, Pearson, et al., 2020).

2.2.3 Ebb-tidal delta dynamics between 1926 and 2002

This study focusses on the ebb-tidal delta dynamics between 2005 and 2020. For an outlook to future change, changes prior to this period are important context. In this section an overview of the morphodynamic changes between 1926 and 2002 (Figure 2.7) is given based on Elias et al. (2019). From 1926 onwards, the sediment bypassing regime is dominated by "main ebb-channel switching", whereby the Akkepollegat and Westgat alternately grow and decay.

Ebb-tidal delta dynamics

Up to 1950, the Akkepollegat [2] was the main ebb-channel and the Westgat [3] a secondary channel (Elias et al., 2019). The Borndiep [1] connected directly to the Akkepollegat and most of the sediment transported out though the inlet was deposited on the seaward side of the ebb-tidal delta. The Westgat had a west-north-westerly orientation along the outer edge of the Boschplaat [5]. The absence of an ebb-shield at the seaward side and the presence of a

sill where the Westgat connected to the Borndiep indicate that the Westgat was flood-dominated.

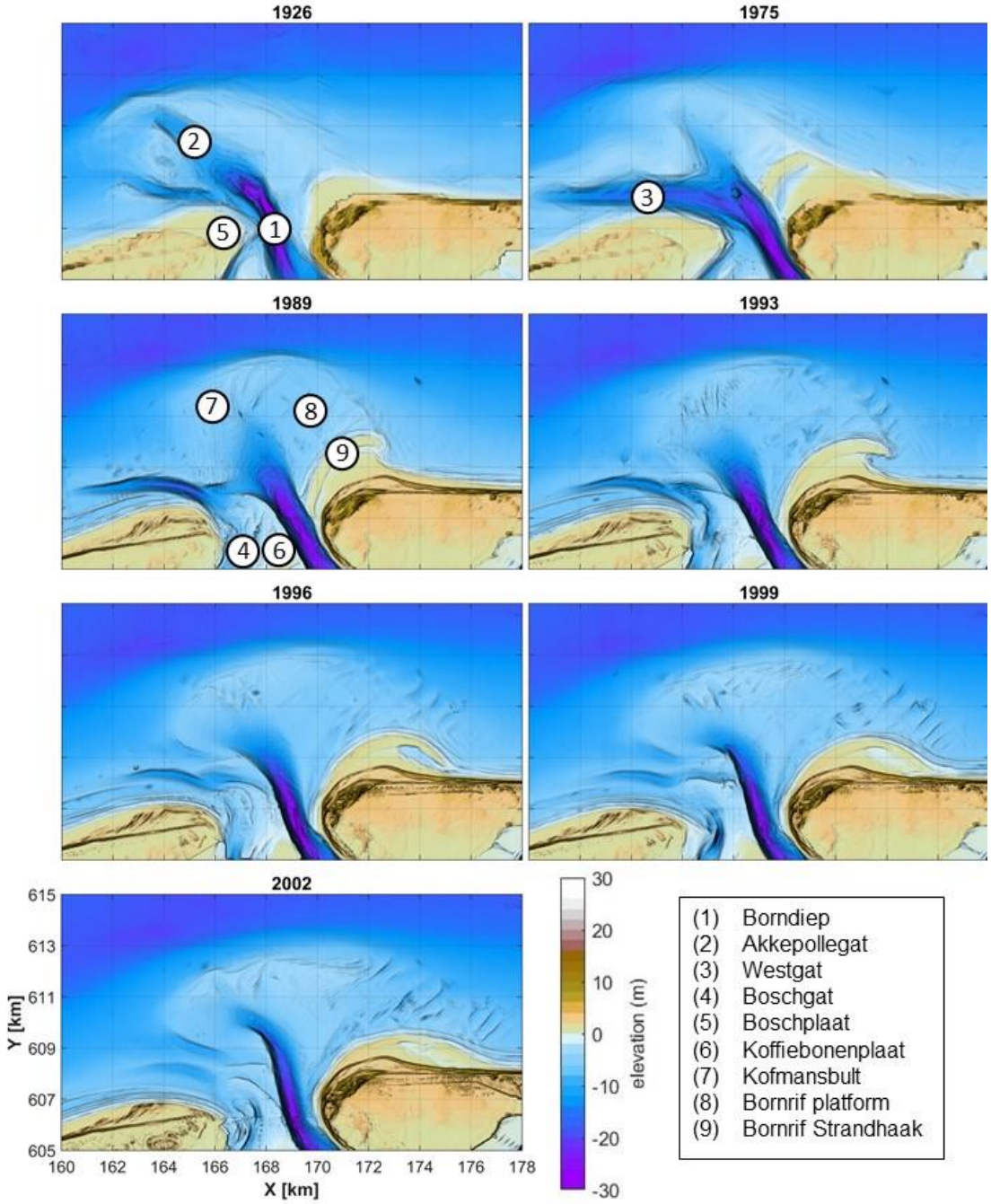

Figure 2.7 – Bathymetric data from 1926 to 2002 showing the morphologic development of the ebb-tidal delta. Key morphologic features are labelled (1) to (9). Only digitised bathymetries are included. For the full set of available bathymetries between 1926 and 2002 see Elias et al. (2019).

Between 1950 and 1985, the more westward-oriented Westgat continued to increase in size and depth and the sill separating the channel from the Borndiep disappeared (Elias et al., 2019). Simultaneously, the Akkepollegat filled up with sediment and a continuous bar formed along the outer edge of the ebb-tidal delta. It is plausible that the Westgat temporarily took over from the Akkepollegat as main ebb-channel. Along the northern margin of the Westgat, large volumes of sediment were deposited, resulting in the outbuilding of the ebb-tidal delta in

the updrift direction close to the coast of Terschelling. By 1982 this sediment formed a linear shoal adjacent to the coast of Terschelling (Elias et al., 2019), sheltering the coast from wave energy during storm events and promoting spit growth of the Boschplaat.

The Westgat maintained its size and position until 1985. At this point the Koffiebonenplaat [6] migrated into the inlet and toward the north between the Boschgat [5] and the Borndiep, cutting off the Westgat from the Borndiep. The Westgat connected temporarily with the Boschgat between 1985 and 1999 following a breach of the spit extending from the Boschplaat. This resulted in a two-channel configuration. After 1999, a distinct Westgat-Boschgat channel no longer existed and a shallow platform dissected by smaller mobile channels formed between the Borndiep and the Boschplaat. Constriction of the Westgat enabled the Akkepollegat to redevelop as main ebb-channel for the Borndiep, and the Westgat changed back from an ebb-dominant to a flood-dominant channel. Increased dominance of the Akkepollegat resulted in the development of the ebb-shields on the Kofmansplaat which form from 2006 onwards.

Outbuilding and retreat of the Boschplaat

In response to changes on the ebb-tidal delta and in the inlet, the Boschplaat and the Terschelling coastline show periods of growth and retreat. In the period before 1926, the tip of the Boschplaat had been building out into the inlet gorge for about 70 years. Between 1926 and 1934, the formation of a channel breaching the Boschplaat caused a sudden > 1km retreat of the tip of Terschelling (Elias et al., 2019). The coastline was then stable until it started to build out again in 1940. The stability of the Boschplaat had been greatly improved by the construction of a sand dike between 1932 and 1936 (Elias et al., 2019), stimulating accretion through the capture of wind-blown sediment and making it more difficult for storm surges to breach the shoal. Beside the sand dike, several other factors contributed to the continuous growth of the Boschplaat between 1940 and 1974. A part of the Koffiebonenplaat attached to the spit on the basin side of the Boschplaat. Also, wave-sheltering by the newly formed shoals along the seaward margin of the Westgat must have contributed to spit growth. By 1974, a long narrow spit had formed which protruded well into the inlet.

The tip of the Boschplaat was breached again between 1974 and 1982, and a shallow subtidal area formed between the Boschplaat and the Borndiep. The formation of a deep channel connecting the Westgat and the Boschgat between 1985 and 1999 introduced large tidal flow velocities. This resulted in erosion of the Boschplaat between 1989 and 1999. After 1999, a distinct channel connecting the Westgat and the Boschgat no longer existed leaving a shallow platform dissected by smaller channels. However, the erosion of the Boschplaat continued. This was related to changes on the adjacent ebb-tidal delta, where the Westgat had reduced in importance and the shoal deposits along its seaward margin could no longer be maintained. An increase in depth of the area between the Kofmansbult and the Boschplaat meant that waves could propagate far into the inlet, resulting in a net eastward transport of sediment from the Boschplaat into the Borndiep.

Based on the observed developments, Elias (2021) has proposed 3 different conceptual models for the erosion or accretion of the Boschplaat based on the morphological configuration (Figure 2.8). The erosion or accretion of the Boschplaat depends on the balance between supply and loss of sediment. Supply of sediment is due to longshore transport along the Terschelling coast (structural), transport from the channel system in the tidal basin (structural), and shoal attachments (episodic). Loss of sediment is due to tide-driven transport through the channels neighbouring the Boschplaat (structural), wave-driven transport across the shallow platform between the Boschplaat and the Borndiep (structural) and breaching by channels (episodic). Episodic processes are generally paired with large volumetric changes, while the effects of structural processes are more gradual.

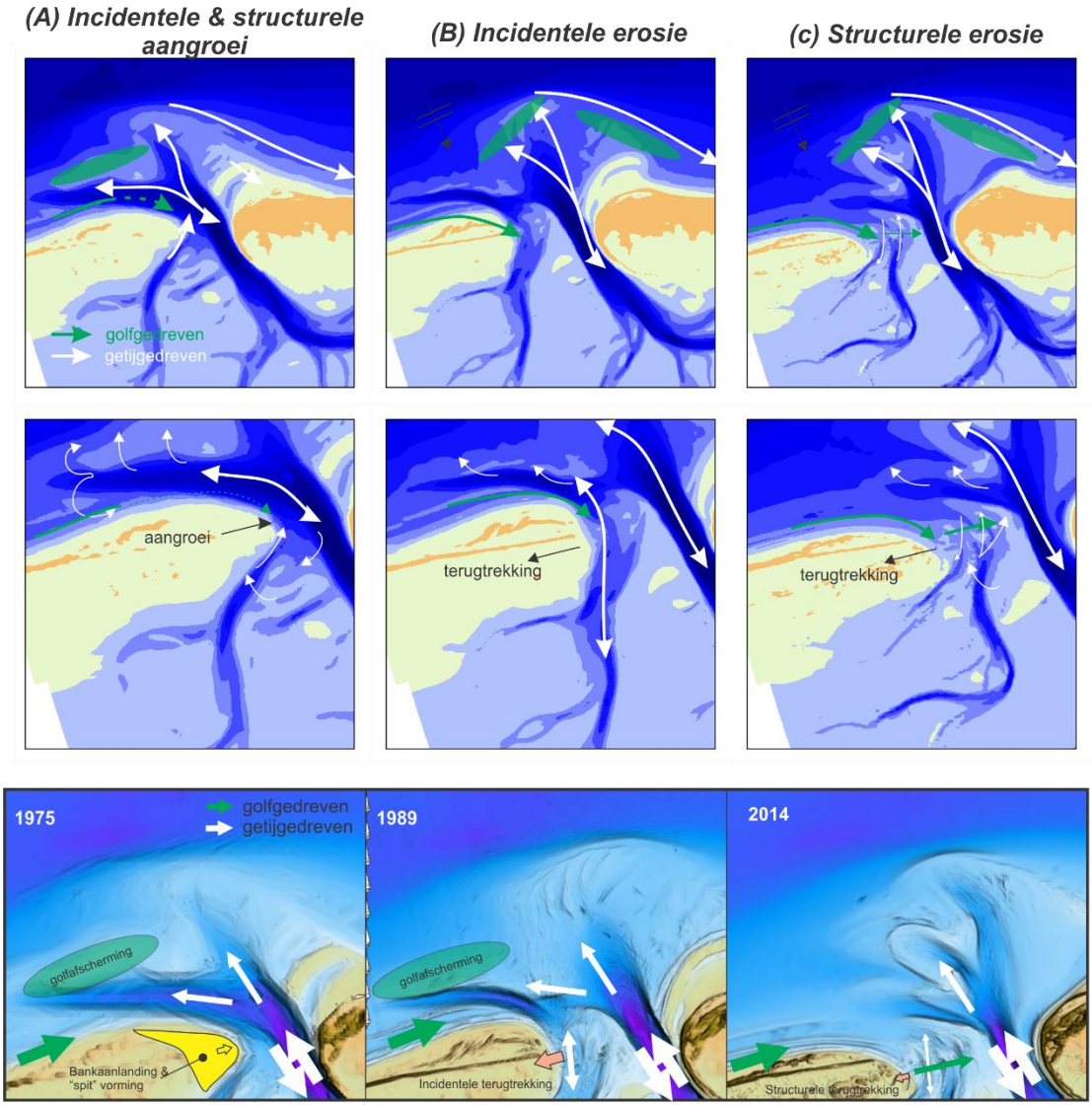

Figure 2.8 – Conceptual descriptions of the sediment transport patterns at the Boschplaat for different morphological configurations: (A) 1975, Episodic and structural accretion, (B) 1989, Episodic erosion and (C) 2014, Structural erosion. Figure from Elias (2021).

Concept A results in episodic and structural accretion, and is characterised by a westward-oriented channel with an ebb-tidal delta which has also built out in westward direction. There are two mechanisms which can lead to accretion of the Boschplaat in this configuration. The first occurs if the wave-driven sediment supply is larger than the loss via the Westgat. Due to wave sheltering, wave energy decreases towards the Boschplaat resulting in a transport gradient and supply of sediment to the Boschplaat. Secondly, this configuration makes it possible for shoals to attach on the basin-side of the Boschplaat. Concept B results in strong but episodic erosion. Strong retreat of the Boschplaat can occur due to the formation of a direct connection between the Westgat and the Boschgat. When the Boschplaat extends far into the inlet, it is sensitive to such a breach during storms. Formation of such a channel is stochastic which means that it is not possible to predict exactly when this will happen. Concept C results in structural erosion. In this configuration, the main ebb-channel passes across the centre of the ebb-tidal delta and the western side of the ebb-tidal delta is relatively deep. This means that waves can propagate far into the inlet. Sediment supplied through

longshore drift is transported further and ends up in the Borndiep rather than on the Boschplaat.

Periodic shoal attachments to the northwest coast of Ameland

Where the southern basin-side of west Ameland is eroding, the northern side shows net accretion as a result of several shoal attachments. The first measured shoal attachment occurred between 1831 and 1903 and can be traced back to a large shallow shoal area on the Bornrif. The resulting bulbous outcrop on the northwest coast of Ameland is still visible when the second shoal attachment (Bornrif Strandhaak [9]) is about to occur. It is difficult to trace back the origin of the Bornrif Strandhaak due to a lack of detail in the depth contours in earlier bathymetries, but JarKus profiles indicate the presence of a shoal near the coast of Ameland in 1970. Between 1970 and 1986, the shoal grows in height, finally attaching to the coast in 1986 towards the Borndiep. This shows that the presence of a flood channel can delay a shoal attachment by more than a decade. Following the attachment, the coast migrated seaward by 1.5km. This was quickly followed by a retreat of 500m as the deposits were eroded and redistributed. Most of the sediment was transported downdrift to feed the Ameland coast, but part of the sediment on the inlet side was also transported into the basin. The third shoal attachment of the Bornrif Bankje occurs in 2017 further downdrift of the two earlier attachments and is discussed in more detail later on as it is part of the study period (2005 – 2020). The origin of the Bornrif Bankje can be traced back to the outbuilding of the ebb-tidal delta between 1989 and 2011 due to the increased dominance of the Akkepollegat.

3 Methodology

This chapter gives an overview of the availability of bathymetric data and the modelling approach. Delft3D FM and SedTRAILS are used to model the sediment transport pathways on the ebb-tidal delta for different bathymetries. Delft3D is a process-based model which is used to compute sediment transport vector fields, and SedTRAILS a tool which visualises particle trajectories based on these transport vector fields.

3.1 Data availability

Since 1986 all bathymetric surveys are stored digitally following a strict protocol (Dillingh, 1990). This includes the standard Vaklodingen as well as surveys performed for other projects (Table 1). Digital elevation models are based on data that is collected at a 3-year interval for the ebb-tidal delta and at a 6-year interval for the tidal basin. Measurements are done using a single-beam echo-sounder at a spacing of about 200m. This data is checked and combined with nearshore coastline measurements (JarKus) and lidar data for the tidal flats in the basin, and then interpolated to 20x20m grids. These are then stored digitally in 10x12.5km blocks which are called Vaklodingen (De Kruif, 2001). In addition, between 2007 and 2010, extra surveys were performed by Rijkswaterstaat as part of the SBW-Waddenzee project (Zijderveld & Peters, 2009). Between 2016 and 2020, (half-)yearly surveys are performed as part of the Kustgenese 2.0 project.

Table 1 – Overview of the available bathymetric data for the basin and ebb-tidal delta between 2005 and 2020. Surveys used for the modelling study are highlighted in blue.

Year	Dataset	Coverage	
		Basin	ETD
2005	Vakloding	X	X
2006	SBW	channels	X
2007	SBW	X	X
2008	Vakloding	X	X
2009	SBW	channels	X
2010	SBW	channels	X
2011	Vakloding	channels	X
2014	Vakloding	X	X

Date	Dataset	Coverage	
		Basin	ETD
31-10-2016	KG2	-	X
21-06-2017	Vakloding	X	X
23-09-2017	KG2	-	Partial
05-06-2018	KG2	-	X
14-10-2018	KG2	-	Partial
18-07-2019	KG2	-	X
2020	KG2	-	X

In addition to the surveys of the full ebb-tidal delta, more frequent surveys of the pilot nourishment are performed during and in the two years after the construction of the pilot nourishment (Table 2). During construction, surveys are performed on a monthly basis and after construction roughly every 3 months.

For this study, the bathymetries between 2005 and 2020 are used. Inaccuracies are believed to exist in the bathymetries prior to 2005 due to unrealistically large changes in sediment budget which are beyond the error range (Elias, 2017). Changes in survey techniques and instruments, positioning systems and correction and registration methods make it difficult to estimate exact accuracy. The vertical accuracy of the Vaklodingen is estimated at 0.11 – 0.40m (Wiegmann et al., 2005). Errors are generally largest along channel slopes due to the steeper gradient in bathymetry here.

Table 2 – Overview of the available bathymetric data for the pilot nourishment. Surveys used for the modelling study are highlighted in blue. Because the surveys of the pilot nourishment cover only a small area, they are embedded in the surveys covering the full ebb-tidal delta which are listed in Table 1.

Survey	Date	Remarks
0	22-02-2018	Baseline measurement. Embedded in 05-06-2018.
1	02-05-2018	
2	08-06-2018	
3	18-07-2018	
4	07-08-2018	
5	27-09-2018	
6	18-10-2018	
7	18-12-2018	
8	25-01-2019	
9	28-02-2019	Nourishment complete. Embedded in 2019.

Survey	Date	Remarks
10	20-06-2019	
11	09-08-2019	
12	22-11-2019	
13	27-03-2020	Embedded in 2020.
14	24-06-2020	
15	21-09-2020	
16	13-12-2020	Embedded in 2020.

For the purpose of this study, incomplete bathymetries are made complete with data from bathymetries which are closest in date and which match best in terms of morphological changes. This is especially important for the bathymetries used in model studies. The nourishment surveys include only a small area which is embedded in the less frequent but larger ebb-tidal delta and basin surveys. To reduce computational time, a limited number of bathymetries are selected for the modelling study (highlighted in blue in Table 1 and Table 2).

3.2 Modelling approach

The extensive bathymetric dataset available at Ameland inlet can be used to describe morphodynamic changes occurring on the ebb-tidal delta in detail. To determine which tide- and wave-driven transport pathways are responsible for the morphodynamic changes observed in subsequent bathymetries, particle trajectories are computed using SedTRAILS. SedTRAILS is a new method which visualises sediment transport pathways based on high resolution sediment transport vector fields computed using Delft3D (Elias & Pearson, 2020). Delft3D is a process-based model which can determine the non-steady flow at pre-defined grid points resulting from tidal, meteorological, and wave forcing. This flow field can then be used to determine the sediment transport fields (Figure 3.1).

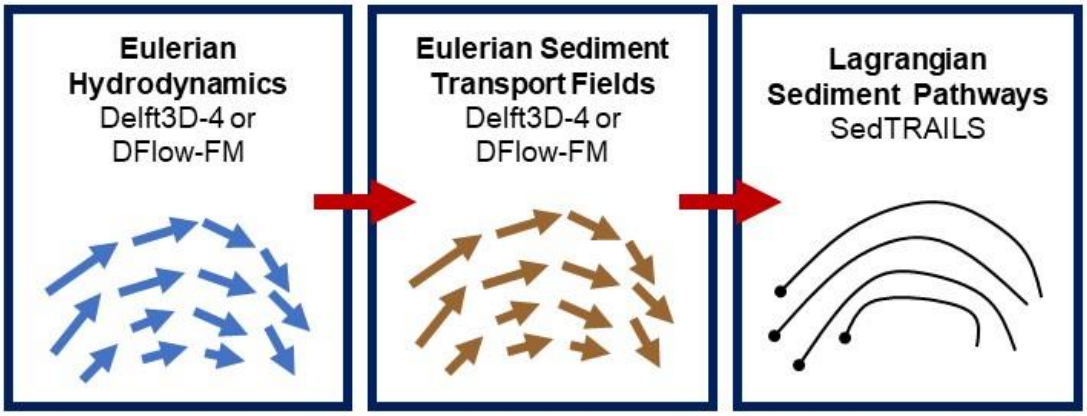

Figure 3.1 – SedTRAILS uses sediment transport field computed using Delft3D to visualise sediment transport pathways (Pearson).

3.2.1 Basics of Delft3D FM

Delft3D includes several modules from which the coupled Delft3D-WAVE and Delft3D-FLOW modules are used. The FLOW module resolves water motion and sediment transport induced by tidal and meteorological forcing by solving the unsteady shallow water equations (Deltares, 2014a). For this study this is done in 2D, meaning that all flow velocities are depth-averaged. Wave effects are integrated using the WAVE module which makes use of the SWAN wave processor. SWAN computes the evolution of random short-crested waves in the nearshore and can accommodate waves in all directions. In coupling with the FLOW module, the effects of flow on waves (through set-up, current refraction and enhanced bottom friction) and the effects of waves on currents (through forcing, enhanced turbulence and enhanced bed shear stress) are accounted for (Deltares, 2014b).

Sediment transport is resolved at each flow timestep and calculated according to the Van Rijn (2007a,b,c) transport equations, which follow the description in Van Rijn (1993). This formulation includes both bed load and suspended load. Bed load transport is the transport of sand particles close to the bed and is based on a parametric formulation which includes the effect of waves. Transport above a certain reference height is considered as suspended load and calculated by solving advection-diffusion equations. Additional formulations are included to account for sediment exchange with the bed and settling velocity.

The interaction between the FLOW and WAVE modules and the calculation of sediment transport within the Delft3D model are shown in Figure 3.2. For the purpose of this investigation, the simulations are run morphostatically, meaning that the bed level is not updated based on the sediment transport. Without morphodynamic feedback, the sediment transport vector field remains unchanged for repeated tides (Elias & Pearson, 2020).

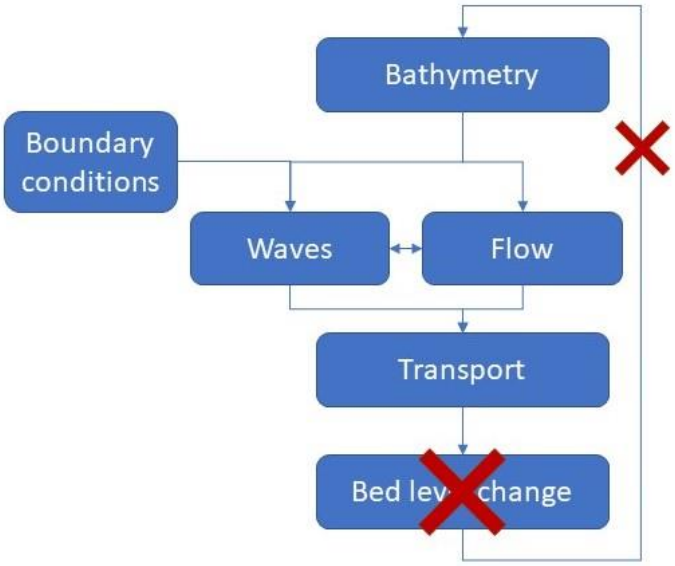

Figure 3.2 – A flow chart showing how the different components of Delft3D interact. For a morphostatic simulation, the bed level is not updated.

3.2.2 SedTRAILS

The sediment transport vector fields computed using Delft3D are the primary input for SedTRAILS (*Sediment TRAnsport visualization & Lagrangian Simulator*). This section describes how SedTRAILS works based on Elias & Pearson (2020). SedTRAILS is a new modelling tool which visualises sediment transport pathways. To do this, virtual particles are released in a sediment transport vector field generated using high resolution Delft3D simulations. The resulting transport pathways can be used to identify links between different

morphological elements within a complex coastal system. An example of a previous application is discussed in Stevens et al. (2020), where insights are used to better align dredge disposal and the nourishment of an eroding beach.

The need for a new approach

SedTRAILS is not a sediment tracking model in a classic sense but rather a visualisation of the sediment transport vector field computed by Delft3D. Before looking in more detail at this newer approach, let us review a more classic particle tracking approach. There are possibilities for particle tracking through Delft3D using Delft3D PART. Multiple sediment fractions with slightly different properties are used so that the movement of the fraction of interest can be followed. This is the approach used by Bak (2017) to evaluate different nourishment strategies at Ameland inlet. However, these simulations are computationally expensive and for smaller tracer deposits are very sensitive to exchange layer thickness (Elias et al., 2011).

Also, while process-based models perform relatively well at the lower and higher ends of the scale cascade (Figure 2.4), the performance of medium-term model simulations (such as those that would be relevant for understanding the sediment bypassing cycle) lags. A study by Lesser (2009) demonstrates that model skill is often worse than simply predicting no morphological change. This can be partly explained by an important lesson from the Kustgenese 2.0 project. Small-scale processes are important on the larger scale of the ebb-tidal delta, with small scale instabilities triggering a new sediment bypassing cycle that will come to dominate the dynamics of the entire ebb-tidal delta (Elias et al., 2019; Elias, Pearson, et al., 2020). These small-scale dynamics are extremely difficult to capture but essential to be able to reproduce the larger scale dynamics. This realisation and the need for a more efficient tool to investigate inlet-scale sediment transport without sacrificing model resolution and accuracy have been the primary driver for the development of the SedTRAILS tool.

Basics of SedTRAILS

SedTRAILS is designed to simulate sediment trajectories in complex coastal systems accurately and in a computationally efficient way over longer time scales. Runtime efficiency is obtained by decoupling the computation of the sediment transport vector field from that of the particle trajectory. Sediment transport vectors are resolved using the advanced flow and sediment transport equations incorporated in Delft3D and with a schematised morphodynamic tide and wave climate applied at the boundaries. Ideally there is a calibrated model of the area available and otherwise one will have to be built. The Delft3D simulation is done morphostatically, and since there is no morphodynamic feedback the sediment transport vector fields remain unchanged for repeated tides. This means that rather than simulating using Delft3D over a longer period, the sediment transport vector fields for a single tide can be repeated to compute particle trajectories over longer timescales. Because the sediment transport vectors are already resolved, the computation of particle motion and the associated trajectory is relatively fast and can be computed over longer periods (months to years).

Important to note is that in its present configuration SedTRAILS can only be used to visualise particle trajectories but can say nothing about the time component. The distance covered in a particular time step does not represent the actual particle velocity. This is firstly because the particle movement has not yet been calibrated, and secondly because processes such as temporary burial in the bed and later resuspension have not been incorporated.

The sediment transport vectors computed in the Delft3D simulations at each time step are derived from the transport formulations by Van Rijn (2007a,b,c) for non-cohesive sediment

transport. The sediment mass flux S_m computed in the Delft3D simulation is converted to a volume flux S_v by dividing by the bulk density ρ_b of the sediment:

$$S_v = \frac{S_m}{\rho_b}$$

This flux represents the volume of sediment per unit width of a given grid cell face, crossing that grid face into the next cell per second. The volume flux is converted to an effective velocity for the transported particles u_{tr}, by dividing by a length scale h_{tr}:

$$u_{tr} = \frac{S_v}{h_{tr}}$$

This length scale h_{tr} should be related to a representative height in the water column over which sediment is transported (depends on transport type). Decreasing the length scale will increase the speed of particle motion. Once the time component is accounted for in SedTRAILS, this will become an important parameter to calibrate. Until then the length scale should only be adjusted to the point where the particle trajectories begin to diverge.

Temporal variations in sediment transport within a tidal cycle are captured by calculating the 10-min mean total sediment transport vectors from the cumulative mean total transport computed in Delft3D. This includes both the bed and the suspended load. Using the mean rather than the instantaneous transport vector has two advantages, namely that any numerical errors and instabilities are averaged out, and that the number of output intervals is reduced, lowering computation time. To compute these particle trajectories within this changing vector field, one particle is released at each source location. At each time step, the particle's new location as dictated by the transport field at that time step is determined. Although particle tracking models are often highly sensitive to the moment of release (during flood or during ebb for example), the small effective particle velocities mean that the exact release time has no significant effect on the overall particle trajectory.

3.3 Model setup

The description of the model set up distinguishes between settings in the Delft3D and in the SedTRAILS model. Choices made in the setup of the Delft3D model will directly translate to the visualisation in SedTRAILS as the transport vector fields from Delft3D form the main input for SedTRAILS.

3.3.1 Delft3D FM

The model is run in 2DH setting. Transports are mainly wave- and tide-driven, and density flows are less important. For these transports a 2D simulation is sufficiently accurate and the increase in runtime for a 3D simulation will not weigh up to the expected improvements in the outputs (Elias, Roelvink, et al., 2020).

Flow model

The basis of this FM model is a structured grid of the entire Wadden Sea as documented in De Graaff (2009), which was converted to Flexible Mesh by Laan (2019). In the Wadden Sea, the unstructured grid has a resolution of 200-300m. Using Flexible Mesh allows for the use of both rectangles and triangles within the grid, making it possible to refine the grid in areas of interest. The unrefined model is of sufficient resolution to resolve large-scale tidal propagation and currents in the Wadden Sea but not for detailed analysis of transport pathways in the Ameland inlet. Through three consecutive refinements, the resolution is reduced to 17m in the inlet (Figure 3.3) (Elias, Roelvink, et al., 2020).

The underlying model bathymetry is largely based on the 2017 Vaklodingen, with missing data filled with older bathymetries (Figure 3.4) as documented in Laan (2019). At the location of Ameland inlet, data from the year of interest is used. Because the Laan (2019) model bathymetry is used, the model calibration and validation remains valid and no additional

verification is necessary. Water levels from the large-scale North Sea model (Zijl et al., 2013) are used for open sea boundary conditions. An output timestep of 10 minutes is used.

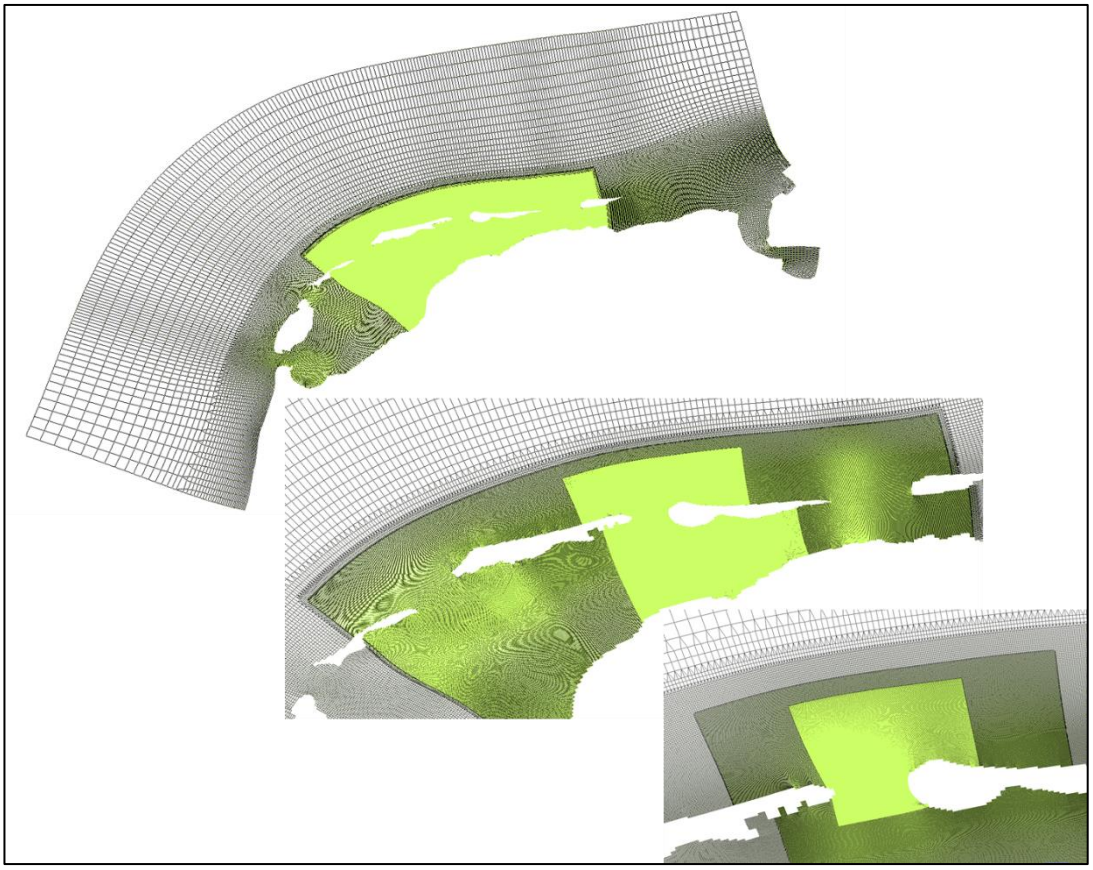

Figure 3.3 – Three refinements of the Flexible Mesh Wadden Sea model grid to a resolution of 17m in the inlet (Elias, Roelvink, et al., 2020) .

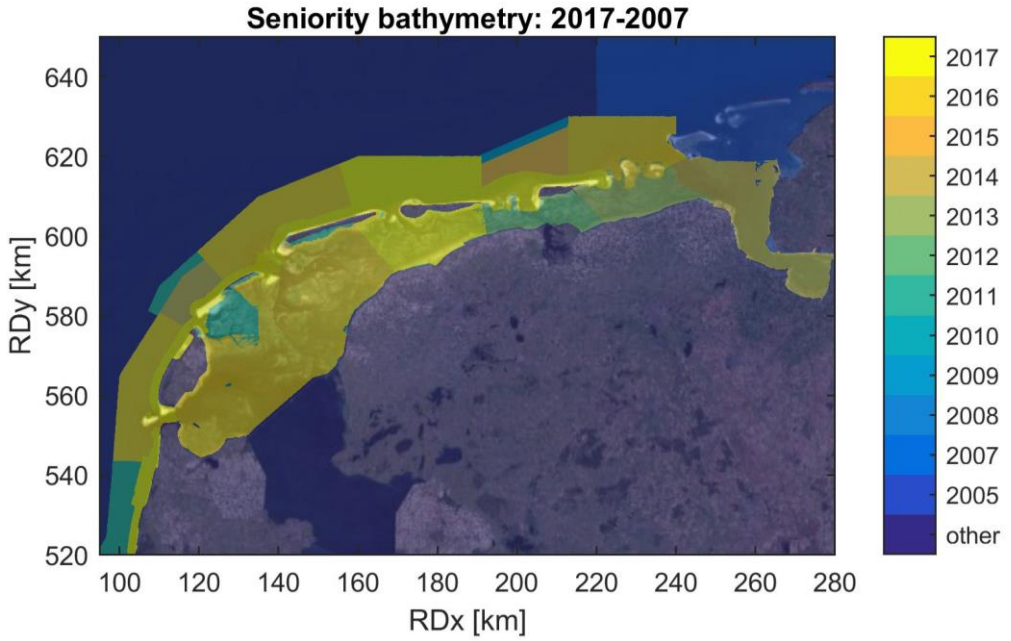

Figure 3.4 – Seniority map of the bathymetry used for the Wadden Sea model (Laan, 2019).

Morphologic tide

The goal of a morphologic tide is to replace a complex time series of water levels and flow velocities with a simplified tide. The residual signal for the complex timeseries and the chosen morphological tide should result in the same outcome. For morphodynamic modelling, the goal is to reproduce morphologic change. However, in a morphostatic simulation this is not possible. The goal then becomes to reproduce residual sediment transport vectors.

For this study, the morphological tide selected for an earlier project on the evaluation of different nourishment strategies in Ameland inlet is used (Elias, Roelvink, et al., 2020). The method to determine the morphological tide consists of two steps. The first step is to simulate the tidal motion over a sufficiently long period. The Wadden Sea model is run for a full year (2017) using boundary conditions from a large-scale North Sea model (Zijl et al., 2013) including wind. For a large number of representative cross sections across tidal inlets, the tidal watersheds and along the islands, transports are determined. These are then used to determine year-averaged transports across each cross section as well as the 25th and 75th percentile. On average, the month of Augustus gives the best approximation of the year-averaged transports.

The second step is to model the tidal inlet in detail for the selected month. Here the sediment transport is averaged over the month August and the tidal period which best represents the month-averaged transports is selected, again based on transport through the cross-sections. The selected tide is from 05/08 13:40 to 06/08 02:00 for Ameland. This selection procedure results in a morphologic tide and matching wind conditions which represent year-averaged transports. This morphologic tide with matching winds is used for the tide-only simulations.

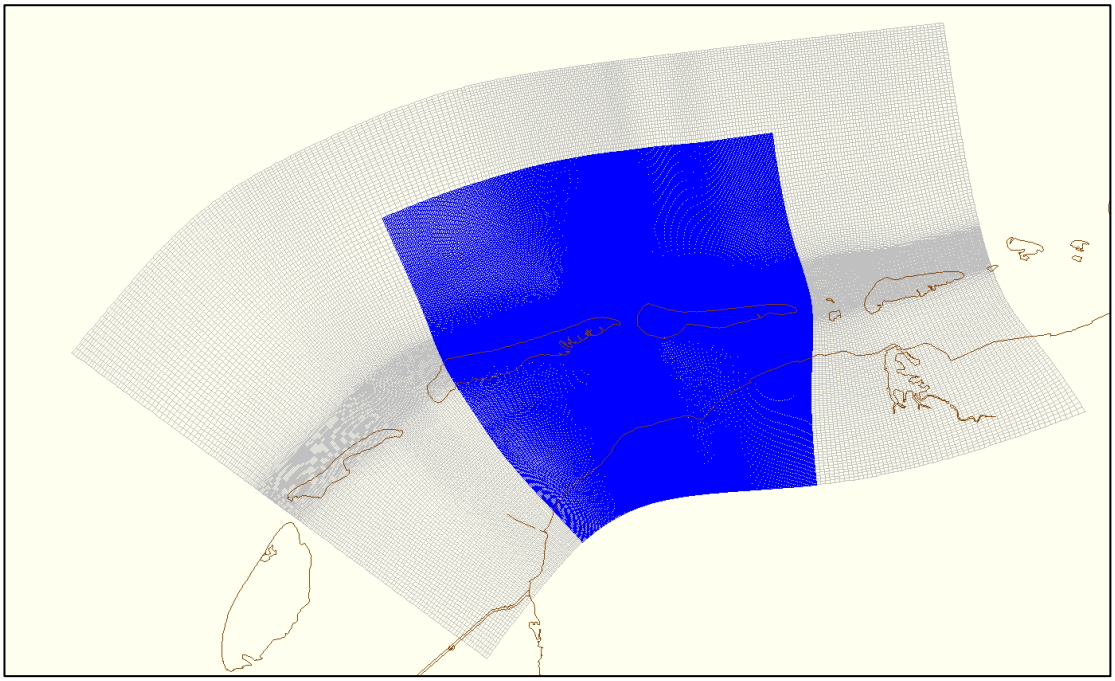

Figure 3.5 – Wave model grid used for Ameland inlet, with a grid resolution of roughly 30m at the centre of the inlet.

Wave model

The SWAN wave model uses a structured grid and can therefore not be directly applied to the unstructured flow grids. The wave model as set up for Kustgenese is applied (for a detailed description see Nederhoff et al. (2019)). This wave model does not cover the full area of the Wadden Sea but is sufficiently large to ensure accurate computation of wave

propagation in Ameland inlet. A nested grid used for a higher resolution at the inlet (Figure 3.5)

Wave driven currents are most important along the island coasts and in the shallower regions on the ebb-tidal deltas as this is where the waves break. To ensure accurate representation of wave-current interaction, the wave model is calculated every 30 minutes and outputs are exchanged between the wave- and the flow-model. Hydrodynamic conditions are communicated with SWAN, a new wave field is calculated, and the wave information is conveyed back to the flow model where it is incorporated in the next 30 minutes of simulation. The settings in the wave model are based on those in the Kustgenese model (Nederhoff et al., 2019). The maximum number of iterations for each wave calculation is set to 50 and the minimum number of accurate wet cells to 98% to reduce numerical instabilities. Wave conditions are defined parametrically using significant wave height, period and direction for a standard JONSWAP spectrum for the schematised wave climate described in the following section.

Wave schematisation

The buoys near Ameland are not suitable for derivation of a wave climate due to the short record and missing data in early summer. Previous studies show that the Schiermonnikoog (SON) buoy best matches the Ameland wave climate and recommend using SON data for wave schematisation (Elias, 2017).

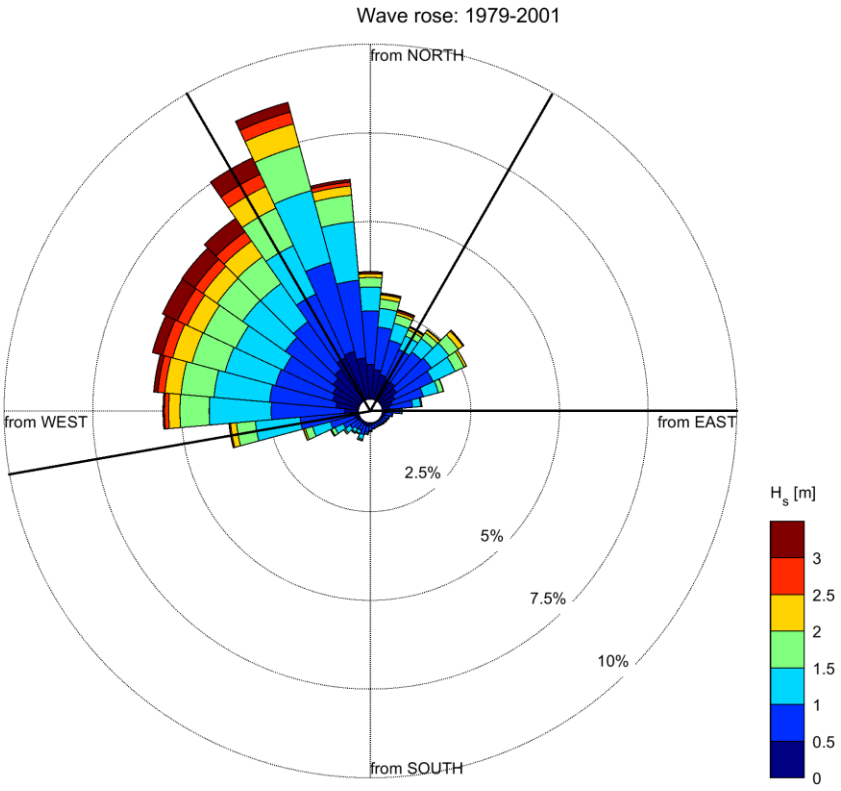

Figure 3.6 – Wave rose for the wave climate recorded at the Schiermonnikoog (SON) buoy (1950-2017). The black lines show the four directional bins that are used to derive a wave climate for the model runs. Figure from van Soest (2021).

To reduce calculation time, the data collected between 1950 and 2017 is reduced to 6 representative wave conditions (Table 3). For the derivation of these 6 wave conditions, 4

direction bins are defined as illustrated in Figure 3.6, and 2 height bins with a cut-off significant wave height of $H_s = 1.2$m. The 6 wave conditions with the highest probability are then selected, giving a high and a low wave condition from the NW, N and NE. The barrier islands and shallow Wadden Sea shelter the ebb-tidal delta from waves from the south. Wind speeds have been derived from a linear correlation of wind speed and wave height (van Soest, 2021). The wind direction is the same as the wave direction.

Table 3 – The 6 wave conditions used in the WAVE module.

Significant wave height (m)	Wave period (s)	Direction (°)	Probability of occurrence (%)	Wind velocity (m/s)	Wind direction (°)
0.8	4.27	293.10	27.41	6.71	293.10
0.75	4.70	352.56	23.97	6.57	352.56
0.75	3.79	56.32	11.92	6.57	56.32
1.87	5.29	298.08	21.35	9.77	298.08
1.83	5.49	346.96	11.83	9.66	346.96
1.66	4.72	51.86	3.52	9.17	51.86

For the coupled tide-wave simulations, these 6 wave conditions including wind in the same direction are used in combination with the morphologic tide. The water levels associated with the morphologic tide are applied at the open sea boundaries.

Sediment transport

This model uses the Van Rijn (2007a,b,c) sediment transport formulations. A single sediment fraction with a grain diameter of 200µm is used and sediment supply is unlimited for these simulations. In reality there will be small variations in grain size with coarser grains in the channels and finer grains on the shoals. Even so, the grainsize distribution on the ebb-tidal delta is remarkably homogenous (Elias et al., 2019; van Prooijen et al., 2020).

3.3.2 SedTRAILS

The boundary conditions, bed level, initial conditions and model schematisation are determined by the Delft3D model setup. A number of settings remain to be determined in SedTRAILS, such as the time frame taken from Delft3D, the number of sources and their locations, and the simulation time.

In the case of Ameland tidal inlet, two tidal periods are used rather than one to account for the daily inequality that is characteristic of the area. The double tidal period is selected from the Delft3D results following spin-up time. It is selected from the velocity signal in open sea, under the assumption that the tidal signal here is relatively undisturbed (Figure 3.7 (left)). The period is selected between the points where the tidal velocity is at its minimum. However, due to phase differences and phase lags across the study area, the velocities at the start and end of the double tidal period do not always match perfectly at different locations on the ebb-tidal delta, resulting in a so-called velocity gap (Figure 3.7 (right)). The velocity gap is defined as the magnitude of the flow velocity at the end of the double tidal period minus the flow velocity at the beginning of the double tidal period, and varies across the ebb-tidal delta. Because the double tidal period is repeated many times, the velocity gap may affect the computed particle trajectories. To minimise these effects, the double tidal period is selected at minimal velocity, since sediment transport should then be zero. Note that due to phase differences, the velocity will not be minimal everywhere on the ebb-tidal delta. Also, the velocity gap is minimised by using 10-minute intervals for the SedTRAILS computation. Increasing this interval directly results in an increase of the velocity gap.

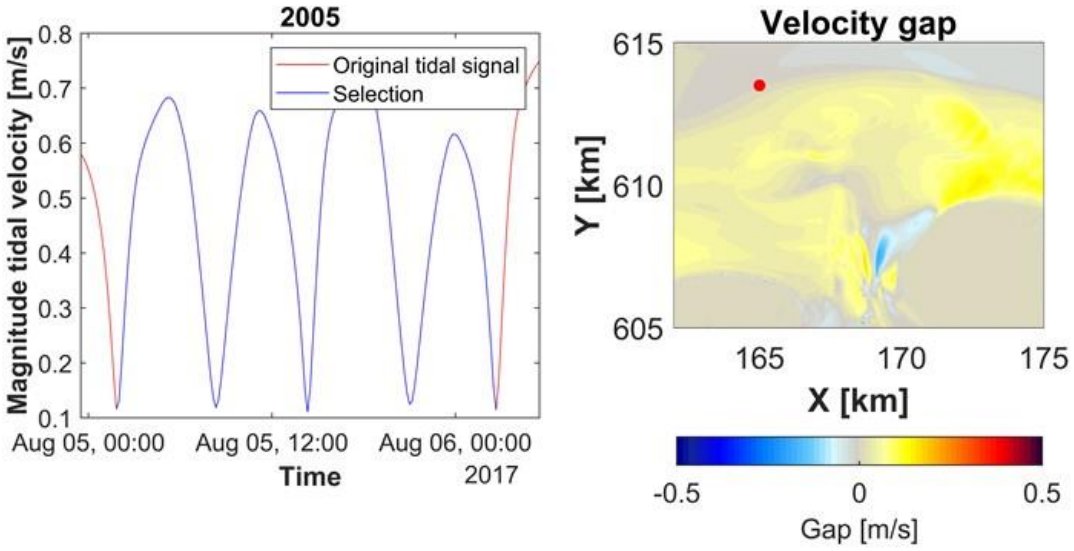

Figure 3.7 – An example of the selection of the double tidal period for SedTRAILS for the 2005 tide-only run. Left: The selected double tidal period based on the tidal signal at open sea. Right: The velocity gap across the domain of interest. The location at open sea used to select the double tidal period is marked in red.

Particle trajectories are visualised using SedTRAILS using 500 initial source locations (Figure 3.8). This ensures a sufficiently high density, whereby the exact position of the source location with respect to the morphology does not matter, and means that the same set of source points can be used for all bathymetries. The density of the source points is adjusted to reflect the complexity of the transport patterns with the highest density in the area where the ebb-shields form, followed by the rest of the ebb-tidal delta and the coastlines, and finally the open sea. The source points within the areas of different density are defined using a clustering algorithm which divides the bathymetric grid into N cells weighted by XY position and bed elevation. The centroid of the cell is then taken as the source location. This is done based on the 2005 bathymetry.

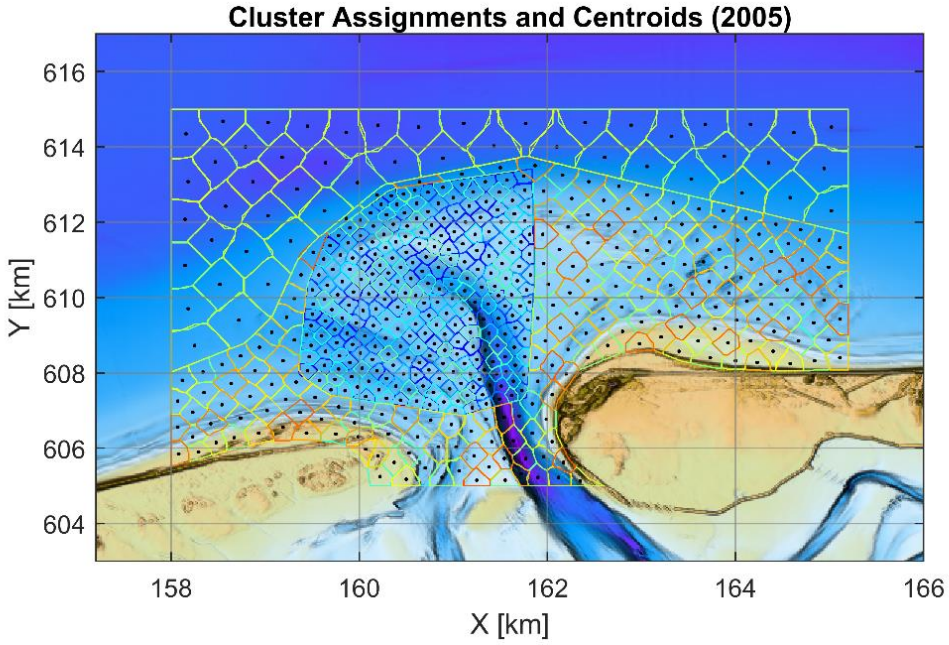

Figure 3.8 – 500 source points as defined using the 2005 bathymetry, with a higher density on the ebb-tidal delta, and an even higher density in the area where the ebb-shield form.

For visualisation using SedTRAILS, a runtime of 500 days is used. The time component of SedTRAILS has not yet been calibrated so this number is arbitrary and cannot be linked to real-time morphodynamic changes on the ebb-tidal delta. This runtime is chosen because after 500 days there are few additions to the existing transport patterns.

3.4 Model simulations

For the model study, both tide-only and coupled tide-wave simulations are performed in Delft3D FM. The tide-only runs include 2 days of spin-up time. The coupled tide-wave run includes 1 day of spin-up time and is run using a restart file generated during the tide-only simulation.

For the coupled tide-wave simulation, a simulation is done for each of the 6 wave conditions and the weighted sum of the calculated transports is taken based on probability of occurrence, to give the year-average representative transports. Both the tide-only and the coupled tide-wave simulation is performed for the 2005, 2007, 2011 and 2017 bathymetries, which gives 28 model runs. Tide-only and coupled tide-wave simulations are also performed for several nourishment surveys, which are embedded in bathymetries of the full ebb-tidal delta. This is done for the nourishment surveys from 22/02/2018, 28/02/2019, 27/03/2020 and 13/12/2020, giving an additional 28 model runs.

For each bathymetry, the particle trajectories for a tide-only and the coupled tide-wave simulations are visualised using SedTRAILS. This is done using the transport vector fields from Delft3D. The computed transports for individual wave conditions are scaled based on the probability of occurrence of the wave condition and summed up to give a combined transport vector field for each bathymetry. This is representative for year-average transports due to waves and tides. For the 8 bathymetries listed above, this gives 16 simulations with SedTRAILS.

3.5 Limits of the followed modelling approach

There are a few limitations of the chosen modelling approach for both Delft3D and SedTRAILS which should be taken into account when considering the results.

Delft3D FM

The morphological tide used is based on transports across cross-sections in the vicinity of the Ameland inlet. This means that gross and net transports correspond well with year-averaged transports. However, there can still be small differences in the details of the transport patterns. For a better match in the small-scale transport patterns, the year-averaged sediment transport vectors should be visually compared with the double-tidal-period-averaged transport vectors for future studies.

The chosen wave conditions represent year-average conditions. This means that the computed sediment transport includes the contribution from storms. This means that the results are suitable for drawing conclusions on transport behaviour under average conditions but not for individual storms.

Because the model run is performed morphostatically, transport which occurs due to morphodynamic change is not included in the individual model results. Pathways will go around a morphodynamic feature, but as the model run is morphostatic, the feature will not move. Morphodynamic change can however be seen when considering a sequence of bathymetries.

Delft3D FM is continuously being developed further but a number of physical processes are not yet included or fully captured in the model, which means that the associated transports will not be visible in the resulting transport pathways. For example, wave-driven transports at the ebb-delta front are known to be underestimated (Elias, 2018a).

SedTRAILS

For this study the tidal velocity signal has been chosen based on the tidal velocity signal at open sea because the tidal signal here is relatively undisturbed. Closer to the inlet, the tidal velocity signal is distorted by local effects, often resulting in a checkerboard pattern, a mild example of which is visible in Figure 3.7 (right). An argument in favour of defining the double tidal period based on velocities in the inlet is that flow velocities are highest in the inlet. The velocity gap is expected to have greater effect if it occurs at higher velocities. The magnitude of these velocities will vary depending on the location on the ebb-tidal delta and the phase in the tidal cycle where the velocity gap is. If the double tidal period is selected in the inlet, velocities will be minimal at the start and end of the period selected, and the effect of the velocity gap should be negligible. Further investigation is needed to define the optimum location for selection of the (double) tidal period.

The velocity gap concept is briefly explained in section 3.3.2. Because SedTRAILS repeats the transports from the same double tidal period a large number of times, the velocity gap and the corresponding sediment transport gap can result in misleading residual transport. This is especially true in areas where transport is negligible. On the ebb-tidal delta, transports are likely sufficiently large that residual transports due to the velocity gap can be considered negligible. Further investigation is needed to determine how large the residual transports due to this velocity gap are, and whether it is actually a problem.

4 Data analysis – Natural inlet dynamics

This section starts with a general description of the morphodynamics of Ameland inlet followed by more details on the behaviour of individual features such as tidal channels and shoals based on analysis of the available data. The sediment volumes actively changing within the ebb-tidal delta are also investigated.

4.1 Morphodynamics of Ameland inlet

This analysis of the meso-scale morphodynamics at Ameland inlet is based on the bathymetries obtained between 2005 and 2020 (Figure 4.1) and expands on the description in Elias et al. (2020) which includes the years 2005 to 2019. The 2005 bathymetry is chosen as starting point because inaccuracies may exist in earlier years (Elias, 2017). Moreover, 2005 is the last bathymetry prior to the formation of a series of ebb-chutes and shields, which can be considered as the starting point of the sediment bypassing cycle (Elias et al., 2019). This links to the emerging idea that the formation of ebb-chute and shield systems and thereby the process of sediment bypassing is triggered by a local instability and may not be cyclic at all (Elias et al., 2019; Elias, Pearson, et al., 2020). Instead, a stochastic trigger marks the start of a sequence of events which together form the sediment bypassing cycle.

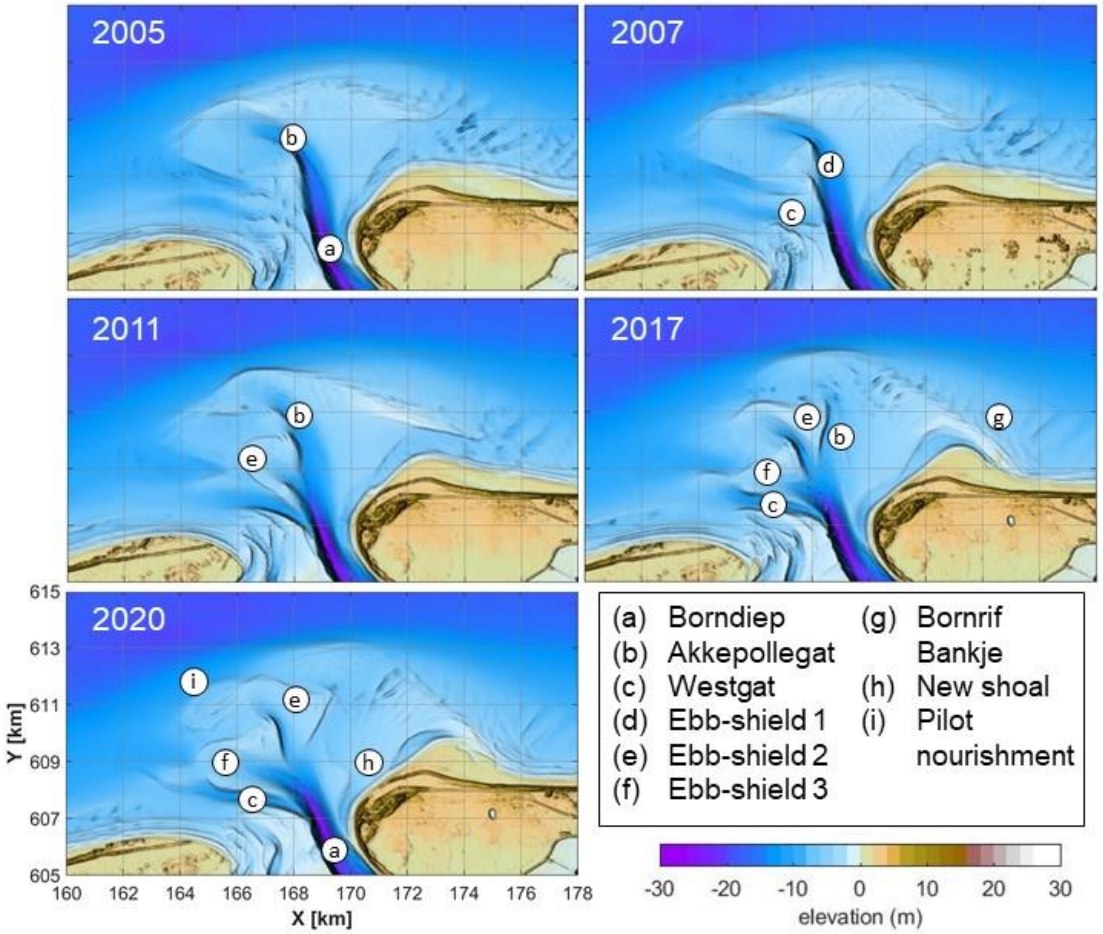

Figure 4.1 – Bathymetries from 2005, 2007, 2011, 2017 and 2020 illustrating the evolution of the Ameland ebb-tidal delta with key features labelled (a)-(i). See Appendix A.1 for the full set of bathymetries and sedimentation-erosion patterns.

Several features remain relatively unchanged during the period described. These are:

1. The inlet between the islands, which consists of a deeper main ebb-channel (Borndiep [a]) along the coast of Ameland and a shallower western part near the tip of Terschelling (Boschplaat).
2. Although its geometry changes, the Westgat [c] maintains its position, connecting the Terschelling foreshore in the west with the Borndiep channel in the east, and separating the ebb-tidal delta from Terschelling.
3. Most of the ebb-delta volume which is stored on the north-east side of Borndiep in the Bornrif platform.
4. In the shallow part of the inlet between Westgat and Boschgat, smaller channels which do not directly connect to a channel on the ebb-delta are present.

Beside these similarities, there are also significant morphodynamic changes taking place. In 2005, the main ebb-channel was bordered by a low elongated shoal on its western side. The Akkepollegat [b], which at that time formed the distal part of the main ebb-channel, deflected westward past the tip of this shoal, and was bordered to the north by the westward reaches of the Bornrif platform known as the Kofmansbult. On this elongated shoal, small instabilities occurred, triggering the formation of a series of ebb-chutes and shields onto the western side of the ebb-tidal delta (2006, 2008, 2014). The first ebb-chute and shield [d] formed between 2005 and 2006 and quickly migrated north, making space for a second ebb-shield. In the study area, during the period of study, the migration of a first ebb-shield creating space always precedes the growth of a second ebb shield. By 2008, a second ebb-shield [e] had formed growing rapidly seaward until 2014 with a mean expansion rate of 385 m/year. As of 2014, the seaward growth had stagnated, and the second ebb-shield covered a large part of the western side of the ebb-tidal delta. Growth was followed by an eastward migration, during which the first ebb-shield was quickly overwhelmed and flow in the Akkepollegat was constricted. As a result, the channel depth was reduced, and the channel rotated from a northwest to a northeast orientation between 2011 and 2020 with a rotation rate of roughly 10°/year.

Between the Westgat [c] and the second ebb-chute, a third ebb-shield [f] started to form in 2014. The ebb-shield initially grew quickly, swallowing the southern trailing end of the second ebb-shield. Growth rates were in the range of 200 - 350m/year between 2016 and 2020. The rotation of this ebb-shield was limited.

These migrating ebb-shields significantly constricted the surrounding channels, reducing the hydraulic efficiency of those channels. Water will always choose the path of least resistance, and this is negatively affected both by the narrowing and the increasing curvature of the channel. Eventually, another path offers less resistance, thus attracting the flow. With less flow through the old channel, the environment switches from erosional to depositional and the channel slowly fills up. Until 2016, Akkepollegat formed the outlet for Borndiep, with the second ebb-chute briefly taking over in 2017. As of 2019, the third ebb-chute formed the main outlet for Borndiep. In this period Westgat continued to deepen, with the sill between Westgat and Borndiep largely gone as of 2014. The development of ebb-shields thus determined the dominant outflow pathways from the inlet.

Changes were also observed on the Bornrif platform. The platform itself remained in place and was a relatively static part of the ebb tidal delta. More dynamic was the formation, migration and merging of the Bornrif Bankje [g] which occurred on top of this platform. Further thoughts on the dynamic and static volumes with in the ebb-tidal delta are elaborated on in section 4.4. Between 2008 and 2010, the Bornrif Bankje started to take shape on the northeast flank of the ebb-tidal delta, shallower than the surrounding platform. Its formation was likely wave-driven, with wave breaking resulting in the coalescing of sand bars and

downdrift sediment transport. The Bornrif Bankje migrated eastward and landward, with an increasingly narrow channel between the Bornrif Bankje and the Bornrif Strandhaak. In 2017 the tip of the Bornrif Bankje attached just downdrift of the Bornrif Strandhaak. On the southern tip of the Bornrif, sediment started to accumulate in 2018 and formed a new shoal [h] in 2020.

While the Ameland coast accreted as a result of the new attachment, the Boschplaat at the tip of Terschelling continued to erode. This was linked to the position of the ebb-tidal delta. After 1999, the Westgat decreased in size and the shoal deposits along its northern margins could no longer be maintained (Elias et al., 2019). The relatively deep area between the Kofmansplaat and the Boschplaat allowed the undisturbed propagation of waves into the inlet and towards the coast. Wave breaking-related transport can induce significant coastal erosion and eastward sediment transport from the Boschplaat towards Borndiep. More recent bathymetries (2016 – 2020) may show the first signs of a reversal of this behaviour as the deposits north of Westgat are growing again, both in height and in westward direction.

4.2 Tidal channel behaviour

The tidal channels in the Ameland inlet are continuously migrating, filling and deepening. This behaviour is mapped for the main ebb and flood channels for the bathymetries between 2005 and 2020.

4.2.1 Akkepollegat

In 2005, Akkepollegat acted as the main ebb channel for Borndiep. Between 2007 and 2020, the distal part of the main ebb channel rotated clockwise, first due to the migration of ebb-shield 1 (2007-2008) and then due to the more sustained growth (2008-2014) and rotation (2014-2020) of ebb-shield 2.

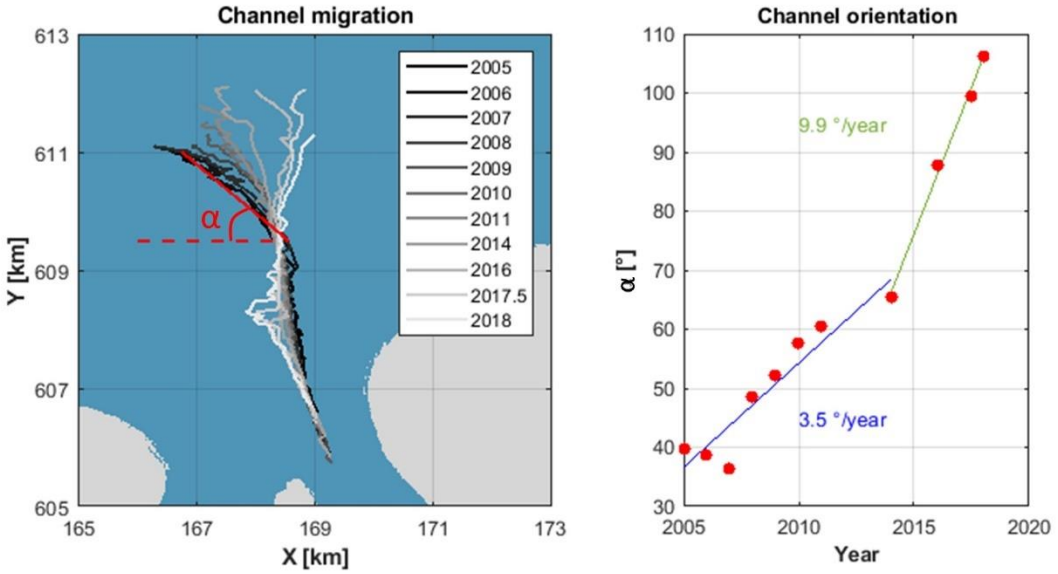

Figure 4.2 – Migration of the Akkepollegat. Left: Main ebb channel trajectories found by following the deepest points. Only years where the depth approach identifies the Akkepollegat as the main ebb channel are included (2005-2018). Right: Orientation of the distal part of the Akkepollegat as the channel migrates. The orientation expresses as the angle to the horizontal (α) is approximated though a linear fit of the distal part of the main ebb channel, which is defined as being north of 609.5km. This is shown for the 2005 trajectory in the left plot. During the growth phase of the 2nd ebb-shield, the migration of the Akkepollegat is approximated at 3.5°/year and during the rotation of the 2nd ebb-shield the migration is approximated at 9.9°/year.

Channel migration is mapped by superimposing subsequent channel trajectories (Figure 4.2 (left)). The channel trajectory is defined starting at the deepest point in the tidal inlet throat and then continues by identifying the deepest point in the region 200m north of the last point. If multiple points have the same depth, then the point closest to the last point is chosen. This is repeated until a depth of 7.5m is reached. This method for identifying the main ebb channel is referred to as the 'depth approach' from hereon. To quantify the migration, a linear fit of the distal part of the main channel is done (north of 609.5km), allowing the orientation to be expressed in an angle to the horizontal 'α' (Figure 4.2 (right)).

During the growth phase of the ebb-shields (2006-2014), the rate of migration was approximated at 3.5°/year. The speed of migration increased to approximately 9.9°/year when the second ebb-shield started to rotate. This suggests that the rotation of the ebb-shields plays an important role in the migration of the Akkepollegat.

The migration of the Akkepollegat was accompanied by an increasing bed level of the channel (Figure 4.3), which can be attributed to siltation. This suggests that flow velocities through the channel are decreasing, resulting in increased deposition of sediment. Shallowing of the Akkepollegat is greatest adjacent to the migrating ebb-shield (608-611km north) with a decrease in depth of roughly 9m between 2008 and 2018.

Between 2011 and 2014, the Akkepollegat and Borndiep temporarily aligned (Figure 4.5), forming a straight hydraulically efficient channel to the ebb-delta front. As a result, sediment was transported beyond the existing ebb-delta front and the ebb-tidal delta built out. Once the Akkepollegat rotated further, this sediment deposit could no longer be maintained and formed the basis of the Bornrif Bankje which formed further downdrift.

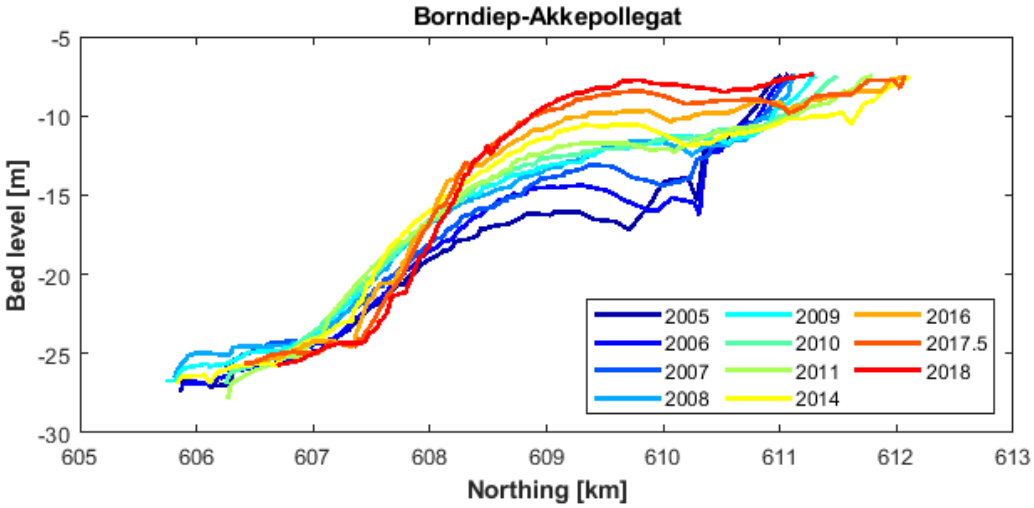

Figure 4.3 – Bed level of the Borndiep-Akkepollegat (2005-2018). The depths are defined along the main ebb channel trajectories shown in Figure 4.2. Because the depth approach no longer identifies the Akkepollegat as the main ebb-channel in 2019 and 2020, these years are not included.

4.2.2 Westgat

Contrary to the main ebb channel, the main flood channel – Westgat – maintained its position (Figure 4.4 (left)). Its trajectory is defined in a similar way to that of the main ebb channel, this time starting at deepest point in the middle of the Westgat (deepest point in the window 166.5-167.0 km E, 607.5-608.0 km N) and following the deepest points east and west.

Where the Akkepollegat was silting up, the Westgat was deepening and the sill where it connected to the Borndiep diminishing in size between 2005 and 2016 (Figure 4.4 (right)). This suggests that flow velocities through the Westgat are increasing, resulting in the erosion

of the channel bed. From 2017 onwards, the depth of the channel and its cross-section stabilises.

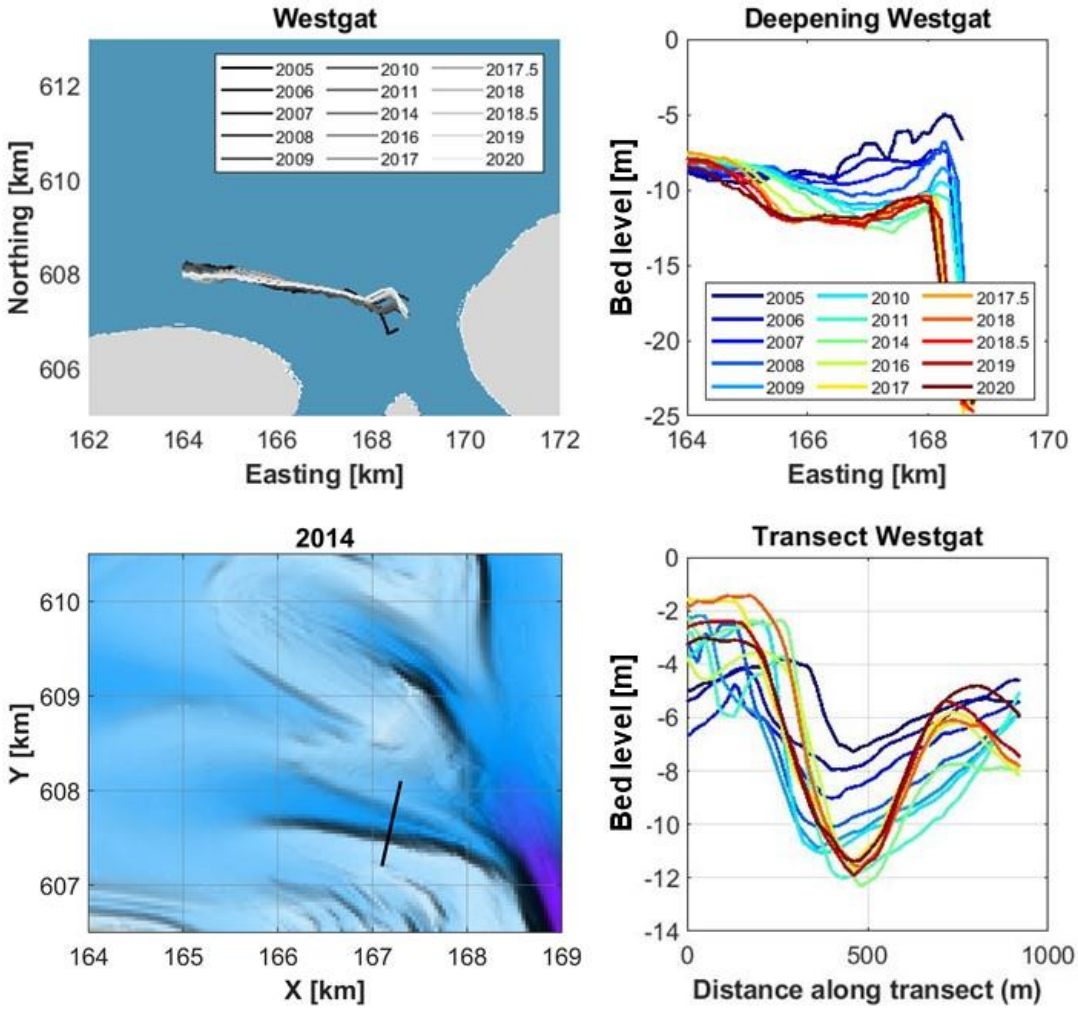

Figure 4.4 - The development of the Westgat and its connection to Borndiep between 2005 and 2020. Top left: the trajectory of the Westgat defined by following the deepest points from the centre of the Westgat. Top right: The depth of the Westgat along the trajectories determined according to the depth approach. Bottom left: The transect used to show the development of the cross-section of the Westgat. Bottom right: Cross-section of the Westgat.

4.2.3 Outer channel switching

The constriction and migration of the Akkepollegat reduced its hydraulic efficiency and led to a switch of the main ebb-channel. Until 2016, the depth-approach described above identifies the Akkepollegat as the main ebb-channel. Following a period with no clear main channel, the third ebb-chute acted as the new main channel from 2019 onwards (Figure 4.5). At the same time, the Westgat was deepening and the sill where it connected to the Borndiep diminishing in size. The diminishing of the sill suggests that the Westgat not only functions as a flood channel but also as an ebb-channel. The Westgat has had a dual role as both flood and ebb channel in the past, for example in 1865 and 1962 (Elias et al., 2019).

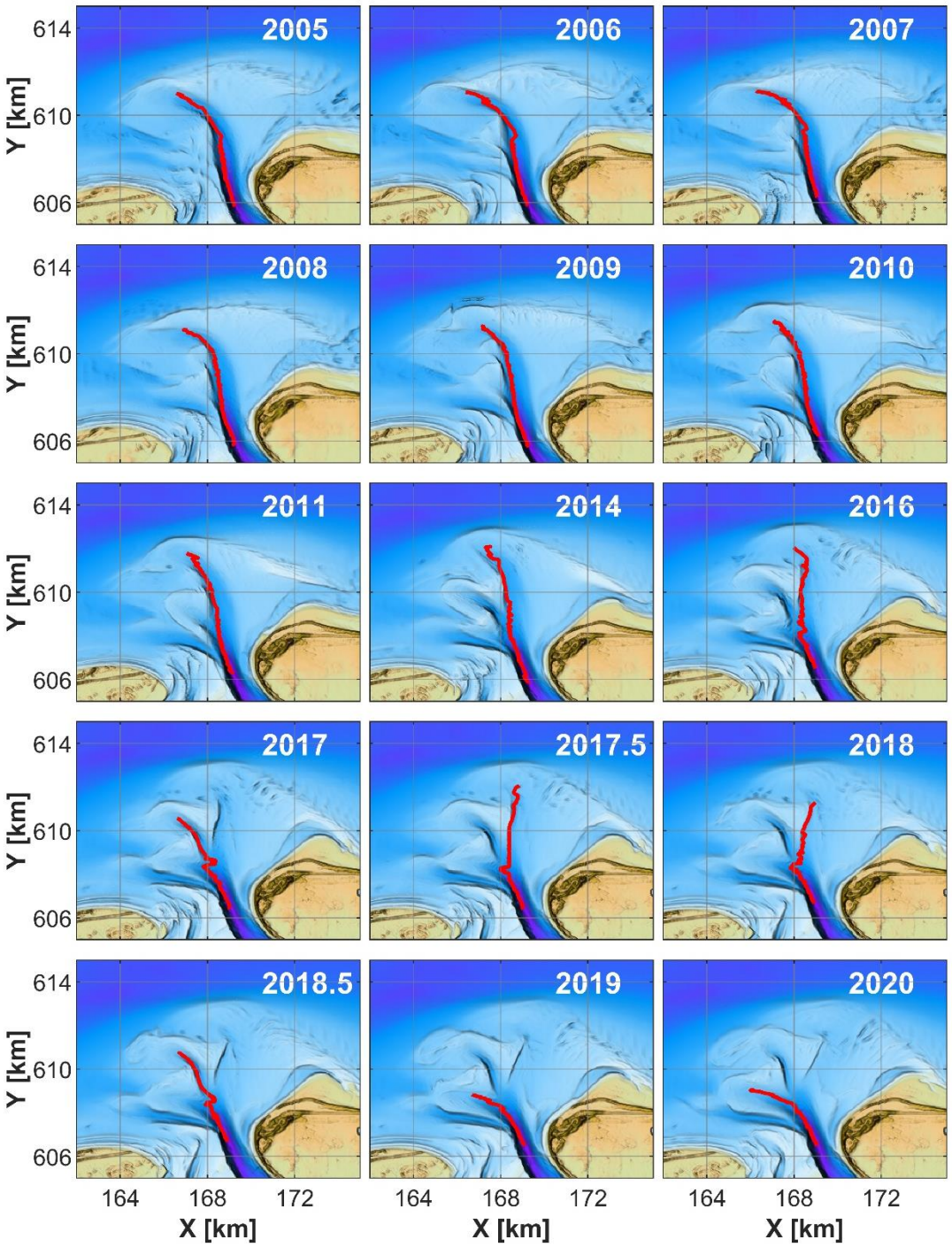

Figure 4.5 – The main ebb-channel trajectory (red) found using the depth approach. Until 2016, the Akkepollegat is identified as main ebb channel. In 2017 and 2018, there is no clear main ebb channel. From 2019 onwards, the 3rd ebb-chute is identified as main ebb-channel.

4.3 Behaviour of ebb-shields and -chutes

The ebb-shields which form on the western side of the ebb-tidal delta grow, migrate and sometimes decay. This behaviour is mapped directly from the bathymetries and further analysed based on the sedimentation-erosion volumes and the hypsometry of the ebb-shields.

4.3.1 Development of ebb-shields and chutes

The development of ebb-shields between 2005 and 2020 is visualised using a series of schematics in which the edge of the ebb-shield is visually determined based on the steepest slopes. In this period, three ebb-shields formed on the western flanks of the Akkepollegat of which the last two are still active in 2020. The ebb-shields are numbered chronologically based on the time of formation.

After formation between 2005 and 2006, the first ebb-shield showed no significant growth. Instead, it migrated northward (Figure 4.6), losing its structure in 2011 with its remnants being swallowed by the second ebb-shield in 2014.

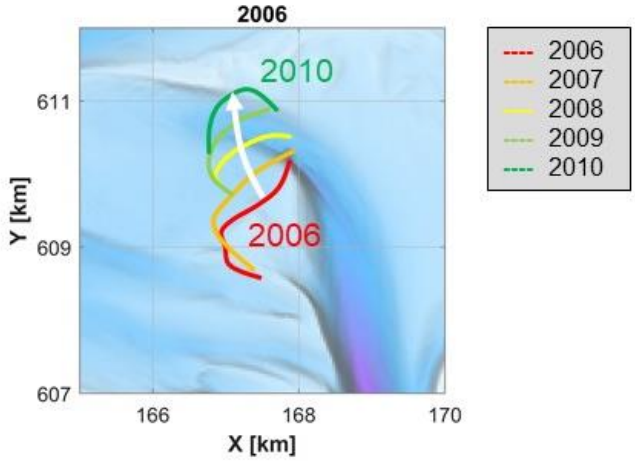

Figure 4.6 – A schematic showing the outer edge of ebb-shield 1 between 2006 (red) and 2010 (green). The 2006 bathymetry is included for reference.

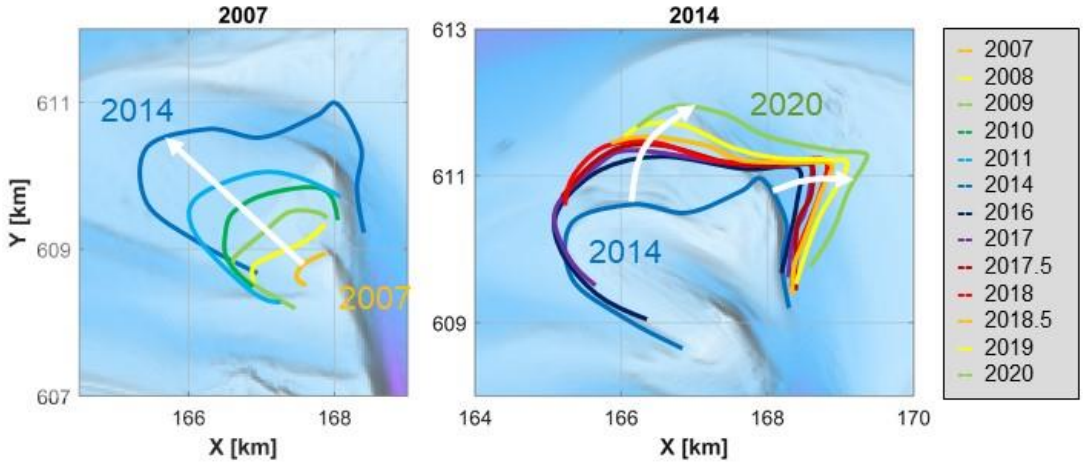

Figure 4.7 – A schematic showing the outer edge of ebb-shield 2 during its growth (left) and rotary phase (right). Left: The rapid growth of the 2nd ebb-shield between 2007 (orange) and 2014 (blue), with the 2007 bathymetry for reference. The remnants of the first ebb-shield are swallowed in 2014. Right: The clockwise rotation of the 2nd ebb-shield between 2014 (blue) and 2020 (green), with the 2014 bathymetry for reference.

The second ebb-shield formed in 2007 and grew rapidly seaward until 2014 with a mean expansion rate of 385 m/year (Figure 4.8). After this, growth stagnated, and the ebb-shield started to migrate across the Akkepollegat. At this point the ebb-shield also lost the roughly symmetric shape it had during the period of growth. From 2014 onwards, the ebb-shield was asymmetric with the bulk of the sediment on the northeast side (Figure 4.7).

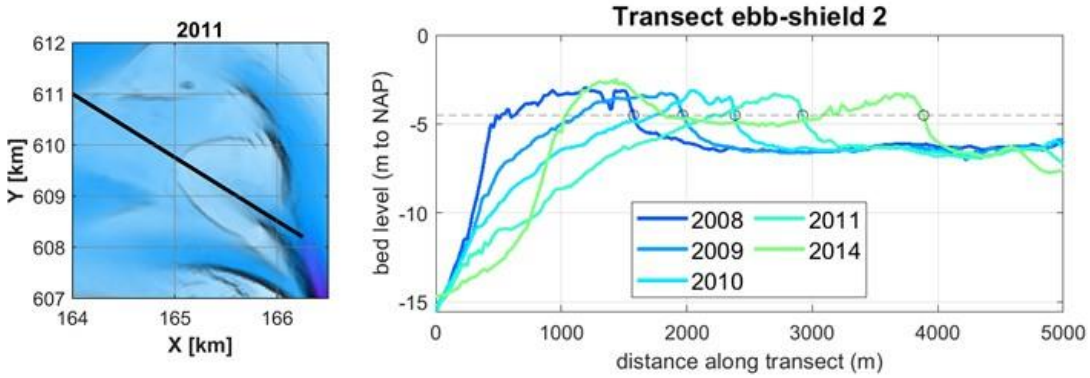

Figure 4.8 – A transect through the second ebb-shield during its growth phase between 2008 and 2014. The mean growth rate is 385 m/year determined based on the -4.5m intersect on the seaward side of the ebb-shield.

The third ebb-shield formed in 2014. Just like the second ebb-shield, the third ebb-shield grew rapidly seaward after formation (Figure 4.9) with a mean growth rate of 260 m/year (Figure 4.10). The ebb-shield was almost directly asymmetric as it directly swallowed the southwestern trailing end of the second ebb-shield. Rotation of the ebb-shield was limited, probably due to wave sheltering by the second ebb-shield.

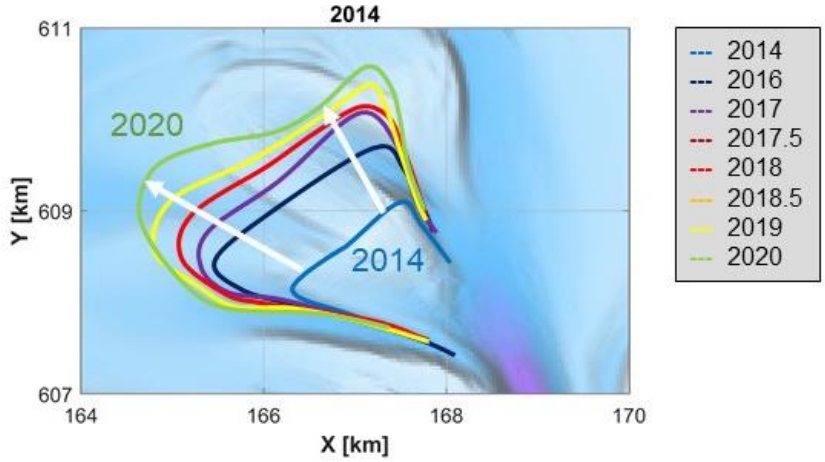

Figure 4.9 – A schematic showing the outer edge of the 3rd ebb shield as it grows between 2014 (blue) and 2020 (blue), with the 2014 bathymetry for reference.

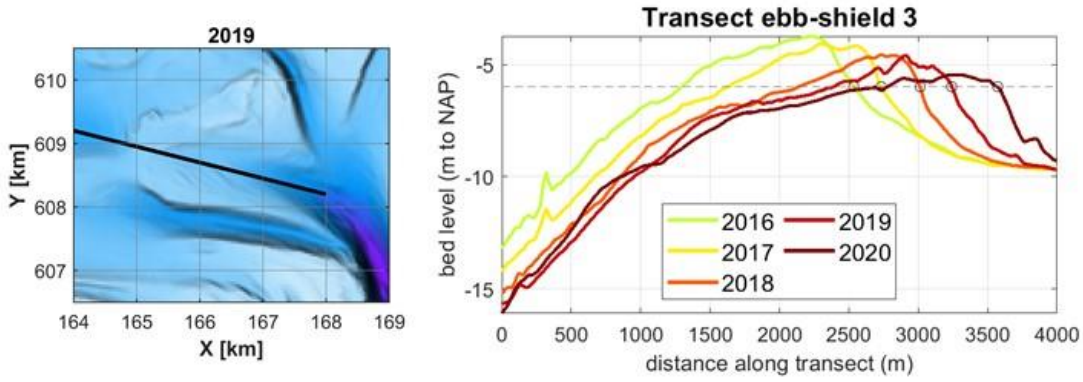

Figure 4.10 – A transect through the second ebb-shield during its growth phase between 2016 and 2020. The mean growth rate is 260 m/year determined based on the -6m intersect on the seaward side of the ebb-shield.

4.3.2 Growth of an ebb-shield

The three ebb-shields whose formation and growth are outlined above behave differently after their formation. The first ebb-shield shows almost no growth, while the second and third ebb-shields grow rapidly for multiple years after formation. For an ebb-shield to form and grow, there are three requirements:

- Space to grow
- Strong ebb flow in seaward direction
- Sediment supply

Space

The behaviour of these three ebb-shields can be characterised by periods of growth and migration, where the migration of an ebb-shield coincides with the formation of the next one (Figure 4.11). Each time, migration precedes growth, which suggests that space must be created to accommodate a new ebb-shield and -chute before it can form. Space is in this case defined as there being limited sediment above the baseline ebb-tidal delta platform discussed in section 4.4.

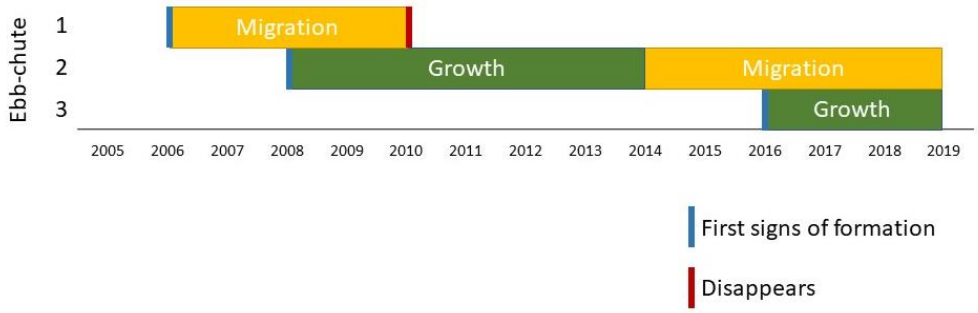

Figure 4.11 – Timeline for the development of the three ebb-shields showing the observed periods of growth and migration.

Flow

Growth occurs through the deposition of sediment on the outer edge of the ebb-shield. This happens when ebb flow velocities decrease from above to below the critical velocity of the local sediment. A condition is thus that the flow is above critical velocity at some point in the ebb-chute. The more flow the chute attracts (water chooses the easiest path), the higher the flow velocities become. In other words, an ebb-chute needs to be one of the more hydraulically efficient paths for ebb flow out of the inlet.

This in turn raises the question what the threshold is after which water will chose a different path, and whether a storm is needed to reach this threshold. The outflow after a storm surge could cause enough erosion to result in a more hydraulically efficient morphology under normal conditions. If a storm is needed to reach the threshold then this is a stochastic process. The fact that period of several years exists when there is no main ebb-channel between the switch from the Akkepollegat to the third ebb-chute (Figure 4.5) suggests that the process is gradual. If storms are key, then multiple will be necessary.

Sediment supply

An ebb-shield's existence and size depend on the critical velocity of local sediment, which is remarkably homogenous in the ebb-tidal delta (Elias et al., 2019; van Prooijen et al., 2020). Flow accelerates in the ebb channel (> v_{crit}) so sand can be eroded. This sand is then deposited when v < v_{crit} which occurs further out to sea for faster flows, so the ebb-shield grows. This description of ebb-shield growth suggests that growth may be largely due to local erosion (i.e. material is eroded from the ebb-chute and deposited on the outer edge of the ebb-shield).

The idea that the growth of an ebb-shield is associated with sand displaced seaward within the ebb-chute and -shield system rather than with sand from outside the system is further investigated by comparing the sedimentation and erosion volumes within each ebb-chute and -shield system. This is done with different polygons for bathymetries from different years, as a universal polygon would not be valid for migrating features over any longer period of time. The definition of these polygons is subjective. An outline of the ebb-shield is defined manually based on a depth plot, taking the steepest slope as the outer edge of the ebb shield. Using the sedimentation erosion patterns in a difference plot, the ebb-shield polygon is then split into a region of erosion and of sedimentation. An example is shown in Figure 4.12, with the sedimentation and erosion polygons for ebb-shield 2.

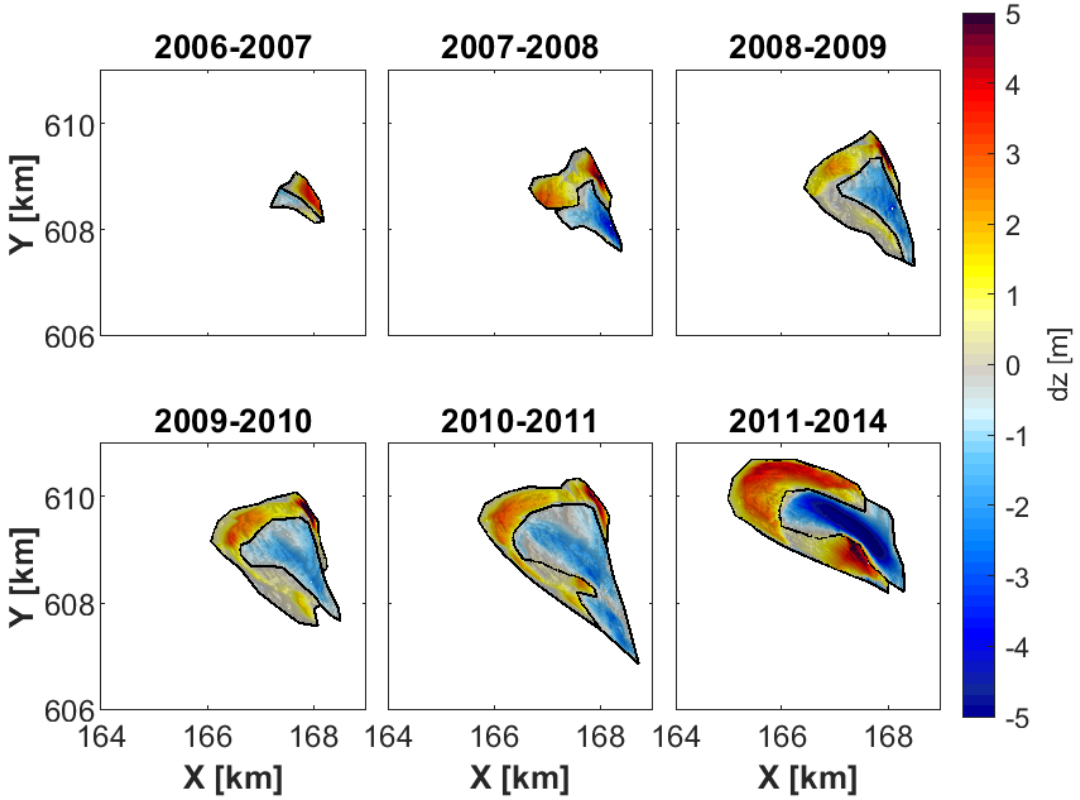

Figure 4.12 – Sedimentation (red) and erosion (blue) areas for the 2nd ebb-shield within the manually defined polygons.

A similar analysis is done for the first ebb-shield. The volumes found through this sedimentation-erosion analysis for ebb-shields 1 and 2 are shown in Figure 4.13. The sedimentation and erosion volumes for ebb-shield 2 are similar from 2008 onwards, which is in line with the idea that the ebb-shields are self-feeding. This is not the case for ebb-shield 1 where sedimentation volumes are considerably larger than erosion volumes. However, the polygon definition is highly subjective, so the resulting volumes remain an estimate and are likely sensitive to changes in polygon definition.

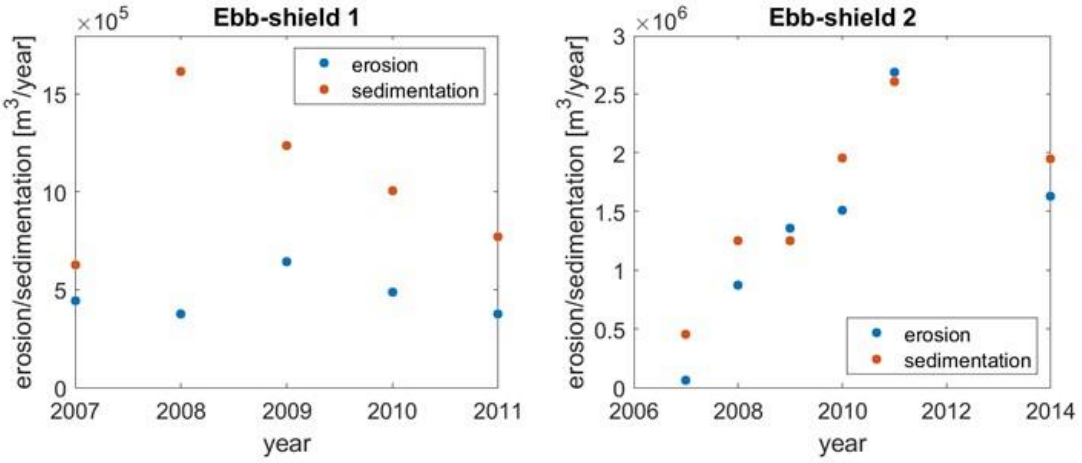

Figure 4.13 – Sedimentation and erosion volumes for ebb-shields 1 and 2 calculated as the volume difference between two subsequent bathymetries within manually defined polygons.

4.3.3 Transition from growth to migratory phase

Growth is characterised by a seaward expansion of a roughly symmetric ebb-shield, while migration is due to a north-eastward movement of a much more asymmetric ebb-shield. Especially ebb-shield 2 shows a transition from a growth to a migratory phase with little apparent overlap. Growth is probably driven by ebb flows while migration is driven by waves and alongshore tidal currents. Alongshore tidal currents are flood-dominant and eastward-directed, and the dominant wave climate is from the northwest (Figure 3.6), which matches the direction of migration of the ebb-shields.

4.3.4 A hypsometric perspective on ebb-shield development

To be able to look at the bathymetric data in a different way, the ebb-shields are reduced to hypsometric curves. A hypsometric curve is a cumulative distribution function of elevation within a geographic area, meaning that it shows the area of land that exists above a certain elevation. In this study, the hypsometric curves are plotted in terms of absolute rather than relative area, allowing the comparison of an ebb-shield in different years with different total areas. The shape of such a curve can be indicative of the geomorphic processes shaping the landscape.

To construct a hypsometric curve for each of the ebb-shields, a polygon is defined around the ebb-shield for each different bathymetry. This is done manually using a bed level plot in which the polygons are drawn slightly outside the steepest outer edge of the ebb-shield. The sensitivity to the choice of polygon should be limited to the greater depths as the ebb-shields are themselves the highest elevation in the area. This is done for all three ebb-shields (Figure 4.14).

In the hypsometric curves for ebb-shield 2, three possible stages can be identified:

1. The **expansion of the base** of the ebb-shield below a pivot point of roughly -3.3m. This is associated with a slight lowering of the top of the ebb-shield. (2007 – 2011)

2. **Growth of the ebb-shield across the full depth range**. Area increases almost equally at all depths. The initial major increase between 2011 and 2014 is due to the swallowing of the remnants of the first ebb-shield. (2011 – 2017.5)
3. The top of the ebb-shield **levels off**. Below a depth of ~-3.5m little changes, but the area above this decreases significantly. (2017.5 – 2019)

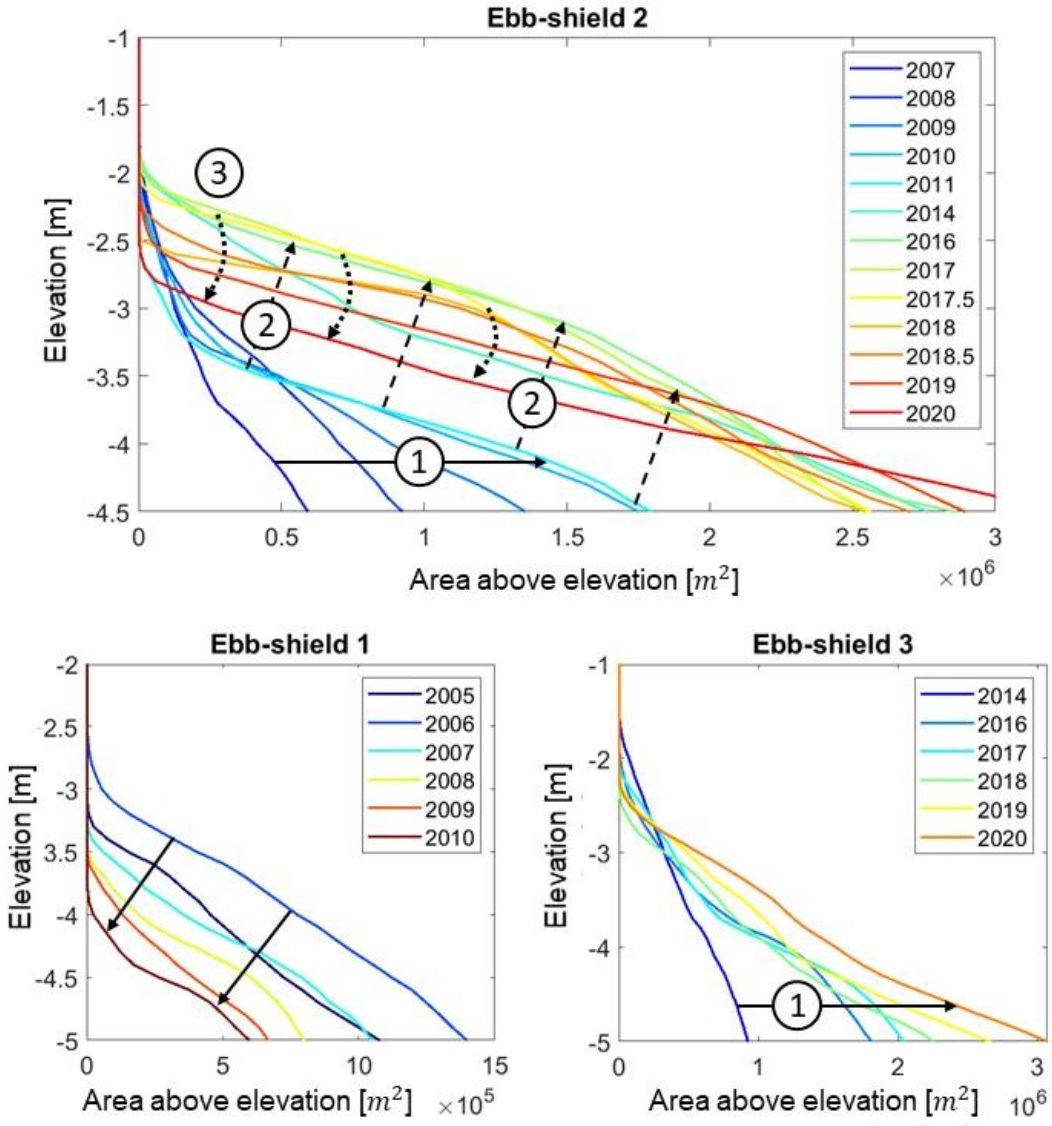

Figure 4.14 – Hypsometric curves for ebb-shields 1, 2 and 3 expressed as the area above a certain elevation. Top: development of ebb-shield 2 with in stages with (1) and expansion of the base, (2) growth over the full depth range, and (3) a levelling off of the top of the ebb-shield. Bottom left: development of ebb-shield 1. Bottom right: development of ebb-shield 3 through expansion of the base (stage 1).

The hypsometric curves for ebb-shields 1 and 3 show less distinct phases. For the first ebb-shield, a short period of growth over the full depth range (2005 – 2006) is followed by the diminishing of the ebb-shield again over the full depth range (2006 – 2011). This decrease in elevation suggests that it is no longer the main recipient of sediment. Notable is also that this ebb-shield is (as a whole) deeper than the other two, something that may have played a role in the lack of further development.

The third ebb-shield shows behaviour very similar to stage 1 identified in ebb-shield 2, with the base expanding while the top lowers slightly. In this case the pivot point is at approximately -3m. For both ebb-shields 2 and 3, the expansion of the base of the ebb-shield labelled as stage 1 corresponds to the main period of growth of the ebb-shield, which suggests that this is characteristic behaviour for a growing ebb-shield.

These results reduce a large amount of data to a simple curve. In order to avoid unsubstantiated simplification, they cannot be considered leading in the understanding of these ebb-shields and will always have to be considered in combination with transects or bathymetries.

4.4 Baseline and dynamic sediment volumes

The motivation for this section is the idea that the ebb-tidal delta consists of a relatively fixed base platform with a dynamic volume of sediment moving across it. This baseline for the ebb-delta platform is then a function of tidal prism and the geological influences which determine it. As a first approximation of this base platform, the minimum elevation over a range of years is used, in this case the bathymetries from 2005 – 2020 (Figure 4.15). Above this base platform there is a dynamic sediment volume, with shoals moving across a base platform, which is controlled by sediment bypassing. By subtracting the baseline surface, this dynamic behaviour can in theory be isolated from the rest.

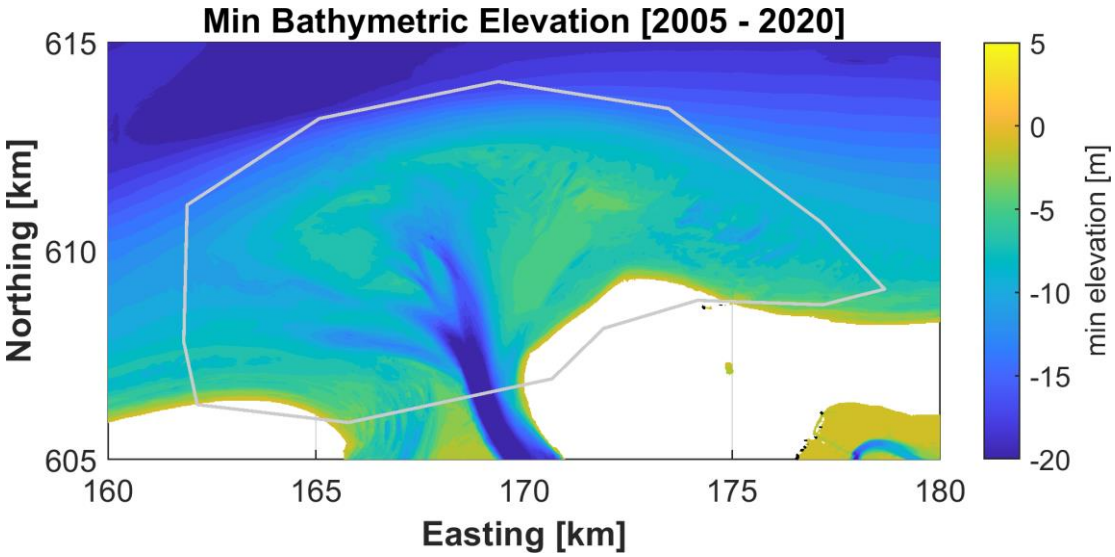

Figure 4.15 – A stable baseline ebb-tidal delta platform approximated as the minimum elevation for every location between the years 2005 and 2020. The polygon used to estimate dynamic volumes for the full ebb-tidal delta is shown in white.

This analysis was done for the full ebb-tidal tidal delta by subtracting the minimum elevation surface from the bathymetries from 2005 to 2020. Any incomplete bathymetries have been made complete using Jarkus data from that year and elevations above 0m MSL have been discarded. The resulting dynamic volumes for each year are shown in Figure 4.16. These numbers suggest that there is 115 million m^3 of dynamic sediment present on the ebb-tidal delta between 2005 and 2011. This increases to more than 125 million m^3 after 2014. To identify the cause of the jump in volume between 2011, a detailed sediment balance will need to be performed. The dynamic sediment volume is of the same order of magnitude as the gross changes of ~200 million m^3 predicted by Elias (2018) for the period 2005 to 2016. The volume of 5.5 million m^3 of sediment present in the nourishment (labelled in Figure 4.16) is

small compared to the total dynamic sediment volume, but of a similar magnitude to other fluctuations observed.

The reliability of any trends in the dynamic volume has not been verified. These volumes are expected to be sensitive to:

- The choice of polygon. The polygon is chosen so that it surrounds the ebb-tidal delta where the volume changes are taking place so this should minimise sensitivity to the choice of polygon.
- The accuracy of the data (although data from 2005 onwards is expected to be relatively accurate (Elias, 2017))
- Beside the pilot nourishment, 9.7 million m^3 of nourishments have been placed at NW Ameland between 2005 and 2020 in the form of beach and shoreface nourishments. These nourishment volumes have not been corrected for. Most of the sediment was placed after 2010.

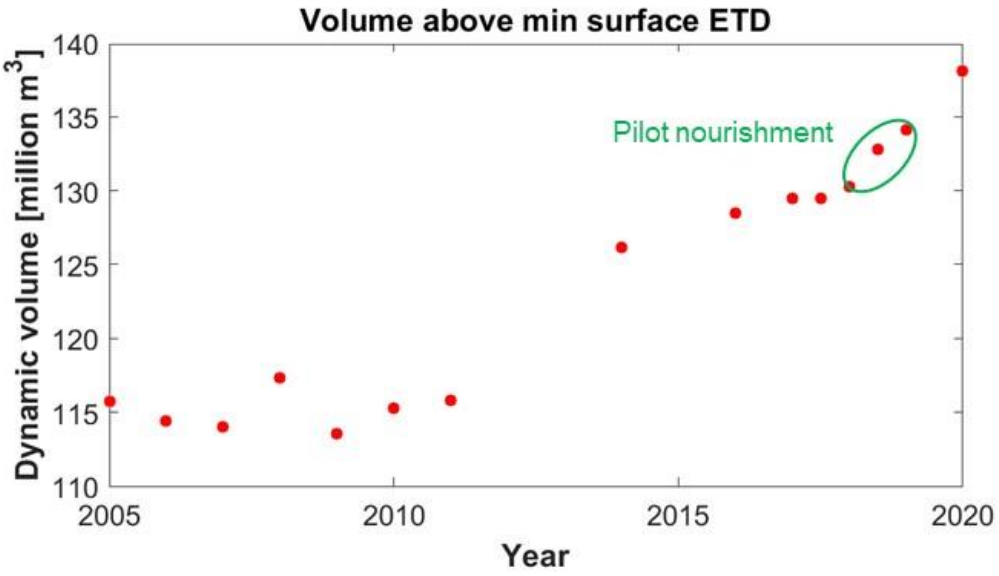

Figure 4.16 – The dynamic volume present on the full ebb-tidal delta calculated by subtracting the minimum bathymetric elevation between 2005 and 2020 from the individual bathymetries in the same period within the polygon shown in Figure 4.15. The average dynamic volume present on the ebb-tidal delta is indicated with the dashed line.

5 Data analysis – Nourishment area

The goal of this chapter is to provide a thorough analysis of the development of the pilot nourishment. This builds on the analysis of the pilot nourishment done by Van Rhijn (2019) and Elias et al. (2020), now also including surveys obtained from 22-11-2019 onwards.

The pilot nourishment in question is constructed just beyond the outer margin of the 2nd ebb-shield between March 2018 and February 2019. Nearly 5.5 million m^3 of sediment is placed on the seaward side of the Kofmansbult. In the original design, the nourishment was directly connected to the ebb-shield, but it was eventually placed with a small trough between the two. As part of Kustgenese 2.0, the nourishment is surveyed regularly both during and after completion (for the complete set of surveys and sedimentation erosion patterns see Appendix 9A.2).

5.1 Nourishment construction

This section summarises the findings of Van Rhijn (2019) on the behaviour of the pilot nourishment during its construction between March 2018 and February 2019. In this period, the nourishment largely kept its place. The changes that did occur were primarily driven by waves. The main transport direction was towards the east, where deposition of sediment is observed along the outer edge of the 2nd ebb-shield. Sedimentation also occurred in the trough between nourishment and the 2nd ebb shield, where sedimentation was not observed before the construction of the nourishment. There was also a seasonality in the response, with stronger erosion in winter than in summer months.

5.2 Post-construction

Following construction, the nourishment continues to evolve under the influence of waves and shore-parallel tidal currents. This behaviour is described using a combination of bathymetries and transects collected during the Kustgenese 2.0 campaign.

5.2.1 Bathymetric analysis

To describe the evolution of the nourishment from before its construction until the most recent survey (13-12-2020), four distinct bathymetries from the Kustgenese 2.0 campaign are chosen (Figure 5.1), and the changes described. These show the nourishment prior to construction (A), directly after completion of the nourishment (B), and roughly 1- and 2-years post-construction (C, D).

Prior to the construction of the nourishment (Figure 5.1A), two large ebb shields dominated the delta platform to the NW of Akkepollegat (ES2 and ES3). These formed in 2007 and 2016 respectively and have been growing seaward and rotating clockwise ever since. From the outer edge of the second ebb-shield, two sandbars (1 & 2) extended towards the southwest. These originated from the earlier ebb-delta front. For a more detailed description of the ebb-tidal delta dynamics prior to the construction of the nourishment, see chapter 4.

During the construction of the nourishment (Figure 5.1B), sandbar 2 was partly buried, but the southwest end continued to exist, also in later years. The nourishment itself can be seen on the west of ES2. Based on the response that followed, the geometry of the nourishment was strongly out of equilibrium with the natural environment.

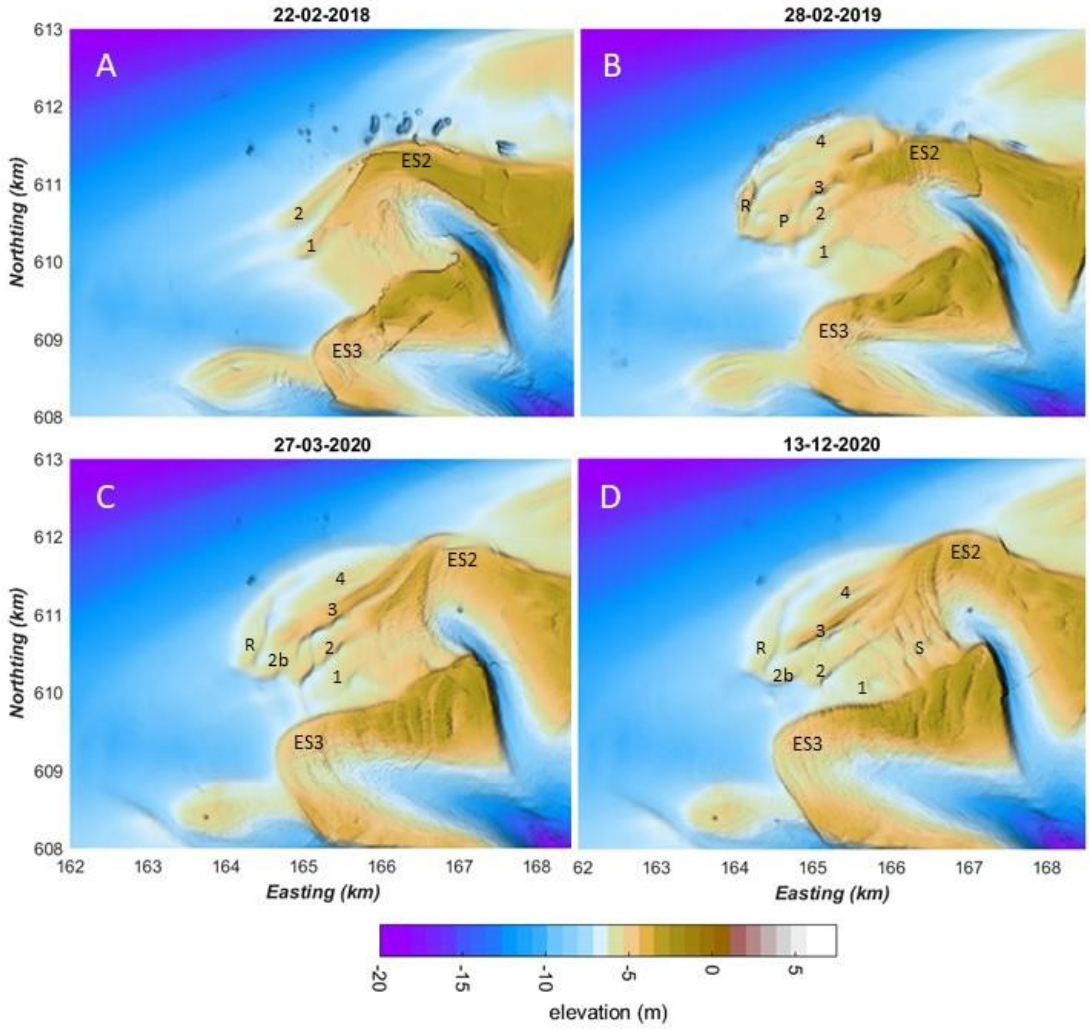

Figure 5.1 - The bathymetry for the location of the pilot nourishment prior to construction (A), directly after completion (B), roughly a year later (C), and the most recent bathymetry available (D). The sand bars are numbered (1-4) and the ebb-shield are labelled ES2 and ES3. R indicates the outer ridge on the nourishment, and P a platform in the centre of the nourishment which is present just after construction. S labels the bar complex which forms perpendicular to the existing nourishment bars.

A first response is clearly visible in Figure 5.1C, with wave-driven eastward sediment transport resulting in smoothing of the nourishment along the outer edge of the 2nd ebb-shield. Bar 4 moved landward, sandbars 2 and 3 elongated and the initial geometry of the nourishment became increasingly streamlined, thus approaching a new equilibrium where the nourishment was more in balance with the wave forcing. Simultaneously, the sand of the nourishments started to form additional sand bars (3 & 4).

This formation of sand bars heralded the second response, a wave-driven landward migration of sandbars. Sandbars started forming and migrating directly after the construction of the nourishment and continued doing so until the most recent survey (Figure 5.1D). In the final surveys, additional sand bars (S) formed perpendicular to the earlier sandbars and parallel to the second ebb-chute. Flood flows drove these bars towards the east.

5.2.2 Volumetric analysis

The development of the nourishment can also be tracked based on its volume (Figure 5.2). Between 22/02/2018 (A) and 28/02/2019 (B) the construction of the nourishment resulted in a continuous increase in volume. Directly after the completion of the nourishment, the volume in the nourishment polygon started decreasing. By 13/12/2020 (D), roughly 38% of the volume had left the nourishment polygon. It should be noted that the nourishment polygon is defined very tightly around the newly constructed nourishment, so any sediment transported just outside this polygon is also considered a loss. Even so, the signal for decreasing sediment volumes and for a seasonal effect is clear.

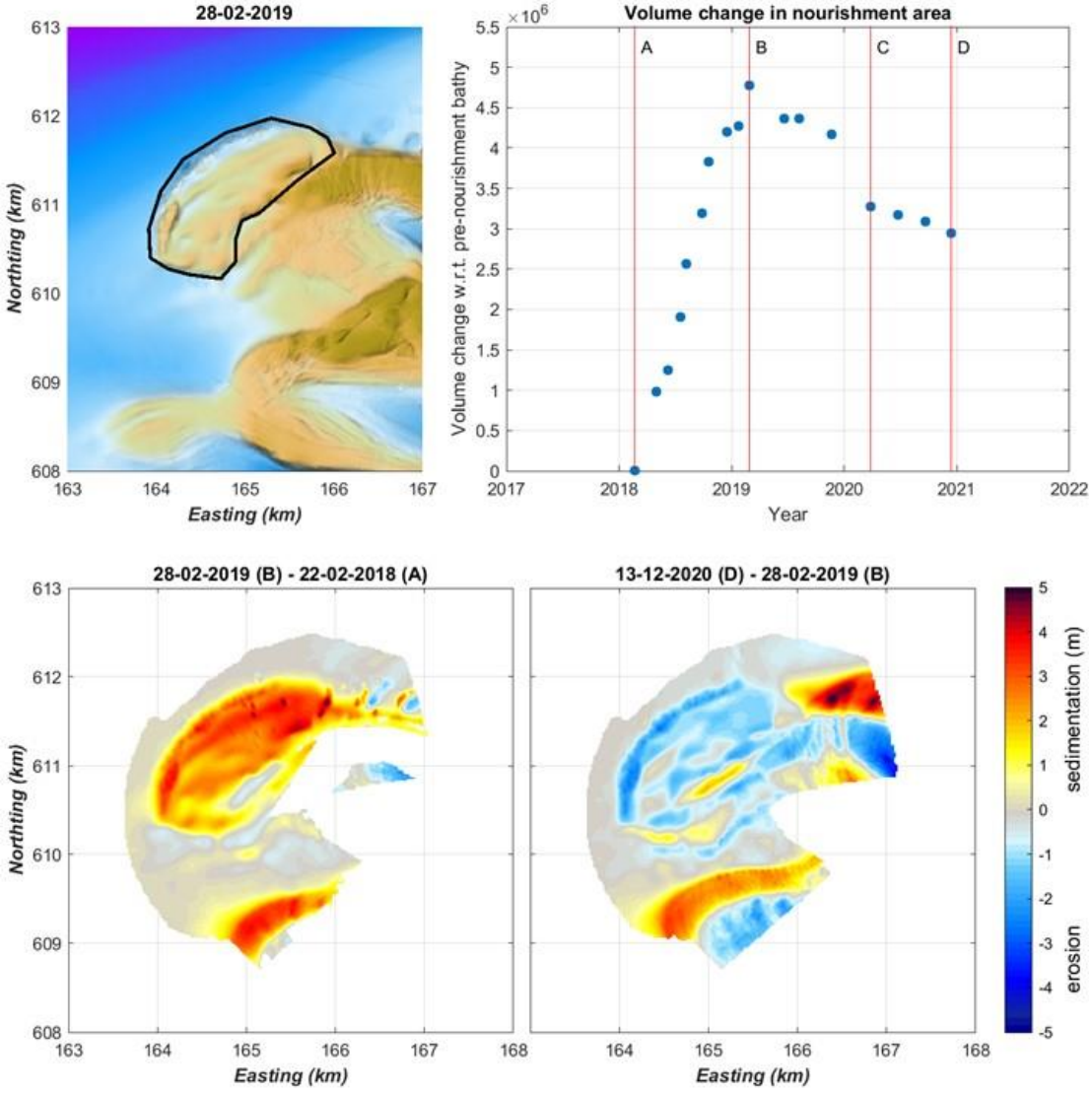

Figure 5.2 – The volumetric development of the nourishment before, during and after the construction of the nourishment. Top left: the nourishment polygon defined based on the bathymetric change before (A: 22/02/2018) and directly after completion of the nourishment (B: 28/02/2019). Top right: volumetric change in the nourishment polygon with respect to the pre-nourishment bathymetry (A). The bathymetries used for the bathymetric analysis in Figure 5.1 are indicated with A, B, C and D. Bottom: the sedimentation erosion patterns between A: 22/02/2018 and B: 28/02/2019 (left) and between B: 28/02/2019 and D: 13/12/2020.

Both in the winter of 2019 and 2020, an increased drop in the sediment volumes was observed with 72% of all volume loss occurring in these winter months. The larger loss observed in the winter of 2020 between the 22/11/2019 and the 27/03/2020 (C) survey

occurred due to erosion mainly on the north-eastern side of the nourishment. This coincided with accumulation of sediment along the outer edge of the ebb-shield to the east of the nourishment polygon, suggesting that strong eastward transport was responsible for this volume loss. This is a clear storm response. Increased erosion during the winter season can be attributed to the more energetic winter conditions.

5.2.3 Cross-sectional analysis

A detailed description of the development of the nourishment and the surrounding area is provided through the analysis of several cross-sections (Figure 5.3).

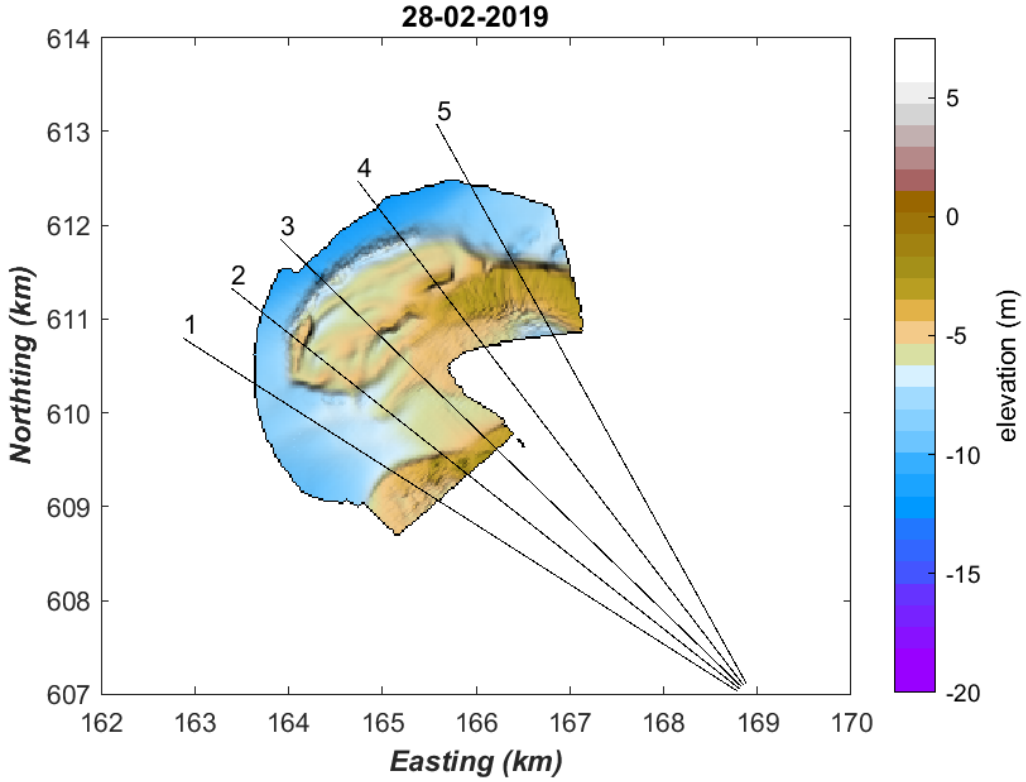

Figure 5.3 - Overview of the selected transects superimposed on the nourishment at the moment of completion (28/02/2019).

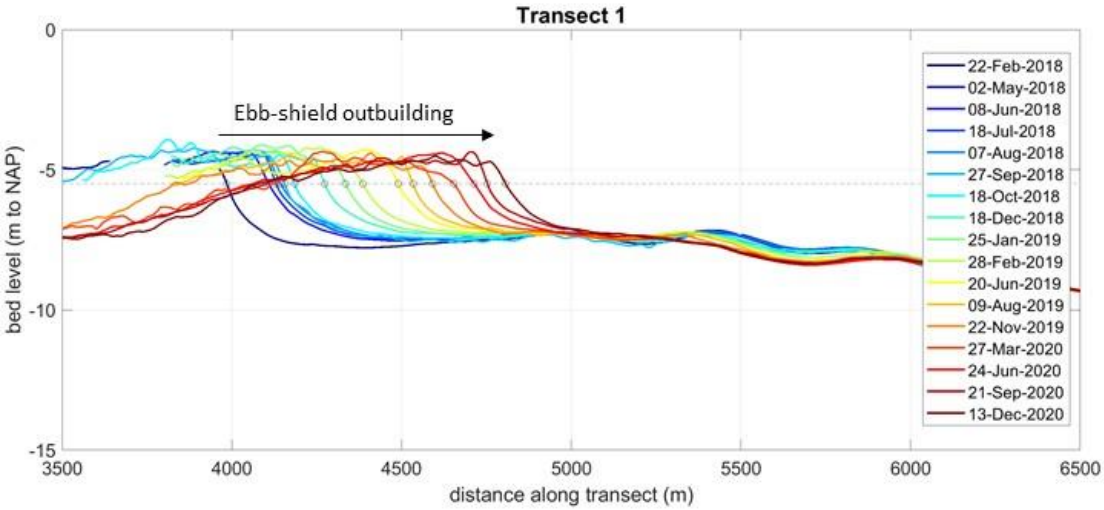

Figure 5.4 - The development of ebb-shield 3 along transect 1 between 22-02-2018 and 13-12-2020. The point at -5.5m NAP use to quantify outbuilding is indicated with a black circle.

Transect 1 (Figure 5.4): This transect is located landward of the pilot nourishment, passing through ebb-shield 3. As in earlier descriptions (Elias, Pearson, et al., 2020; Van Rhijn, 2019), no clear influence of the nourishment on the ebb-shield is observed. However, this transect does give a detailed view of the ebb-shield's growth, outbuilding just over 800m in 2 years. Distinct differences in expansion rate are observed (Figure 5.5). Until summer 2019, there were strong seasonal differences with much larger expansion rates in the winter than in the summer months. From the summer of 2019 onwards, the expansion rate stabilises around 15-20 m/month. Throughout this period of growth, a steeper seaward and gentler landward slope is maintained.

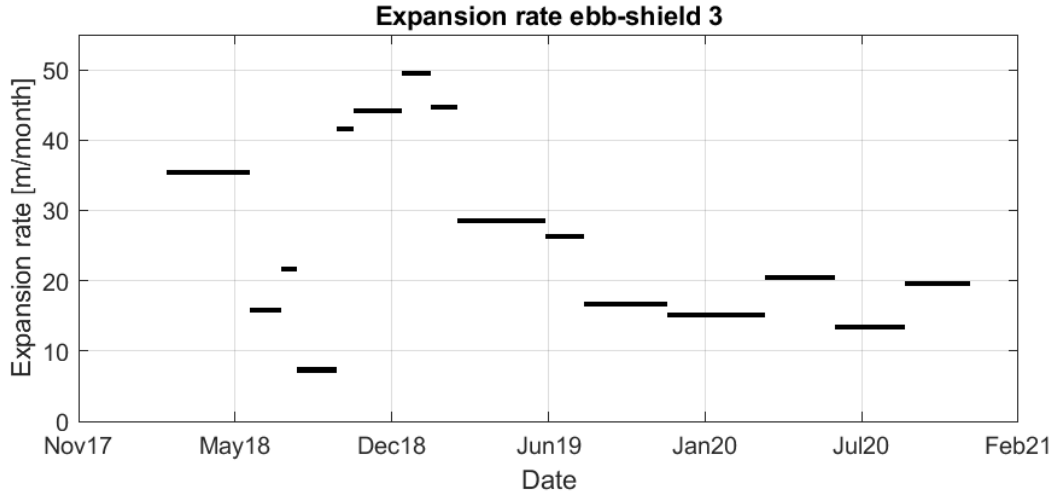

Figure 5.5 - The expansion rate of ebb-shield 3 in m/month, with the length of the line corresponding to the period between surveys. The distance along the transect of the ebb-shield at -5.5m NAP is used to quantify the extent of the ebb-shield.

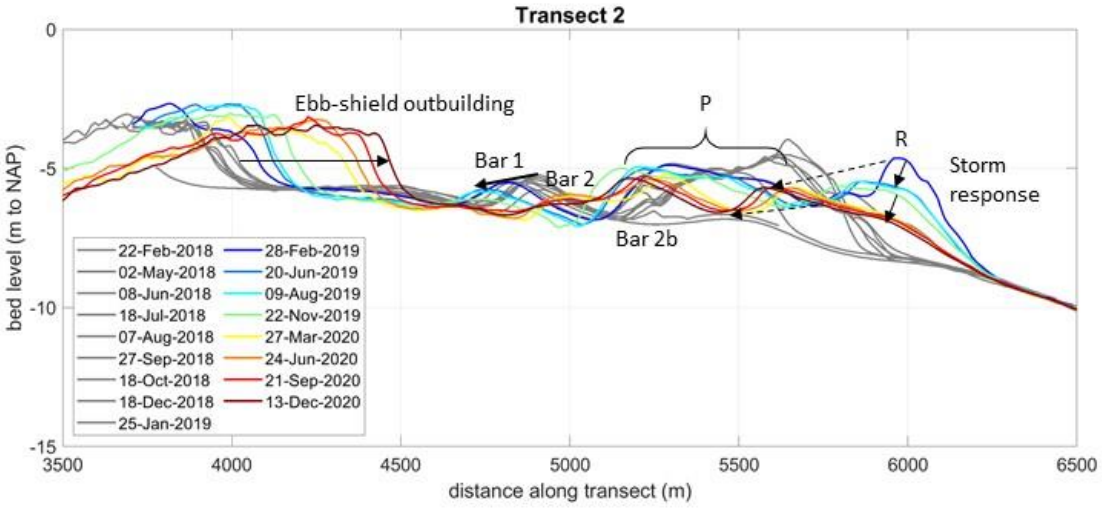

Figure 5.6 – The development of ebb-shield 3 and the landward side of the nourishment along transect 2 between 22-02-2018 and 13-12-2020. Profiles during the period of construction are shown in grey.

Transect 2 (Figure 5.6)**:** Transect 2 passes both through the 3rd ebb-shield and through the landward side of the nourishment. As in transect 1, the ebb-shield was seen to build out, especially after January 2019. This was accompanied by an increase in height.

There are also several sandbars visible in this transect. Bar 1 existed before the nourishment was placed, migrating landward and decreasing in height between 22-02-2018 and 09-08-2019, after which it migrated out of the transect. The 2nd sandbar is not initially visible in this transect. Upon completion of the nourishment (28-02-2019), the sandbar was buried under the platform visible between 5200-5700m (P). This section of the nourishment migrated landward and separated into two distinct bars which are visible from 27-03-2020 onwards. The most landward bar formed an extension of the original sandbar 2, while the other formed a shorter bar (2b) lying between the seaward ends of bars 2 and 3.

During construction, a steep ridge (R) was placed on the outer edge of the nourishment (6000m mark on 28-02-2019). During the two winters following construction (Feb-Jun 2019 and Nov 2019 – Mar 2020) a strong decrease in height and in the slope of the outer edge of the nourishment was observed, with limited change in between. This is likely a storm response. Simultaneously, the crest of the ridge migrated roughly 400m landward in 2 years, considerably faster than the more landward sandbars. Also, by 27-03-2020, the trough landward of this ridge approaches the original depths prior to the placement of the nourishment.

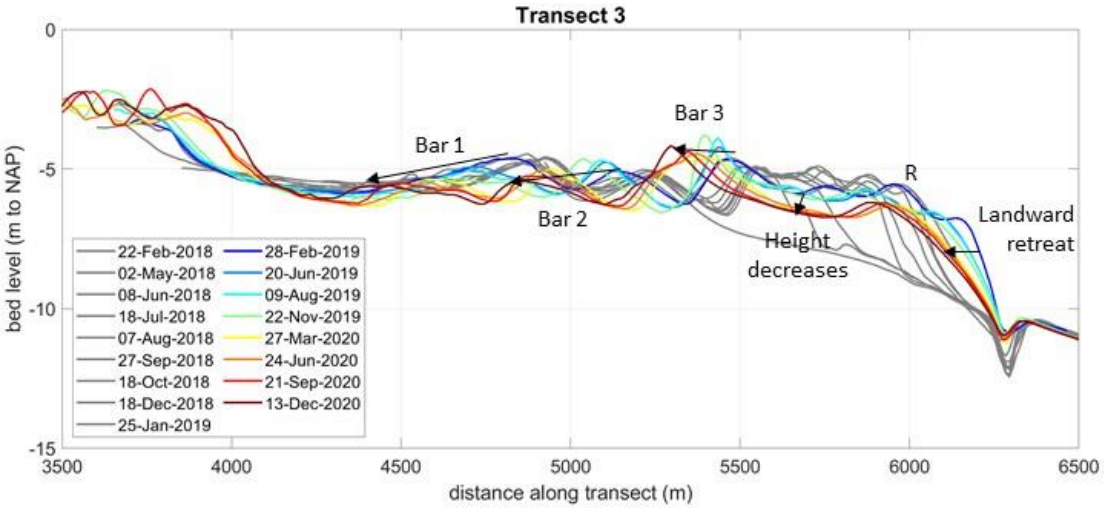

Figure 5.7 – Developments in the middle of the pilot nourishment along transect 3 between 22-02-2018 and 13-12-2020. Profiles during the period of construction are shown in grey.

Transect 3 (Figure 5.7)**:** Transect 3 passes through the 3rd ebb shield and the middle of the nourishment. On the seaward side, the transect also passes through a hole of unknown origin. This is a very local feature which filled up over the period surveyed and appeared to have little effect on the behaviour. As in previous transects, ebb-shield 3 was seen to build out, though by less (only about 100m). This is because the transect passes through the flank of the ebb-shield rather than in the extension of the ebb-chute, where most growth is expected to take place.

The behaviour of sandbar 1 was similar in this transect to in transect 2, with the bar migrating landward and lowering over time. Migration of the 2nd sand bar was limited until the construction of the nourishment was almost complete. From 18-12-2018 onwards, the sandbar migrated landward, increasing in height until 22-11-2019 after which it decreased in height. The 3rd sandbar formed from the material on the landward side of the nourishment. The crest of the sandbar migrated landward while the trough seaward of the sandbar deepened. The ridge (R) was much less prominent where it intersects transect 3 than transect 2. Even so, a similar gentling of the slope was visible, with again the largest changes in winter.

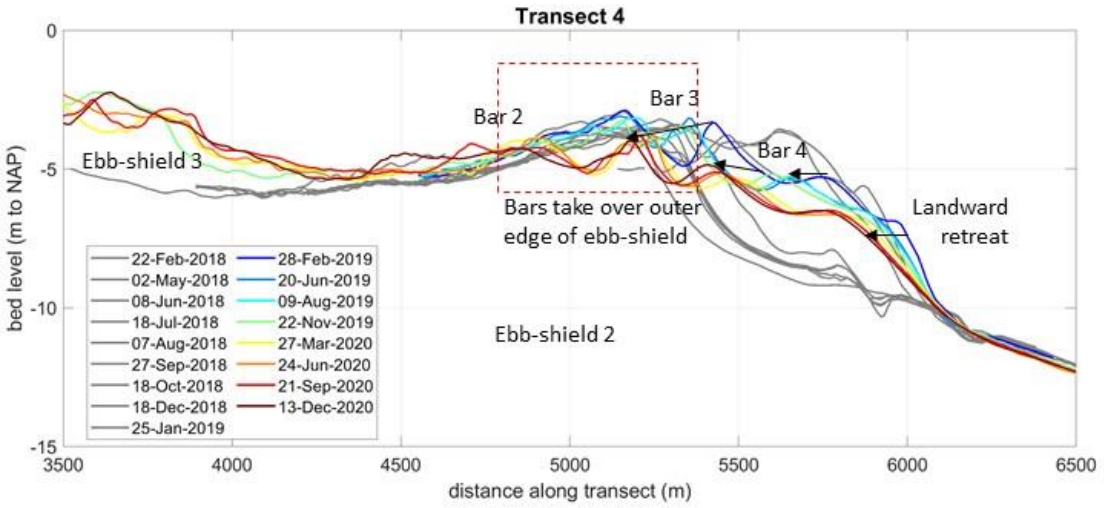

Figure 5.8 - Development of the northern side of the pilot nourishment along transect 4 between 22-02-2018 and 13-12-2020. Profiles during the period of construction are shown in grey.

Transect 4 (Figure 5.8)**:** Transect 4 passes through the northern part of the nourishment, the western part of ebb-shield 2 (ES2) and the eastern side of ebb-shield 3 (ES3). At the outer edge of the 2nd ebb-shield, outbuilding or retreat of the ebb-shield is difficult to distinguish from the construction activities. From 27-03-2020 onwards, the outer edge of the ebb-shield was dominated by laterally extending sandbars 2 and 3, and no longer distinguishable. Sandbar 2 migrated landwards after this extension into transect 4. The 3rd sandbar is visible from 25-01-2019 onwards and migrated landward until 13-12-2020. A 4th sand bar is visible close to the outer edge of the nourishment, which migrated rapidly landward (400m in under 2 years), especially during the winter months. The outer slope of the nourishment again retreated resulting in gentling of the outer slope. The toe of the slope did remain in place.

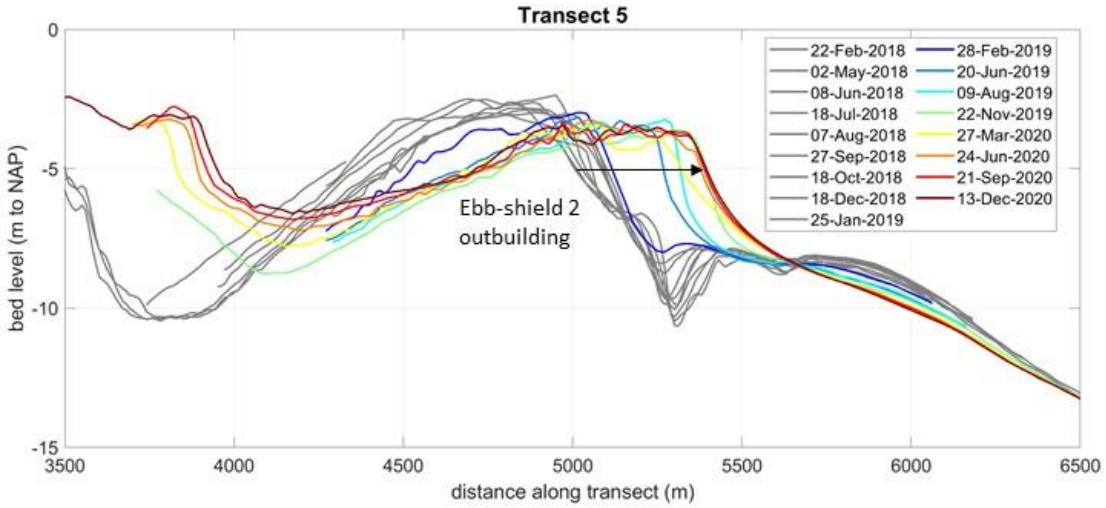

Figure 5.9 - Outbuilding of ebb-shield 2 to the north of the pilot nourishment along transect 5 between 22-02-2018 and 13-12-2020. Profiles during the period of construction are shown in grey.

Transect 5 (Figure 5.9)**:** This transect is located to the north of the nourishment and passes through the middle of the 2nd ebb-shield (ES2). Before construction (grey), the ebb-shield built out slowly seaward, until a very strong seaward movement between 28-02-2019 and 20-06-2019. This coincided with the completion of the nourishment and likely corresponds to the first response described in more detail in section 5.2.1, where the nourishment is smoothed by rapid eastward wave-driven transport. This interval of increased outbuilding was followed by a period of slower ebb-shield growth, until the outer edge of the ebb-shield remained stable from 24-06-2020 onwards. This suggests that after an initial pulse, eastward transport from the nourishment decreases.

6 Modelling study

Analysis of the historic bathymetry gives many insights into the ebb-tidal delta dynamics. However, they remain snapshots of a continuously evolving area. A modelling study is performed to fill in the missing process-based links between the different bathymetries. For each of the bathymetries a tide-only and a coupled tide-wave run is performed using Delft3D FM and the resulting transport patterns are visualised using SedTRAILS (see sections 3.2 and 3.3 respectively for more details). Bathymetries both before and after the placement of the nourishment are included in the modelling study.

6.1 Natural ebb-tidal delta dynamics

This section includes the model results for bathymetries before the placement of the nourishment, starting with the general transport patterns across the entire ebb-tidal delta and then zooming in on the ebb-shields.

6.1.1 Transport patterns at ebb-tidal delta scale

In the following section, transport pathways for bathymetries at different stages in the sediment bypassing cycle are visualised using SedTRAILS. This is done for year-average conditions, which include both tides and waves. To produce these results, a morphological tide is selected which generates sediment transports that are representative for year-average conditions. Delft3D FM is run morphostatically for the selected period to generate a sediment transport vector field at a 10-minute interval. SedTRAILS is then used to visualise the resultant transport pathways. A particle is released in the sediment transport vector field from Delft3D and its position is computed every 10 minutes. The selected morphological tide can then be repeated until the desired runtime is reached. Due to the low acceleration factor used, the particle trajectories represent net and not gross particle motion. For a more detailed description of the modelling approach see sections 3.2 and 3.3.

Patterns in the SedTRAILS results can be extremely complex and difficult to interpret. Important to note is that the particle trajectories represent only the pathway that the particle follows and say nothing about the volume following these pathways. This is inherent to Lagrangian approaches. To interpret the transport patterns, the SedTRAILS results have been annotated (Figure 6.2). Trajectories where pathways converge are shown in red. Zones where the net transport pathways diverge are indicated with white dashed lines. These lines divide the residual transport which means that transport across them is possible, but that the net changes are roughly subdivided by these lines. In the areas between these lines of convergence and divergence, pathways often follow trajectories which are similar or roughly parallel to each other. These general transport patterns are indicated with yellow arrows.

This analysis is performed for a select number of bathymetries which represent different stages in the sediment bypassing process. Bathymetries shown are:

- 2005: prior to the formation of the first ebb-shields
- 2011: during the growth phase of the 2nd ebb-shield
- 2017: prior to the placement of the nourishment when the ebb-shields are mature and have started rotating
- 2020: 2 years after the construction of the nourishment and following a switch of the main ebb-channel

Prior to ebb-shield formation (2005)

The transport pathways prior to the formation of the ebb-shields are shown in Figure 6.2A. Based on these pathways, the ebb-tidal delta can be split in 3 separate areas with little or no exchange between them (Figure 6.1). These areas have a strong internal connectivity but a limited external connectivity.

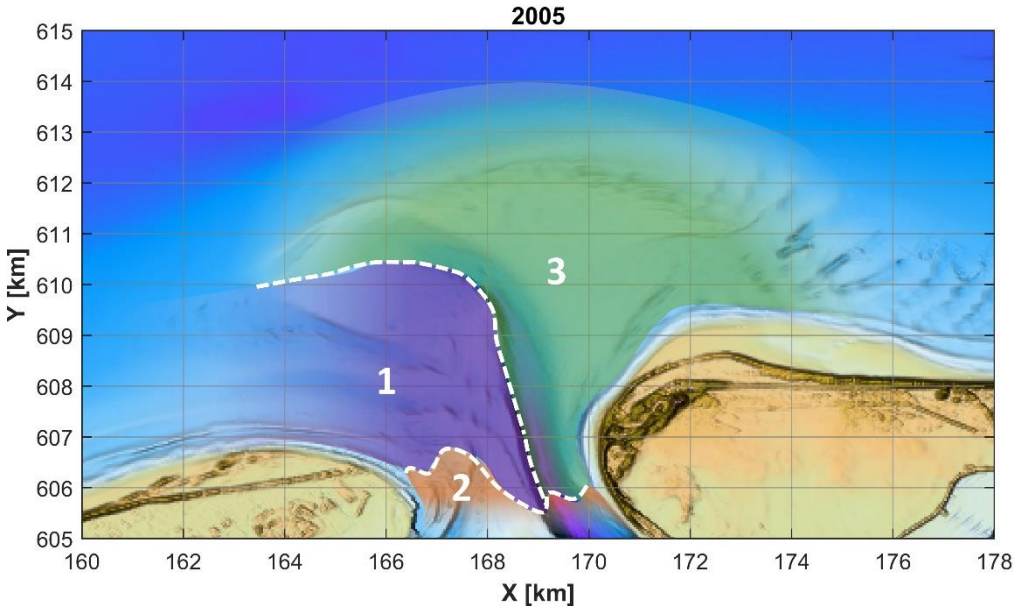

Figure 6.1 - In 2005, the ebb-tidal delta is split into 3 areas with little to no exchange between them based on the transport pathways: (1) the Kofmansbult where the ebb-shields form, (2) the Boschgat and basin-side of the Borndiep, and (3) the Akkepollegat and Bornrif.

Area (1) is the landward side of the western part of the ebb-tidal delta also known as the Kofmansplaat, where the ebb-shields later form. This area acts as a sediment trap, capturing any sediment coming in from the west. Sediment already present in this area continues to circulate in the same area, and no sediment appears to exit this area to join the major transport pathways along the ebb-delta front. All this suggests that sediment accumulates in area (1).

The zone supplying the western side of the tidal basin forms a second distinct area (area (2)). In 2005, only particles starting in the tidal inlet throat move into the basin and any particles north of this line are redirected into area (1). Along the shoreline, sediment is directed to the Boschgat area, where it feeds the channels and shoals that are present here. Partly, this sediment moves into the basin through the shoals, while a major part of the sediment seems to migrate eastward over the shoals and towards Borndiep. It should be noted that transport along the shoreline of Terschelling is not well resolved in this model and that this may still play a significant role in feeding the basin.

Area (3) is the Akkepollegat and the part of the ebb-tidal delta which lies east of this channel. Most of the sediment in this area converges towards a major transport pathway along the outer edge of the ebb-tidal delta. Waves are the primary driver of transport along the ebb-delta front and across the Bornrif platform, with a contribution from shore-parallel tidal currents on the western side (Appendix B.1). At this stage, the particle trajectories do not reach the Ameland coast but stop on the eastern tip of the Bornrif where sedimentation is observed. Sediment may reach the coast indirectly via the migration of large bars offshore of the ebb-delta platform, a process that is not captured in a morphostatic run. On the southern tip of the Bornrif, almost in the inlet throat, there is an area where sediment recirculates.

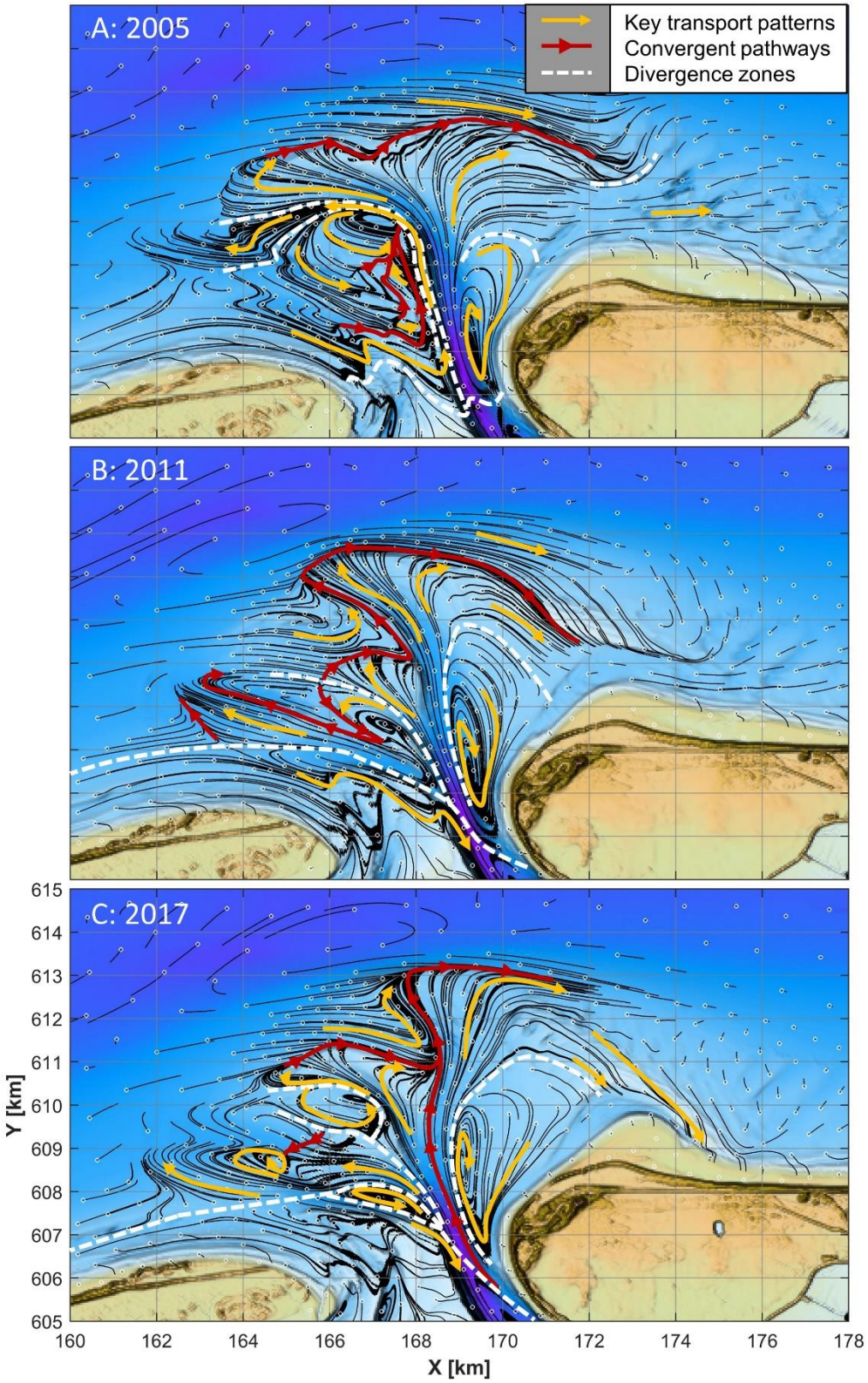

Figure 6.2 - Schematised SedTRAILS results for a coupled tide and wave simulation performed using the bathymetries for: (A) 2005, (B) 2011 and (C) 2017. Source locations are indicated with a white circle and particle trajectories with a white line. Key transport patterns are illustrated with the yellow arrows, trajectories where the particles converge are shown in red and zones where the particle behaviour diverges are shown with dashed white lines.

Ebb-shield growth (2011)
In 2011, the second ebb-shield is in its growth phase, and the transport pathways on the Kofmansplaat (previously area (1)) connect to the major transport pathway along the ebb-delta front (Figure 6.2B). At this stage, the second ebb-shield extends roughly 2km onto the Kofmansplaat. Sediment for the growth of ebb-shield is supplied from its ebb-chute and the western bank of the main ebb channel, passing through the chute and diverging towards the outer edge of the ebb-shield. Particles reaching the northern half of the outer edge of the ebb-shield continue seaward, eventually joining the major transport pathway along the ebb-delta front. On the other hand, particles reaching the edge of the ebb-shield south of the divergence zone are driven landwards by waves until they are transported westward out to sea by ebb flows passing through the Westgat. The ebb flows passing through the Westgat peak in 2011 (see Appendix B.2).

There are also more transport pathways in the Boschgat area leading into the tidal basin than in 2005, with all particles starting south of the Westgat travelling into or towards the basin. This could indicate increased transport into the basin. Simultaneously, the major transport pathway along the ebb-delta front continues to supply sediment to the southeast tip of the Bornrif, where sediment accumulates, and the pathways do not directly connect to the Ameland coast. The connection of the second ebb-shield to the major pathway along the ebb-delta front and northward shift of the line separating particles travelling into the basin and onto the delta are all indications that area (1) is no longer acting as a sediment trap.

Ebb-shield rotation (2017)
By 2017, the third ebb-shield has formed and both ebb-shields have also started rotating, pushing the Akkepollegat further east. This is also the first year that transport pathways form a direct connection between the Bornrif platform and the coast (Figure 6.2C).

In 2017, the Kofmansplaat remains connected to the major transport pathway along the ebb-delta front with the connection from outer edge of the second ebb-shield still active. The rotation of this ebb-shield brings sediment further east. At this stage, the third ebb-shield is well-connected to the Borndiep via the ebb-chute but transport connections from the ebb-shield to the rest of the ebb tidal delta are limited. Sediment for the growth of the ebb-shield is supplied through the chute, and upon reaching the outer edge of the ebb-shield is transported landward by waves. Ebb flows through the third ebb-chute are strong and transport sediment westward into open sea.

As in 2011, all sediment starting south of the Westgat follows a net trajectory towards or into the tidal basin. Also, this is the first year that a direct connection forms between the Bornrif platform and the Ameland coast. This connection forms through the attachment of the Bornrif Bankje, closing off the flood channel which passes along the coast of Ameland.

Section synthesis
This series of SedTRAILS results gives several insights on the transport behaviour of the Ameland ebb-tidal delta over time. The Kofmansplaat initially acts as a sediment trap where almost all particles coming in from the west are trapped and recirculate. This includes particles starting south of the Westgat which in later years travel into the tidal basin rather than onto the western part of the ebb-delta platform. Accumulation on the Kofmansplaat continues until an instability triggers the formation of a series of ebb-shields which allow for a transport connection to form with the major transport pathway passing along the ebb-delta front. This major transport pathway is present in all the bathymetries considered and continuously supplies sediment to the south-eastern tip of the Bornrif. Transport across the Bornrif is almost completely wave-driven. Sediment accumulates at the south-eastern tip of the Bornrif as the Bornrif Bankje and is pushed closer to the coast by waves until pathways make a direct connection with the Ameland coast in 2017.

6.1.2 Ebb-shield dynamics

The SedTRAILS results can also be used to explain the transport behaviour of individual features such as ebb-shields. This section discusses what the transport pathways show about the processes governing the behaviour of ebb-shields in terms of their growth, rotation, and the transition between the two.

Ebb-shield growth

Growth of the ebb-shields is predominantly tide-driven, with material being transported through the ebb-chute to the outer edge of the shield. As can be seen in Figure 6.3B, the general transport patterns within the ebb-shield are very similar for the tide-only and the coupled tide-wave simulation during growth. The limited difference between the tide-only and coupled simulations suggests that waves play a minor role and that growth is tide-dominated. In the coupled simulation, particles do travel further. This can be explained by the fact that waves stir up additional sediment which is then transported by tidal currents, and that they generate wave-driven currents especially along the outer edges of shoals.

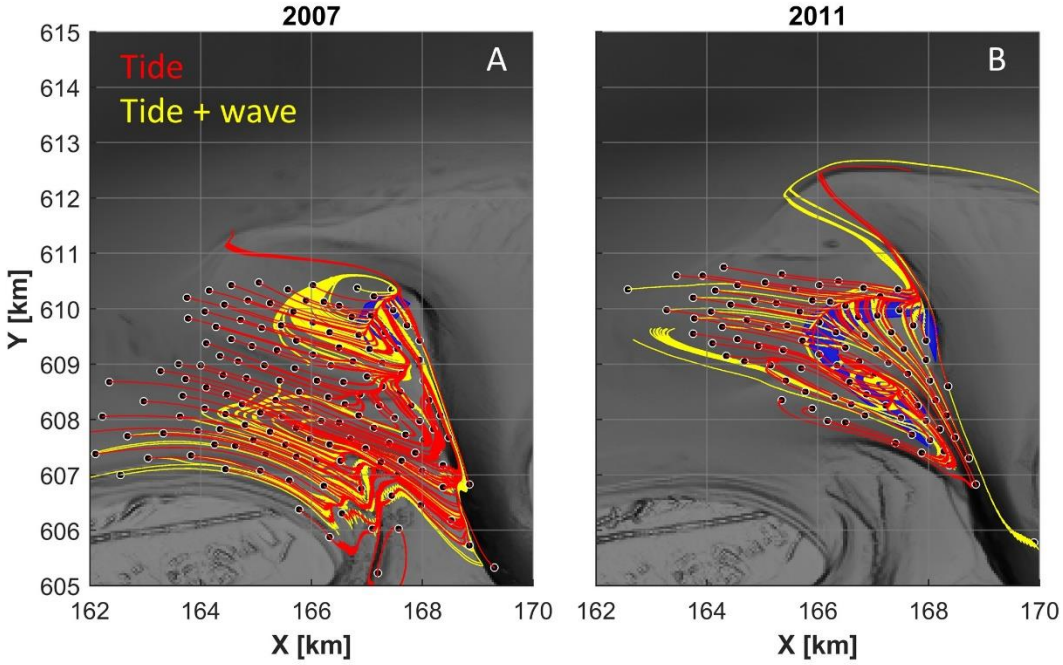

Figure 6.3 - The particle trajectories passing through a the outer edge of an ebb-shield (blue) during the growth phase for the tide only (red) and the coupled tide and wave simulation (yellow). Left (A): the particle trajectories passing through the accreting outer edge of the 1st ebb-shield during its growth phase in 2007. The polygon is defined as the area of sedimentation on the outer edge of the ebb-shield when comparing the 2006 and 2007 bathymetries. Right (B): the particle trajectories passing through the accreting outer edge of the 2nd ebb-shield during its growth phase in 2011. The polygon is defined as the area of sedimentation on the outer edge of the ebb-shield when comparing the 2010 and 2011 bathymetries.

For younger ebb-shields (2006 – 2008), sediment for growth is supplied from a large area including not only the ebb-chute but also the area offshore of Terschelling (Figure 6.3A). More developed ebb-shields are largely fed by sediment originating from the ebb-chute and the bordering west bank of the main ebb channel (Figure 6.3B), which are in turn fed by the Borndiep. Although the transport pathways do not indicate what volumes are transported, the difference in catchment area does correlate with the findings shown in section 4.3.2, where sedimentation volumes far exceed erosion volumes within the ebb-shield for young and small ebb-shields, while they are roughly equal for more developed ebb-shields. This could be coupled to the ebb-shield becoming increasingly ebb-dominant in time. A younger smaller

ebb-shield is subject to a more mixed environment, where both tides and waves play an important role. As the ebb-shield grows it modifies the surrounding flow field, thereby reinforcing its own ebb-dominance. Changes in the surrounding morphology may also play a role. However, the general trend does match an increasing ebb-dominance.

Ebb-shield rotation

Rotation of the ebb-shields is driven by a combination of shore-parallel tidal currents and waves. To illustrate this, a polygon surrounding the area of sedimentation in the main channel is selected based on the sedimentation-erosion patterns for subsequent bathymetries. Sedimentation in the main channel at the eastern border of the ebb-shield is a direct consequence of the rotation of the ebb-shields, which makes this a suitable polygon to isolate the behaviour of particles involved in this rotation. As can be seen in Figure 6.4, particle trajectories for the tide-only simulation converge along the outer edge of the ebb-shield, suggesting that shore-parallel tidal currents drive transport mainly along the outer edge of the second ebb-shield. In the coupled simulation, the particle trajectories pass across the surface of the ebb-shield following distinct paths towards the area of sedimentation in the channel, which are almost perpendicular to the tidal pathways. This difference between the tide-only and the coupled simulation suggests that waves play an important role in driving sediment across the surface of the ebb-shield. This is supported by the wave-breaking induced transports for the higher wave conditions (4, 5 and 6) observed on the right flank of the ebb-shield in model results. The fact that waves drive transport across the surface of the ebb-shield suggests that they are important for the rotation of the ebb-shield. Shore-parallel tidal currents responsible for transport along the outer edge of the ebb-shield are of secondary importance. During rotation, the ebb-shield can continue to grow through ebb-driven transports.

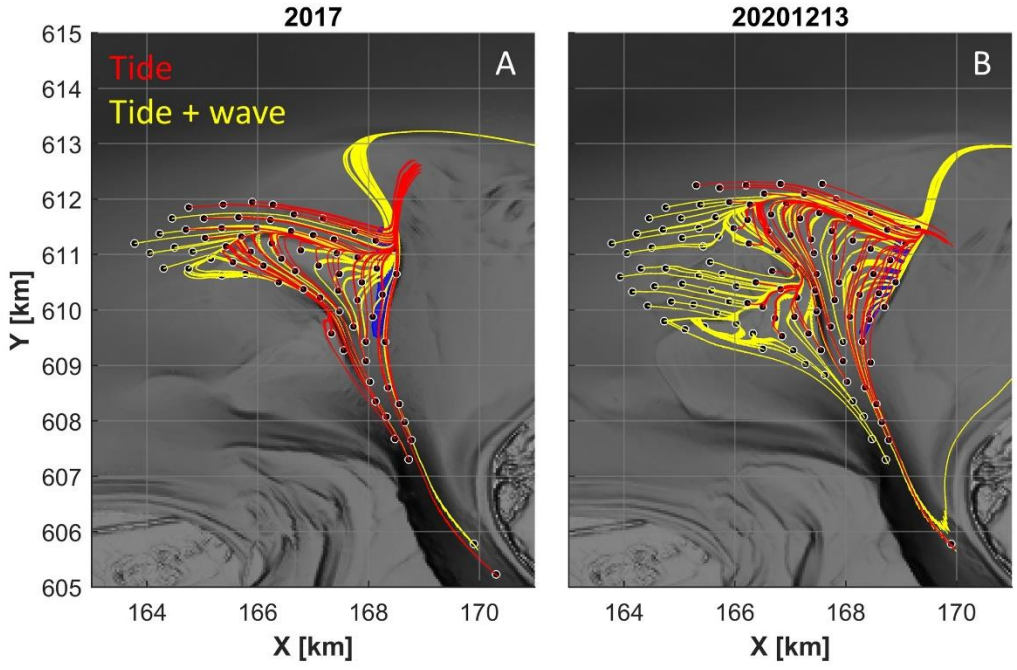

Figure 6.4 – Rotation of the ebb-shields results in sedimentation in the main channel (polygon in blue) and is mainly wave-driven. Particle trajectories passing through the sedimentation polygon of the 2nd ebb-shield for the tide-only simulation (red) and the coupled tide-wave simulation (yellow) are shown for the 2017 bathymetry (A) and the 13/12/2020 nourishment survey embedded in the 2020 bathymetry (B).

Transition from ebb-shield growth to rotation

In progressing from a growth phase to a rotary phase, the ebb-shield transitions from a tide-dominated process to one where waves also play an important role. The cause for the increased importance of waves is twofold.

First is the depth of the ebb-shield. In 2011, the ebb-shield is deep, so the majority of waves do not break here, while in 2017 the ebb-shield is shallower, and waves do break. The difference in depth of the second ebb-shield between the two years is confirmed by the hypsometry shown in Figure 4.14. The depth of the ebb-shield is key for the occurrence of wave breaking and thus for wave breaking induced transports (Battjes & Janssen, 1978).

Secondly, wave sheltering by the shallow ebb-delta front can influence local wave dominance at the ebb-shields. In the report by Elias et al. (2020), analysis of the wave measurements shows that waves exceeding 2m wave height at open sea break on the ebb-delta front, resulting in important wave reduction. In 2011, the ebb-delta front is shallower and extends further to the west which could be a reason to expect more wave sheltering than in 2017. Because the model simulates year-averaged conditions, wave sheltering effects that occur under storm conditions are not fully represented by the model.

6.2 Post-nourishment behaviour

This section includes model results after the placement of the nourishment, starting with the general transport patterns and then zooming in on the nourishment.

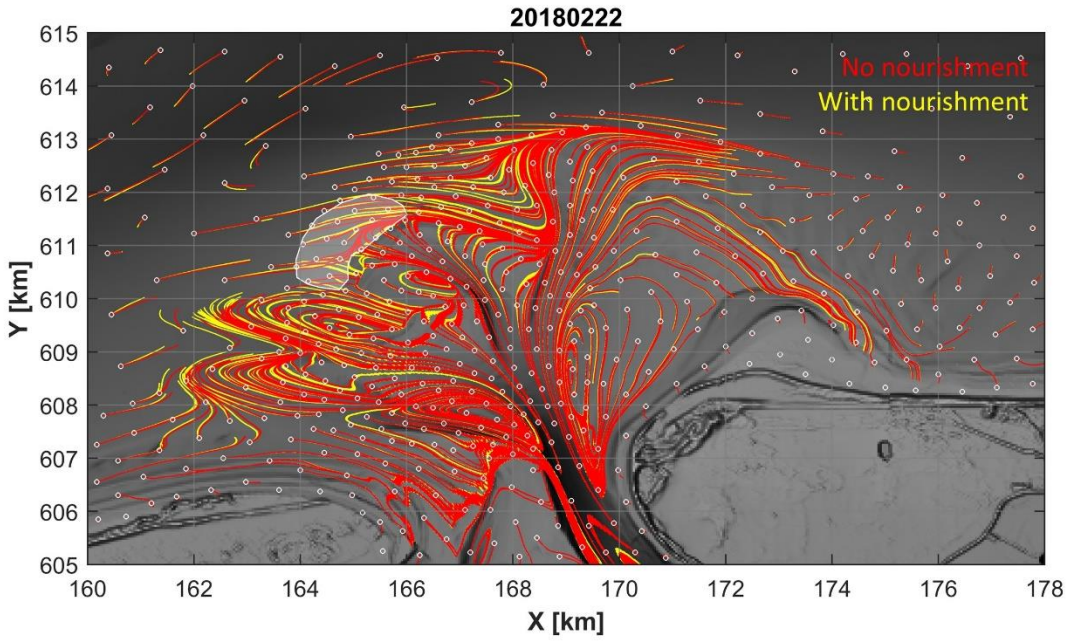

Figure 6.5 – Transport pathways for a coupled tide-wave simulation for the 22/02/2018 bathymetry with the nourishment superimposed (yellow) and without the nourishment (red). The nourishment is highlighted in white.

6.2.1 Isolating the effect of the nourishment

To isolate the direct effect of the nourishment, a model run is performed using the 22/02/2018 bathymetry with and without the nourishment (Figure 6.5). This is done by superimposing the nourishment from the 28/02/2019 bathymetry (directly following the completion of the nourishment) on the 22/02/2018 bathymetry (directly prior to the construction of the nourishment. The effects of the nourishment on the surrounding transport patterns are

minimal, with only a minor shift of the pathways with respect to the no-nourishment simulation. The general patterns outside the nourishment polygon do not change. In the nourishment polygon, the line dividing particles which pass south-eastward into the ebb-chute rather than along the outer edge of the ebb-shield shifts to the north when the nourishment is added. As the changes in transport patterns surrounding the nourishment are minimal, pathways starting in the nourishment polygon will be used to illustrate the changes in transport patterns before and after the placement of the nourishment in section 6.2.3.

6.2.2 Transport patterns at ebb-tidal delta scale

The following section discusses the results for behaviour at the ebb-tidal delta scale after the placement of the pilot nourishment. Again, model results for a coupled tide-wave run are visualised using SedTRAILS.

By 2020, transport pathways along the northern outer edge the third ebb-shield have also connected to the major pathway along the ebb-delta front via the ebb-chute and outer edge of the second ebb-shield. Both ebb-shields also continue to rotate clockwise, bringing sediment from the ebb-shield area further east. By 2020, the third ebb-chute takes over as main ebb-channel, funnelling sediment westward into the open sea. Any material south of the Westgat is still transported into the tidal basin. On the Bornrif, sediment from the Bornrif Bankje continues to be transported to the Ameland coast. On the southern tip of the Bornrif, in the area where circulation occurs for all the bathymetries, a shield-like feature has started to form. This is the same location where the Bornrif Strandhaak forms, later attaching to the coastline in 1985 (Elias et al., 2019).

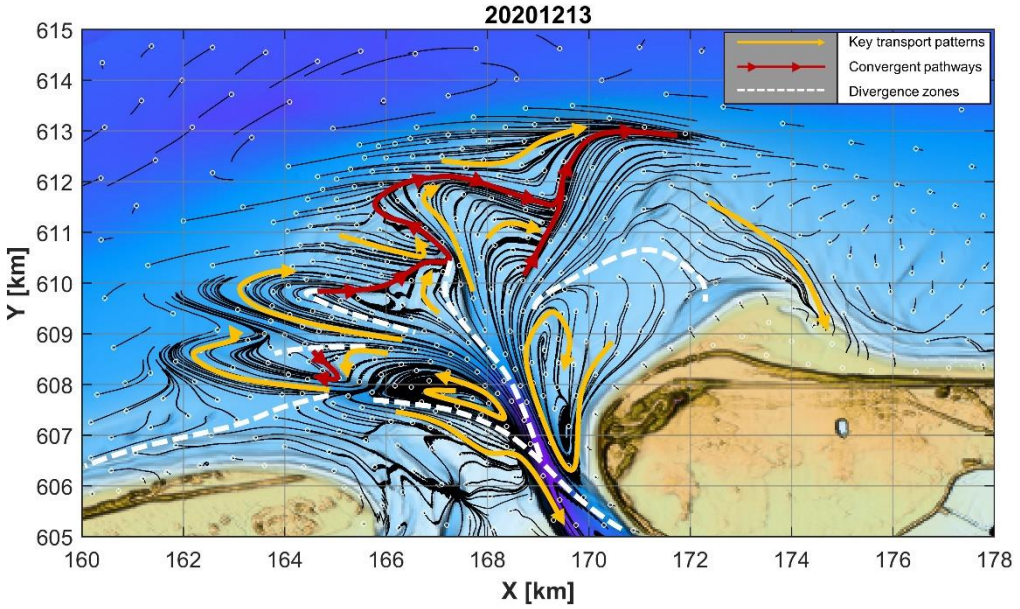

Figure 6.6 – Schematised SedTRAILS results for a coupled tide and wave simulation performed using the 13/12/2020 bathymetry which includes the pilot nourishment. Source locations are indicated with a white circle and particle trajectories with a white line. Key transport patterns are illustrated with the yellow arrows, trajectories where the particles converge are shown in red and zones where the particle behaviour diverges are shown with dashed white lines.

By the end of 2020, the nourishment has been interacting with the ebb-tidal delta for almost 2 years. Even so, general transport patterns remain very similar to 2017, and any changes appear to be part of the natural evolution of the ebb-tidal delta rather than an effect of the nourishment (compare Figure 6.2C to Figure 6.6).

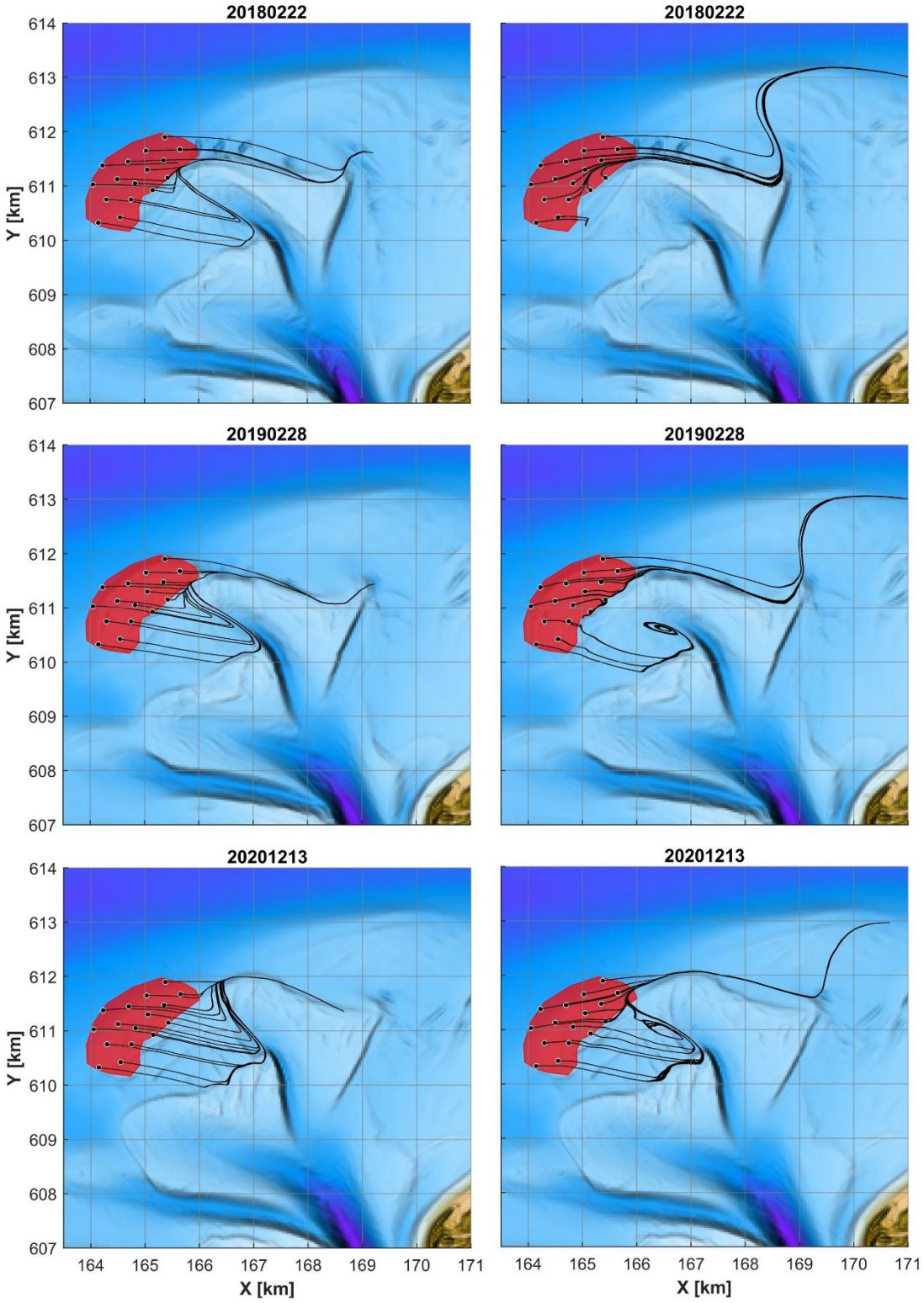

Figure 6.7 – The pathways of the nourished sediment originating in the nourishment polygon (red). SedTRAILS results for a tide-only simulation are shown on the left and for a coupled tide-wave simulation on the right. Source points are indicated with white circles and particle trajectories in black. 22/02/2018 is directly prior to the construction of the nourishment, 28/02/2019 directly after completion of the nourishment, and 13/12/2020 almost 2 years after the completion of the nourishment.

6.2.3 Transport pathways from the nourishment

As Figure 6.5 shows that the effect of the nourishment on surrounding transport patterns is limited, the change in transport behaviour can be described by isolating particle trajectories originating in the nourishment polygon before and after the placement of the nourishment. The nourishment is placed on the outer edge of the second ebb-shield. Effects on the tidal response of the nourishment are limited, but the importance of waves does change in response to the nourishment (Figure 6.7).

Based on the particle trajectories in Figure 6.7, two main pathways can be identified. The first pathway passes along the outer edge of the second ebb-shield and is driven mainly by waves. This can be seen because the coupled tide-wave simulations force more particles along the outer edge than the tide-only simulation. The second pathway is tide-dominated and passes further south. Particles from the nourishment are transported towards the east and into the ebb-chute by shore-parallel tidal currents. In the ebb-chute, ebb currents transport the sediment to the outer edge of the ebb-shield where this second pathway re-joins the first pathway.

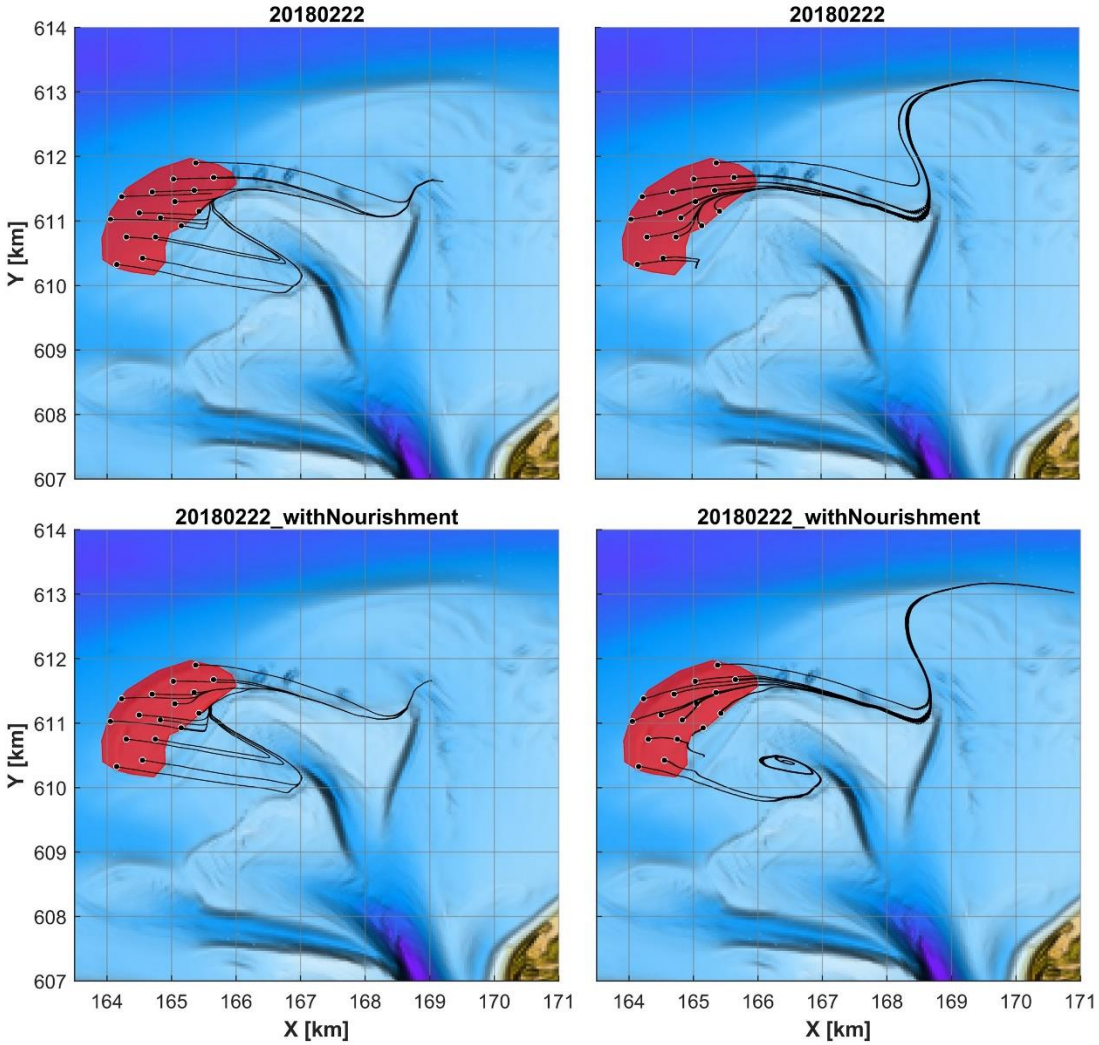

Figure 6.8 – A comparison of the pathways followed by sediment originating in the nourishment polygon (red) for the 22/02/2018 bathymetry with (bottom) and without (top) the nourishment. The tide-only result is shown on the left and the couple tide-wave result on the right.

Before and after the placement of the nourishment, the tidal response is unchanged. In each of the tide-only transport pathways (left) in Figure 6.7, the trajectories follow the same pattern, moving towards the east until they reach either the ebb-chute or the outer edge of the ebb-shield. This means that the tidal response is not affected by the nourishment.

Waves initially force more pathways to pass along the outer edge of the ebb-shield with respect to the tide-only simulation. By 2020, the coupled transport pathways closely resemble the tide-only transport pathways, suggesting that wave-driven transport has become less important. As sediment is transported away from the nourishment, the nourishment becomes deeper and more in equilibrium with its surroundings, and tidal transports take over from wave-driven transports. This corresponds to the first wave-dominated response and the second tide-dominated response described in section 5.2.1.

During the period of study, not only is the nourishment adapting to its surroundings, but the ebb-shield which it borders also continues to rotate clockwise. To isolate the effects of the rotation of the ebb-shield from those of the nourishment a model run has been performed using the 22/02/2018 bathymetry with the nourishment superimposed (Figure 6.8). The SedTRAILS results show the same trends before and after the placement of the nourishment described above, with the southernmost particles following the southern path into the ebb-chutes after the placement of the nourishment. This means that the changing transport patterns cannot be solely attributed to the rotating ebb-shield but are also due in part to the construction of the nourishment.

6.3 Evolution of ebb-tidal delta dynamics from 2005 to 2020

The changing transport patterns and connections between 2005 and 2020 (Figure 6.9) reflect the morphodynamic complexity of the ebb-tidal delta. Zones of different behaviour have shifted their boundaries and the connections between them have changed.

Where in 2005, area 1 and 3 were poorly connected in terms of transport pathways, in 2020 they are well-connected by major transport pathways along the ebb-shields. Sediment travels through the ebb-chute and then along the outer edge of the ebb-shield to the next ebb-shield or the major transport pathway along the ebb-delta front. Area 1 (where the ebb-shields form) has grown to cover the entire western half of the ebb-tidal delta at the cost of the Akkepollegat and part of the Bornrif. This has forced the switch of the main ebb-channel from its long stable position along the western edge of the Bornrif to the more dynamic ebb-shield area. Area 2, the area feeding the tidal basin, has expanded northward with a net transport of all particles south of the Westgat into the tidal basin. This occurs either via the Boschplaat or via the Borndiep.

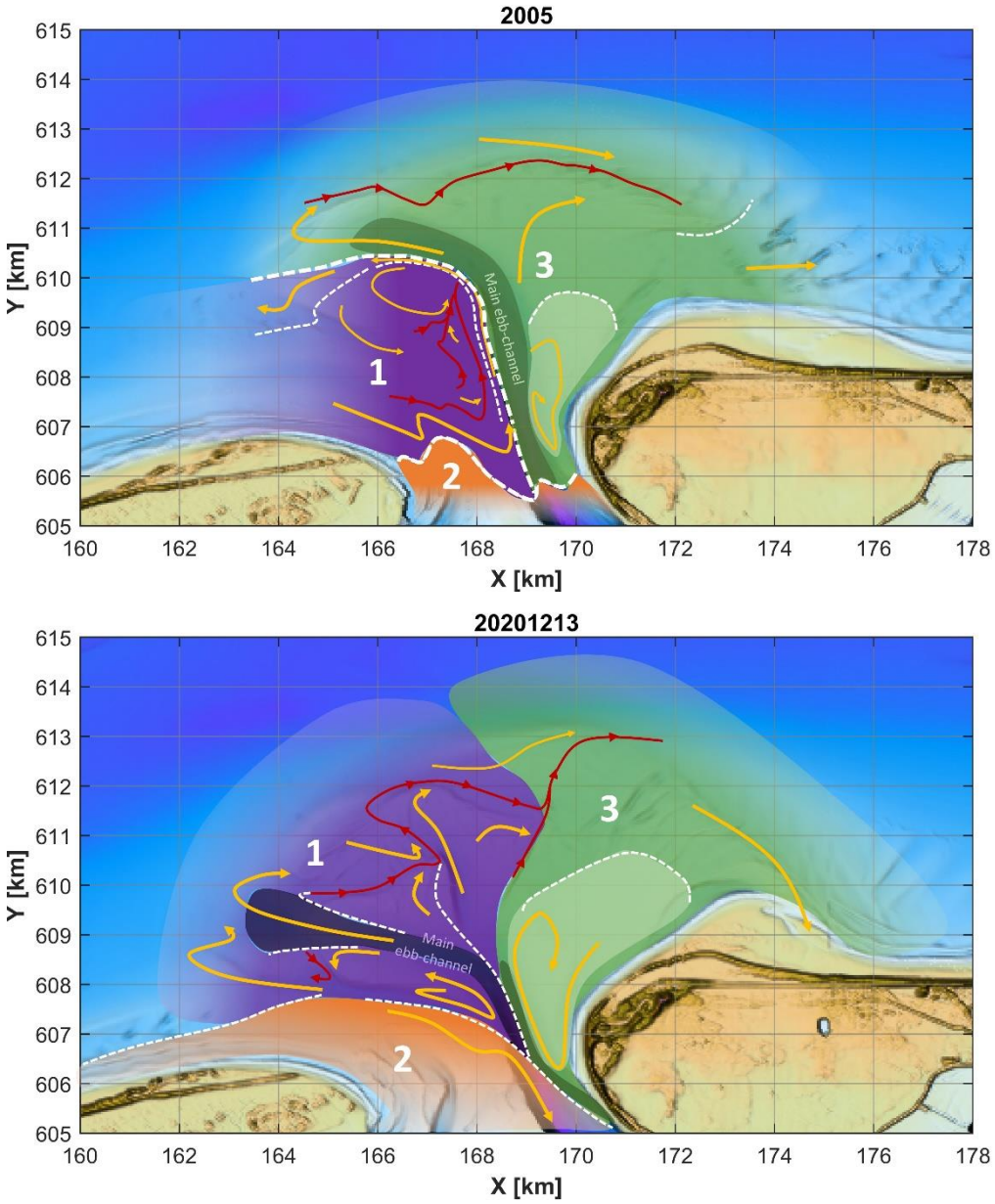

Figure 6.9 – Evolution of the transport patterns on the Ameland ebb-tidal delta between 2005 (top) and 2020 (bottom). The areas are defined in the same way as in Figure 6.1 as: (1) the Kofmansplaat where the ebb-shields form, (2) the Boschgat and basin-side of the Borndiep, and (3) the Akkepollegat and Bornrif. Key transport patterns are illustrated with the yellow arrows, trajectories where the particles converge are shown in red and zones where the particle behaviour diverges are shown with dashed white lines.

7 Synthesis and discussion

In this chapter the combined understanding of the ebb-tidal delta system during the period of study is synthesised, followed by a discussion of the further implications for ebb-tidal delta dynamics.

7.1 Conceptual models

The combined understanding of the ebb-tidal delta system between 2005 and 2020 from the data analysis and modelling studies is synthesised in a series of conceptual models which illustrate the residual transports and morphological response on the Ameland ebb-tidal delta at different stages in the sediment bypassing cycle (Figure 7.1). This includes behaviour both before and after the placement of the nourishment.

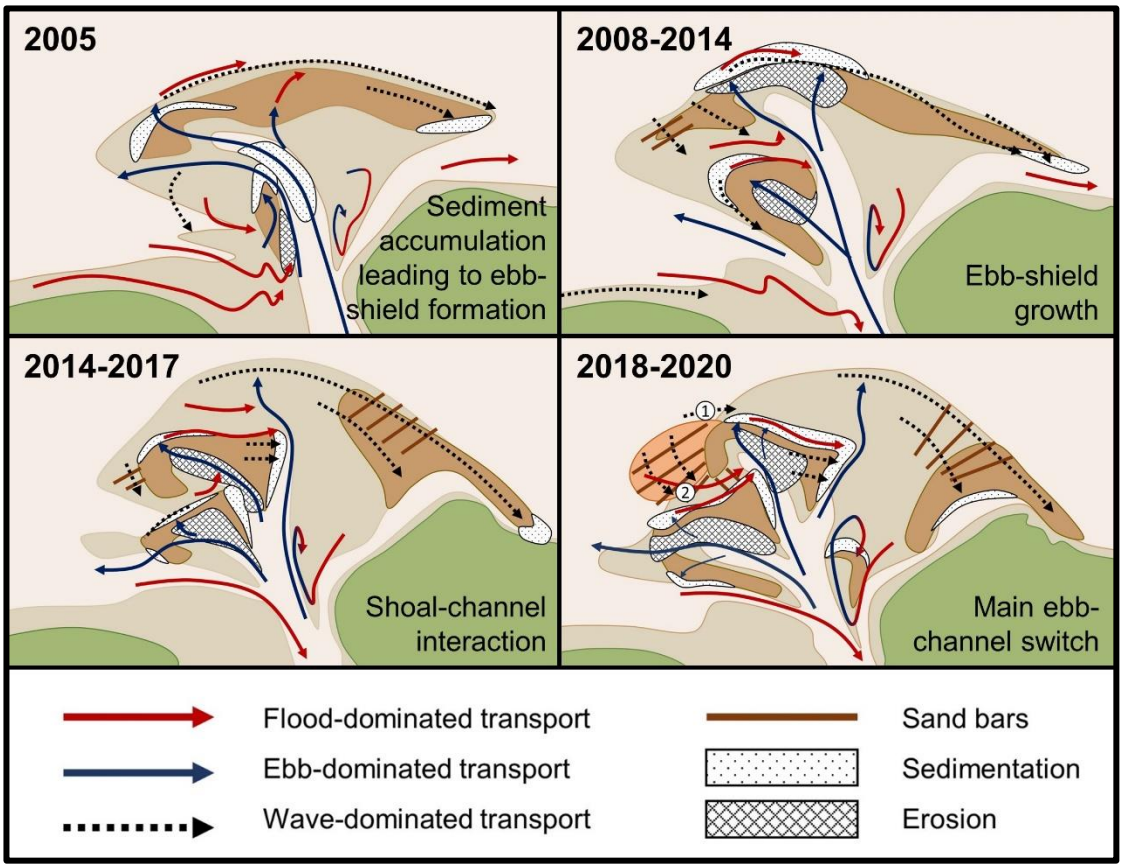

Figure 7.1 – The different stages of the sediment bypassing described through the series of conceptual modes: (1) sediment accumulation leading to ebb-shield formation, (2) ebb-shield growth, (3) shoal channel interaction and (4) main ebb-channel switch.

7.1.1 Natural sediment bypassing

The phases of the sediment bypassing cycle described in the following section are analogous to the description in Elias et al. (2020). More detail, especially on the role of the ebb-shields and the interactions between different features is included, as well as a clearer distinction between the wave and tide-driven processes that link the evolving morphologies in consecutive bathymetries.

Throughout the different phases discussed below, there is always a major transport pathway along the outer edge of the ebb-tidal delta which is driven mainly by waves and in part by shore-parallel tidal currents. This steadily drives sediment towards the Ameland coast until the shoal attachment in 2017. Supply to this major transport pathway along the ebb-delta front is initially dominated by transport from the Akkepollegat and later by sediment coming from the ebb-shields on the Kofmansplaat. This sequence is described in four distinct stages which are ebb-shield formation, ebb-shield growth, and shoal-channel interaction, and main ebb-channel switch.

Ebb-shield formation (ca. 2005)

The first conceptual model describes the behaviour on the ebb-tidal delta around 2005, prior to the formation of the first ebb-shield (Figure 7.2). Sediment coming in from the west was trapped on the Kofmansplaat where it circulated. The Kofmansplaat was disconnected from the rest of the ebb-tidal delta in terms of transport pathways. Through the Akkepollegat and across parts of the Bornrif ebb flows brought sediment seaward to the ebb-delta front.

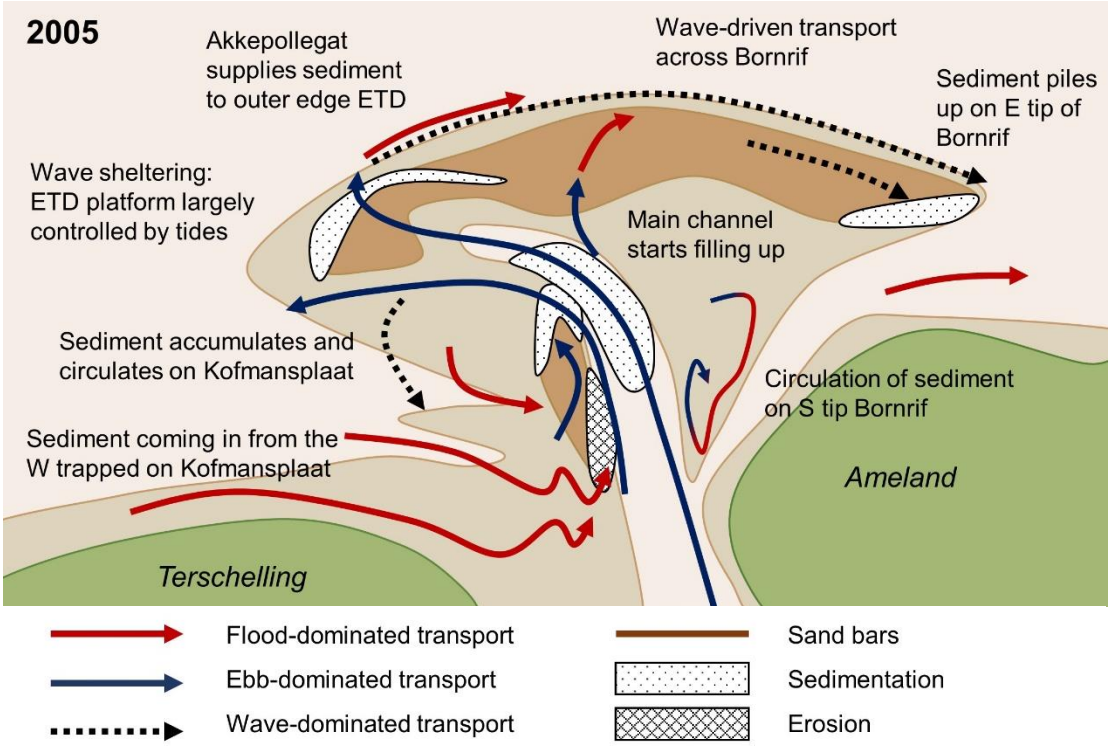

Figure 7.2 - Conceptual model illustrating sediment bypassing behaviour on the Ameland ebb-tidal delta around 2005, shortly before the formation of the first ebb-shields, including residual transports and areas of sedimentation and erosion.

Prior to 2005, sediment had accumulated on the western bank of the Akkepollegat as an elongate bar (Elias, Pearson, et al., 2020). Sediment was delivered from the updrift Terschelling coast and the western margin of the ebb-tidal delta, with any sediment passing north of the tip of the island of Terschelling being redirected onto the Kofmansplaat (area (1) in Figure 6.1). All the sediment present on the Kofmansplaat circulated here, with no net transport pathways connecting to the area east of the Kofmansplaat. This circulation was driven by both tides and waves, with waves mainly contributing on the western margin of the ebb-tidal delta. The combination of accumulating and trapped circulating sediment formed a potential site for the morphodynamic instabilities which mark the start of ebb-shield development. The results do not show what the trigger for these instabilities was.

In 2005, the Akkepollegat dominated the ebb-tidal delta platform, extending far onto the ebb-tidal delta and thereby determining the behaviour of the ebb-tidal delta platform. Ebb-dominated transports fed the northwest tip of the ebb-delta front (Kofmansbult), maintaining a shallower area along the outer edge of the ebb-delta front which sheltered the central part of the ebb-tidal delta from waves. Wave-driven transport across the outer edge of the Bornrif brought sediment to the eastern tip of the Bornrif, extending it towards the southeast. The eastern flood channel separated the sediment piling up from the Ameland coast.

Ebb-shield growth (ca. 2009-2014)

This conceptual model describes the behaviour of the ebb-tidal delta between 2009 and 2014 (Figure 7.3), when the ebb-shields have already formed and are in their growing phase. Tides dominated the central part of the ebb-tidal delta, expanding the existing ebb-shields and bringing sediment to the ebb-delta front through the main ebb channel. Waves were dominant mainly on ebb-delta front, driving transport across the Bornrif.

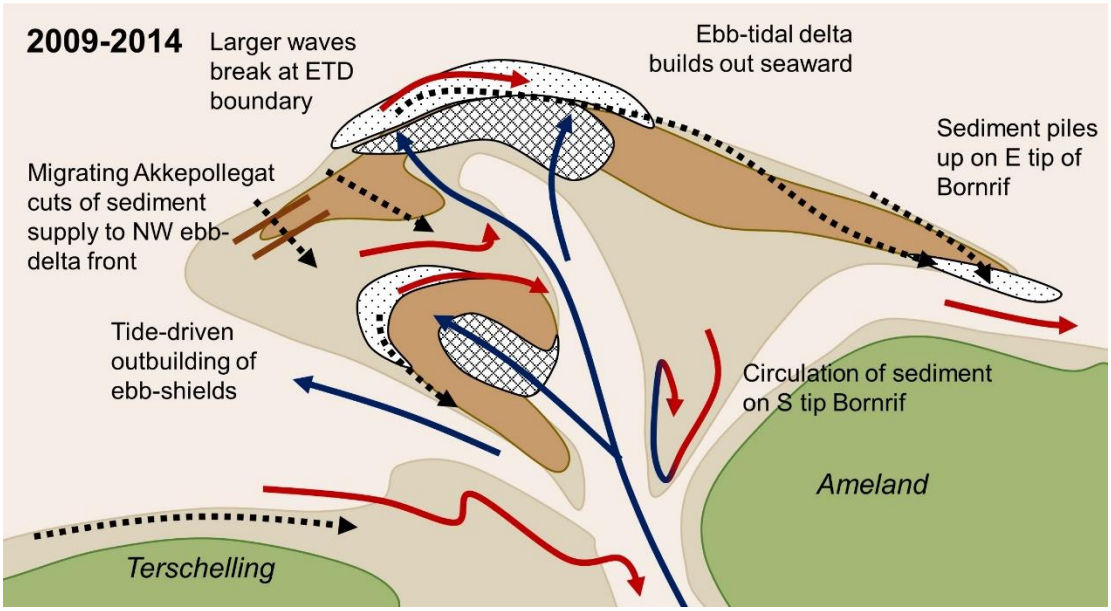

Figure 7.3 - Conceptual model illustrating sediment bypassing behaviour during the period of significant ebb-shield growth between 2009 and 2014, showing residual transports and areas of sedimentation and erosion.

During the initial growth of the ebb-shields, they were sheltered from larger waves by the shallower outer edge of the ebb-tidal delta. With waves exceeding 2m wave height breaking on the ebb-delta front (Elias, Pearson, et al., 2020), tide-driven outbuilding of the ebb-shields could occur relatively undisturbed. This resulted in fast growth of roughly symmetric ebb-shields. Sediment reaching the northern edge of the ebb-shield was transported east by flood-dominated shore-parallel tidal currents until reaching the Akkepollegat, where ebb-dominant tidal inlet currents brought sediment to the ebb-delta front. Sediment reaching the southern edge of the ebb-shield rim was transported towards the Westgat by a combination of waves and flood currents.

Simultaneously, the main ebb channel (Akkepollegat) migrated from a northwest to a northward orientation, shifting the destination of the sediment-laden ebb-currents. In its northward orientation, the Akkepollegat was aligned with the Borndiep, which is the hydraulically most efficient configuration. This allowed sediment to be transport beyond the existing ebb-delta front, leading to seaward outbuilding of the central part of the ebb-tidal delta. The migration of the Akkepollegat also resulted in cutting off the sediment supply to the Kofmansbult. While sediment was supplied by ebb flows through the Akkepollegat (until

2011), the Kofmansbult appeared relatively stable in a mixed tide- and wave-environment. With the departure of Akkepollegat, the area became wave-dominated. Sediment was eroded and transported landward and large sandbars formed.

The preferential north-westerly orientation of the main ebb-channel is due to interactions between the shore-parallel and inlet tidal currents. The shore-parallel tidal currents immediately updrift of the inlet are reinforced by the inlet tidal currents, while the shore-parallel tidal currents downdrift of the inlet are counteracted (see section 2.1.2 for a more detailed explanation) (Sha, 1989). In 2011, eastward migration of the Akkepollegat occurred due to the growth of the ebb-shields, which constricted the ebb-channel.

Where the central part of the ebb-tidal delta platform was dominated by tides, along the outer edge waves played a more important role. Waves broke on the shallower outer edge of the Bornrif and drove transport across the outer edge of the ebb-tidal delta, bringing sediment across the Bornrif towards Ameland where it piled up on the eastern tip of the Bornrif. The shoal that emerged is known as the Bornrif Bankje and separated from Ameland by a flood channel.

Shoal-channel interactions (ca. 2014-2017)
This conceptual model describes the behaviour between 2014 and 2017 (Figure 7.4), when the ebb-shields rotated and constricted the Akkepollegat. Wave action continued to erode the ebb-delta front, reducing the wave sheltering effects for features located further landward. Simultaneously, continued migration of the Akkepollegat led to its abandonment, with the third ebb-chute becoming the new dominant pathway for ebb flow.

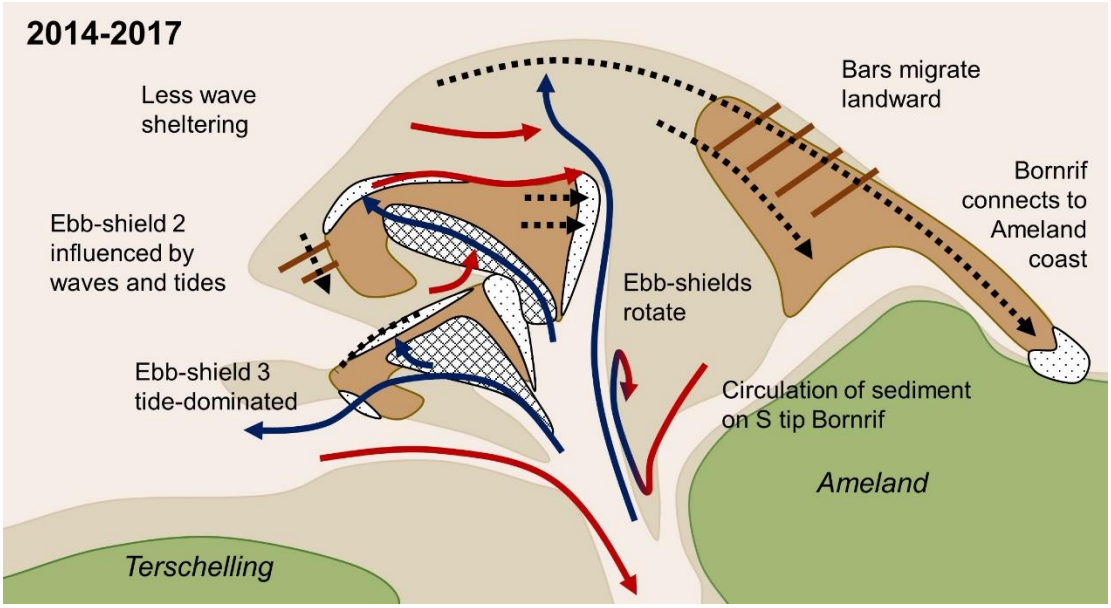

Figure 7.4 - Conceptual model illustrating sediment bypassing behaviour during a period characterized by significant channel-shoal interactions between 2014 and 2017, showing residual transports and areas of sedimentation.

Reduced wave sheltering left ebb-shield 2 (the outer ebb-shield) more exposed, and where it was previously tide-dominated, waves began to play a more important role. The development of the 3rd ebb-shield as new main ebb channel left ebb-shield 2 tide-starved, with only limited tide-driven outbuilding. Flows through the 2nd ebb-shield decreased in magnitude while those through the 3rd ebb-shield increased. This is also because the second ebb-shield is further away from the inlet. A combination of shore-parallel tidal currents along the outer edge of the

ebb-shield and wave-driven transports across the surface of the ebb-shield caused a net eastward sediment transport which resulted in the clockwise rotation of the ebb-shield and its asymmetric shape. Rotation of the ebb-shield constrained the Akkepollegat and resulted in its migration. Sediment reaching the Akkepollegat along the outer edge of the ebb-shield was transported through the Akkepollegat to the ebb-delta front. The sand bars to the west of the 2nd ebb-shield continued to migrate landward under the influence of waves.

The 3rd ebb-shield remained partly sheltered from waves by the 2nd ebb-shield and was largely tide-dominated. Ebb flows through the ebb-chute originating in the Borndiep resulted in rapid outbuilding of the ebb-shield by roughly 260m/year. Due to wave sheltering of the eastern part of the 3rd ebb-shield by the 2nd ebb-shield, the 3rd ebb-shield rotated clockwise less than the second ebb-shield. Sediment reaching the ebb-shield edge further to the west was transported west by waves to join the ebb-dominated transports exiting the tip of the ebb-shield towards open sea. At this stage, the 3rd ebb-chute was well-connected to the Borndiep by transport due to the reversing tidal currents. This resulted in a net accumulation of sediment on the ebb-shield. However, there are limited transport pathways connecting the ebb-shield to the rest of the ebb-tidal delta.

As the Akkepollegat migrated eastward, it became increasingly hydraulically inefficient, causing tidal flows to decrease. The reduced dominance of the Akkepollegat meant that there was less sediment supply to counter the wave-induced erosion on the outer ebb-tidal delta. Eroded sediment was deposited further landward by waves. On the eastern side of the Bornrif platform, wave action led to the formation of large bar complexes which migrated towards Ameland. At this stage, the sediment piling up on the eastern tip as the Bornrif Bankje traversed the eastern flood channel and attached to the Ameland coastline just downdrift of the Strandhaak.

7.1.2 Sediment bypassing under the influence of a nourishment (ca. 2018-2020)

The final conceptual model includes the nourishment and illustrates the morphological behaviour in its vicinity between the start of 2018 and the end of 2020 (Figure 7.5). The general setting was similar to the last pre-nourishment model (Figure 7.4), with limited wave sheltering at the ebb-delta front and increased dominance of the 3rd ebb-chute as main ebb channel. Under these conditions, the 2nd ebb-shield continued to rotate under the influence of waves and shore-parallel tidal currents. The continued constriction of the Akkepollegat and its decreasing hydraulic efficiency had led to a channel switch. The 3rd ebb-shield had established itself as the new main ebb-channel, remaining tide-dominated and continuing to build out. This meant that the main ebb-channel switch introduced in section 2.2.1, had taken place. The bars on Bornrif continued to migrate landward. This is probably the natural continuation of the sediment bypassing cycle of which the earlier phases are described in section 7.1.1.

A new development was the emerging shoal on the southern tip of the Bornrif. Throughout the earlier stages of sediment bypassing described, sediment had been circulating in this area. In 2016, a channel-parallel bar formed and developed into a shield-like feature in 2020.

The influence of the nourishment was limited, with little to no effect on sediment bypassing at ebb-tidal delta scale or on local transport pathways at a smaller scale. Sediment originating from the nourishment re-joined the major transport pathway passing along the outer edge of the 2nd ebb-shield and then the ebb-tidal delta perimeter. In the short-term this happened directly via the outer edge of the ebb-shield (first response) and in the long-term this happened via the 2nd ebb-chute (second response). This reinforced transport through the ebb-chute but did not significantly alter the existing pathways, which move with the ebb-shield.

The nourishment was positioned in an area which was sheltered from the inlet tidal currents, so waves and open sea tides formed the dominant transport mechanisms. A new feature constructed over a short period of time (March 2018 and February 2019), the nourishment was initially out of equilibrium with its environment and responded accordingly. The first response (see (1) in Figure 7.5), was a smoothing of the nourishment in the eastward direction along the outer edge of ebb-shield 2, also visible in the bathymetries in Figure 5.1. Wave-driven transports and shore-parallel tidal currents smoothened the nourishment in the eastward direction, allowing it to find a new equilibrium within the wave-dominated environment. This eastward transport caused a short period of increased outbuilding of ebb-shield 2. Waves also drove the sandbars on the nourishment landward and lowered the outer edge of the nourishment, so that the outer slopes approached their pre-construction angles.

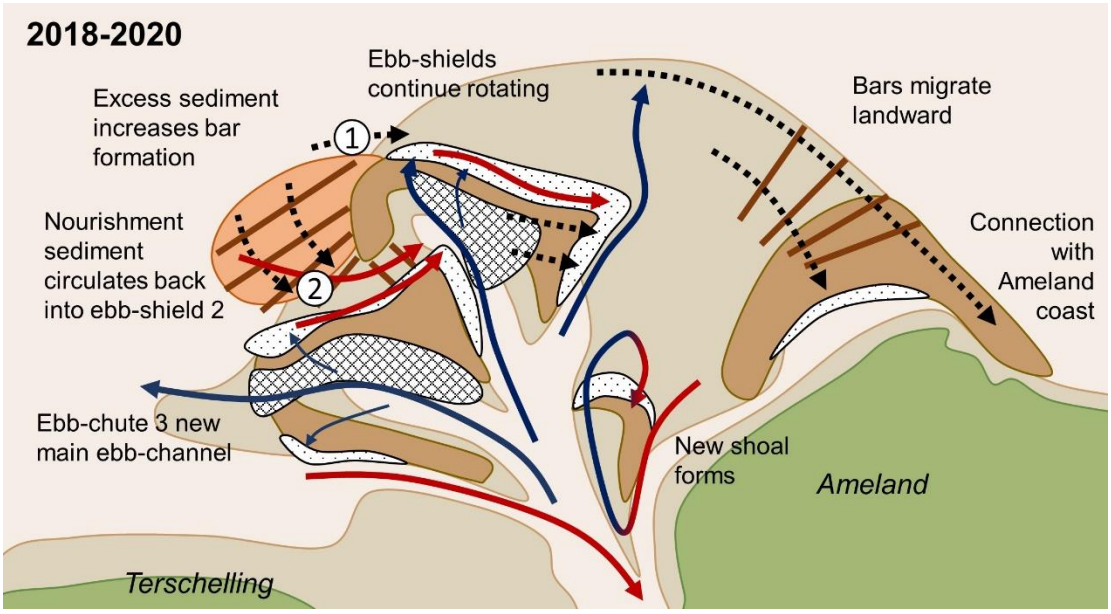

Figure 7.5 - Conceptual model illustrating sediment bypassing behaviour after the construction of the nourishment, from 2018 until 2020. The diagram includes residual transports (arrows) and areas of sedimentation and erosion (shaded areas). The first and second response are labelled with 1 and 2.

Simultaneously, a second response mechanism was active (see (2) in Figure 7.5). When the nourishment was closer to equilibrium with its surroundings, the role of waves was less important and shore-parallel tidal currents dominated. Sediment was transported east into the 2nd ebb-chute, both continuously and through the migration of sand bars observed in Figure 5.1. Sediment then passed through the chute back to the outer edge of ebb-shield. Of secondary importance were the sand bars which formed on the nourishment and migrated landward under the influence of waves.

7.2 Implications for the ebb-tidal delta dynamics

Discussion of the implications of the research results for ebb-tidal delta dynamics is split into a section on the natural dynamics and a section on the pilot nourishment.

7.2.1 Natural dynamics

The conceptual models in the previous section focus specifically on sediment bypassing processes between 2005 and 2020. The following section relates the lessons learnt from this period to the broader understanding of sediment bypassing processes at Ameland inlet.

Since 1926, the Ameland ebb-tidal delta has been in a regime described as main ebb-channel switching (Elias et al., 2019), where the Akkepollegat and Westgat remain roughly in place but alternately grow and decay. Until 2016, the Akkepollegat acted as the main ebb channel based on the depth approach adopted in section 4.2.3. Constriction by the rotating ebb-shields meant that the Akkepollegat became increasingly hydraulically inefficient. Following a period in which there was no clear main ebb-channel, the depth approach defines the 3rd ebb-chute as the main ebb-channel from 2019 onwards, as is also predicted by Elias et al. (2019, 2020). This period of transition suggests that the main ebb-channel switch is gradual and cannot be attributed to a single event such as a storm. With this switch, the orientation of the main channel becomes more favourable with respect to inlet and shore-parallel tidal current interactions (Sha, 1989).

The main ebb-channel migration leading up to the channel switch is a consequence of the growth and migration of the ebb-shields on the Kofmansplaat. During the growth of the ebb-shields (2006 – 2011), the Akkepollegat migrated slowly with a clockwise rotation of the distal part of the channel of roughly 3.5°/year. This accelerated when the ebb-shields started rotating to roughly 9.9°/year (2011-2017). Significant rotation of the ebb-shields is linked to the transition from a tide-dominated environment to a mixed environment.

Although shore-parallel tidal currents contribute to rotation of the ebb-shields, waves are the primary driver. This is a combination of transport driven by wave breaking when the ebb-shields are shallow enough and a decrease in wave sheltering as the northwest ebb-delta front erodes. Erosion of the NW ebb-delta front is part of a positive feedback loop. The migration of Akkepollegat reduces sediment supply to the NW ebb-delta front, allowing for its erosion by waves, thus reducing wave sheltering of the ebb-shields landward of the ebb-delta front and accelerating their wave-driven rotation which in turn further constricts the Akkepollegat. Over time, the Akkepollegat becomes increasingly hydraulically inefficient, causing tidal flow velocities to decrease and eventually leading up to a channel switch.

The formation of a new channel (ebb-chute 3) in the westward direction could reverse the continued structural erosion of the Boschplaat which has been observed since 1974 (Elias, Pearson, et al., 2020). Reduced importance of the Westgat cut off the sediment supply to the shoal deposits along the northern margin of the Westgat, resulting in their erosion (1999 – 2005). The deep area that formed between the Kofmansplaat and the Boschplaat (2005 – 2016) meant that waves could propagate far into the inlet, eroding sediment from the Boschplaat (Elias, 2017). The new position of the channel supplies sediment to the western and landward margin of the ebb-tidal delta, which can provide sheltering for the Boschplaat as occurred in the period between 1940 and 1974 (Elias et al., 2019). Reduced wave activity close to the inlet results in a negative gradient in sediment transport from the Terschelling coast into the inlet, which leads to sedimentation on the Boschplaat. There is also a second mechanism which could lead to progradation of the Boschplaat. If new shoals form along the Westgat or 3rd ebb-chute then these may also migrate and attach to the Boschplaat like the Koffiebonenplaat in the 1960s (Elias, 2021).

The erosion or sedimentation of the Boschplaat is highly dependent on supply along the Terschelling coast and sheltering by the Western side of the ebb-tidal delta, as exchange with the ebb-tidal delta seaward of the Westgat or the Borndiep is limited. This is supported by the observed transport pathways in the SedTRAILS results, which include the zone of divergence that persists through the Westgat and the net transport pathways from the Boschplaat area into the Borndiep. Moreover, earlier conclusions show that the ebb-tidal delta can be subdivided into two parts: (1) the area between Terschelling and the Boschgat which exchanges with the Boschgat and the Terschelling side of the tidal basin and is largely flood-dominated, and (2) the Borndiep which exchanges sediment with the part of the ebb-tidal delta seaward of the Westgat and is largely ebb-dominated (Elias, 2017).

Sediment on the ebb-tidal delta platform is eventually delivered to the Ameland coast, a process that occurs both directly in the form of shoal attachments, and indirectly through the migration of large sand bars slightly offshore of the Bornrif platform. Shoal attachments occur with a low frequency, bringing sediment to the Ameland coast in pulses which can lead to outbuilding of the coast in the order of a kilometre (Elias, Pearson, et al., 2020). Following attachment, the shoal plays a role similar to that of a mega nourishment, supplying sediment to the downdrift coast over a longer period of time. The migration of sandbars offshore of the ebb-tidal delta platform is clearly visible in bathymetric data but poorly captured in the model. The volumes delivered to the Ameland coast by these sand bars is likely much smaller but also more continuous than the shoal attachments.

The Ameland ebb-tidal delta is part of a larger sediment-sharing system, which not only includes the barrier islands but also the tidal basin. Based on the SedTRAILS results, the Ameland ebb-tidal delta does not directly contribute to the sediment demand of the tidal basin. There is a clear signal that the Wadden Sea and the Ameland tidal basin are accreting (Elias, 2019; Wang et al., 2018). However, SedTRAILS results suggest that a net export occurs through the Borndiep, a result supported by previous modelling studies (de Fockert, 2008; Laan, 2019; Teske, 2013). This makes it unlikely that the Ameland tidal basin is fed by sediment from the Ameland ebb-tidal delta. Sand import most likely occurs along the Terschelling coast and from the Boschplaat, but less is known about net transport in this area. Another possible contribution to the sediment demand of the tidal basin is sediment that is supplied across the tidal watersheds separating the tidal basins. According to the SedTRAILS results, the Westgat forms the divide between sediment which remains outside the basin to the north and sediment which travels along the Terschelling coast and into the basin to the south (Figure 7.6). An exception occurs during large shoal attachments at the Ameland coast, when large volumes of sediment from the attaching shoal can be transported into the basin as is observed during the attachment of the Bornrif Strandhaak (Elias & Bruens, 2013).

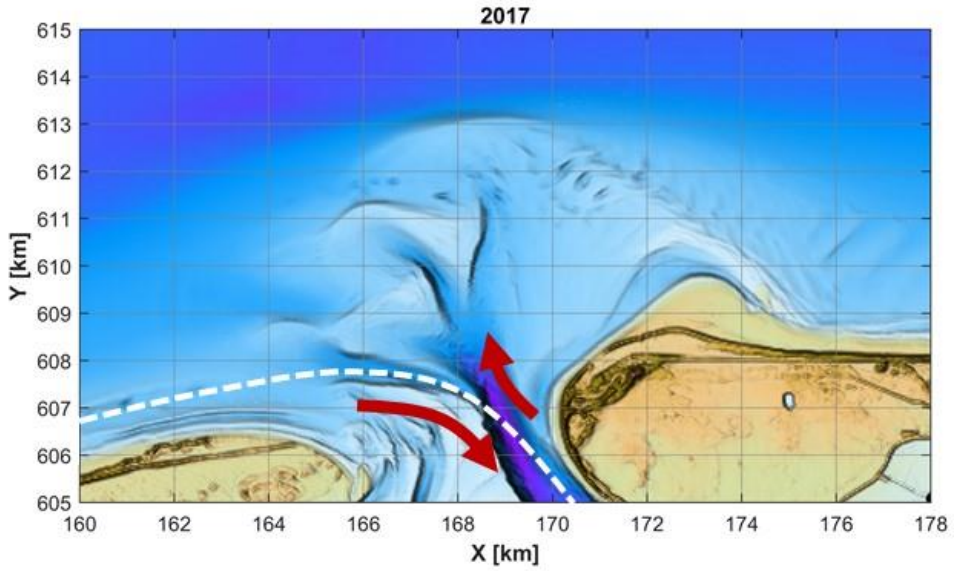

Figure 7.6 - Transport into and out of the Amleand tidal basin from 2011 onwards. The Borndiep shows a net export of sediment which means that sediment for the accretion of the Wadden Sea is likely supplied from the Terschelling coast and Boschplaat area rather than the outer ebb-tidal delta.

7.2.2 Thoughts on the pilot nourishment

New insights about the development of the pilot nourishment give rise to several points for discussion, such as how the behaviour of the nourishment compares to that of the naturally existing ebb-shields, where sediment from the nourishment goes and how it would behave for a different size or location.

The development of the pilot nourishment is different to the development of existing ebb-tidal delta features such as the ebb-shields. Even though the pilot nourishment is placed on the outer edge of the platform on which the ebb-shields develop, as an extension to the second ebb-shield, its morphology and development cannot be considered similar to that of the natural ebb-shields. Volumes in the nourishment polygon decrease and the nourishment retreats landward rather than expanding seaward as the ebb-shields do. This is because the pilot nourishment barely interacts with the tidal inlet currents which are the primary driver for the development of the natural ebb-shields. The nourishment is subject mainly to shore-parallel tidal currents and waves.

The influence of the nourishment is mainly passive, as an additional source of sediment. Change in the transport patterns for consecutive bathymetries are limited which suggests that the nourishment has little effect on the natural behaviour. However, as no volumes are associated with the morphostatically determined transport pathways, a morphodynamic run is necessary to confirm that the changes in transport patterns are indeed insignificant. In both the bathymetries and in the model results there is no clear indication that active effects such as wave sheltering play a role.

Most of the sediment originating in the nourishment will eventually supply the Ameland coast, following the transport pathways that also existed prior to the placement of the nourishment. Sediment travels to the major transport pathway along the ebb-delta front either directly along the outer edge of the second ebb-shield or indirectly via the ebb-chute and then the outer edge of the ebb-shield. The particle trajectories then lead to the coast of Ameland, following the same motion that the Bornrif Bankje did. Sediment from the nourishment does not feed the Terschelling coast and is unlikely to significantly feed the tidal basin. This matches the conclusions from the morphodynamic tracer study previously performed by Bak (2017).

With its current design, the pilot nourishment has a volume of roughly 5 million m^3 and plays a very passive role in the ebb-tidal delta dynamics. The effect on local transport mechanisms is temporary with an increase in wave-dominated transports for ±1 year. Increasing the volume and more specifically the height of the nourishment could result in wave sheltering effects, although the effect is likely very short-lived. No features on the ebb-tidal delta grow very high which suggest that there is a limited elevation which can be sustained, especially if there is no tide-driven sediment supply to counter wave-driven erosion.

The improved understanding of the ebb-tidal delta dynamics as well as the SedTRAILS results could be used to inform the choice of other possible nourishment locations. At the present location seaward of the second ebb-shield the role of the nourishment is largely passive as the effect on existing transport pathways is limited. If this can be assumed true at other locations, the SedTRAILS results and in particular the lines of divergence can be used to distinguish between different nourishment zones depending on the desired final destination. For example, to feed the Boschplaat or the Terschelling side of the tidal basin, a nourishment should be placed south of the line of divergence passing through the Westgat. To feed Ameland, the nourishment should be placed somewhere on the ebb-delta which links directly to the major transport pathway along the ebb-delta front, as this appears to be the most direct link with the Ameland coast. The concepts of divergence and convergence cannot only be deduced from SedTRAILS results but also as a mathematical description of the transport vector field. For flow fields, researchers have taken this a step further using the

concept of Lagrangian coherent structures which are used to identify key material lines that organise the fluid flow transport (Kuitenbrouwer et al., 2018; Peacock & Haller, 2013; Samelson, 2013). Key material lines are lines that play a dominant role in attracting or repelling neighbouring fluid elements. It would be interesting to investigate whether this is also applicable to sediment transport vector fields. If the role of the nourishment is not passive at other locations then its design will be more complicated and require additional morphodynamic modelling.

7.3 An outlook to future change

Although the development of the ebb-tidal delta is in part deterministic and thus predictable, the system can be very sensitive to small changes. A local instability or the breach of a shoal by a channel is likely caused by a stochastic event such as a storm, and can affect the inlet and ebb-tidal delta dynamics as a whole, despite their origin at the smallest scales (Elias et al., 2019). The system may be fundamentally chaotic, which means that it is predictable for a while and then appears to become random. With this is mind, the following section discusses possible developments after 2020, sometimes through multiple possible scenarios.

The end of the period of study (2005 – 2020) is marked by a switch of the main ebb-channel from a north-eastward oriented Akkepollegat to a west-north-westward oriented third ebb-chute. This switch is likely to lead the developments of the ebb-tidal delta in the years following 2020.

In 2020, the third ebb-chute is the dominant outflow for the Borndiep, and will likely remain so in the near future. This configuration with a westward-oriented main ebb-channel is also observed between 1958 and 1985 when it led to the outbuilding of the ebb-tidal delta in updrift direction. With increased ebb flow and sediment transport through the third ebb-chute this can be expected to occur again. Moreover, the bathymetries from 2016 onwards already show signs that the deposits north of the Westgat are growing.

The Westgat itself has stopped deepening and widening since 2017. Given the continued development of the third ebb-chute as the main ebb outflow for the Borndiep, it is unlikely that the Westgat will develop into an ebb-dominant channel. Instead it will remain flood-dominant. There is also a possibility that the Westgat will temporarily reconnect with the Boschgat like between 1985 and 1999, resulting in a two-channel system.

7.3.1 Development of the Boschplaat

In the measured bathymetries, no decrease in the erosion of the Boschplaat has been observed (Elias, 2021). The current morphological changes occurring at the Boschplaat correspond to the structural erosion described in Concept C (section 2.2.3). The westward side of the ebb-tidal delta is relatively deep, which means that waves can propagate far into the inlet and transport sediment eastward from the Boschplaat into the Borndiep. However, there are morphological characteristics which suggest that a transition to Concept A (structural and episodic accretion) is imminent.

With the new westward orientation of the main ebb-channel, the ebb-tidal delta is likely to build out in the updrift (westward) direction, as occurred between 1958 and 1985. The westward extension of the ebb-tidal delta could shelter the Terschelling coast and the northern side of the Boschplaat from the waves which now penetrate far into the inlet. This means that wave-driven transport along the seaward boundary of the Boschplaat will be reduced. The structural accretion or erosion of the tip of the Boschplaat is a balance between the supply of sediment through longshore transport, and the loss of sediment through wave-driven transport across the shallow platform and through tide-driven transport through channels from the Boschplaat to the Borndiep. Reduced wave activity around the Boschplaat

leads to a transport gradient in wave-driven transport which could reverse the balance between supply and loss of sediment, resulting in accretion and spit formation at the tip of the Boschplaat. This updrift expansion of the ebb-tidal delta for a westward-oriented channel, leading to increased wave sheltering and growth of the Boschplaat is largely deterministic as it is driven by tidal processes. Additional accretion through an episodic event such as a shoal attachment seems unlikely in the short-term.

The transition to structural accretion described above is largely deterministic. However, this can be interrupted by a stochastic process such as the breaching of the Boschplaat by a channel connecting the Westgat and the Boschgat. This corresponds to the episodic erosion described in Concept B. A large part of the Boschplaat is protected from breaches during storms by the manmade sand dike. However, if a spit forms, it will be vulnerable to episodic erosion through over wash and breaching during a storm event. Also, if a channel connecting the Westgat and the Boschgat has already formed, spit growth will be limited. The formation of such a channel is a stochastic process and it is thus not possible to predict exactly if or when it will happen. Once formed, such a channel can transport large volumes of sediment away from the Boschplaat, leading to longer term structural erosion as was the case between 1989 and 1999. A stochastic event such the formation of a channel during a storm can cause a sudden switch from an accretionary to an erosive regime, resulting in a very different development of the Boschplaat. This is what makes the development of morphodynamic features so difficult to predict.

7.3.2 Shoal attachments

The two most recent shoal attachments, that of the Bornrif Bankje and the Bornrif Strandhaak, are analogous to possible upcoming shoal attachments. The Bornrif platform is less dynamic than the western side of the ebb-tidal delta, and thus may be slightly more predictable.

With the switch of the main ebb-channel, sediment supply by ebb flows passing through the Borndiep is now westward directed. This means that less sediment is supplied to the northern ebb-delta front to counter erosion by waves, and the ebb-delta front will likely continue eroding as is already observed since 2017. In the past, the Bornrif Bankje formed from sediment which was deposited further out to sea during the alignment of the Borndiep and the Akkepollegat between 2011 and 2014. The Bornrif Bankje migrated along the outer edge of the ebb-tidal delta and attached to the coast downdrift of the Bornrif Strandhaak. The sediment eroded from the ebb-delta front following the recent channel switch could form another shoal which follows the path of the Bornrif Bankje, migrating along the ebb-delta margin and attaching to the coast downdrift of the Bornrif Strandhaak. Alternatively, waves could drive the sediment continuously along the ebb-delta front and across the direct connection between the Bornrif and the Ameland coast now established by the Bornrif Bankje. This is what is observed in the SedTRAILS results following the attachment of the Bornrif Bankje. The decrease in sediment supply to the ebb-delta front due to the switching of the main ebb-channel is much larger than the decrease due to the changing alignment of the Akkepollegat and the Borndiep. For this reason, the sediment volume supplied to the downdrift coast following the erosion of the ebb-delta front is expected to be much larger than that of the Bornrif Bankje. If sediment is supplied to the coast continuously or through an attachment, sediment from the ebb-delta front is unlikely to counter erosion of the northwest Ameland coast towards Borndiep because it will reach the coast too far to the east.

The switch of the main ebb-channel towards the west also means that the central part of the ebb-tidal delta around the former Akkepollegat will be less tide-dominated, with most of the ebb flows passing through the third ebb-chute. As a result, tides will play a less important role in determining the morphology of the second ebb-shield and waves will become more

dominant. Initially, the outer edge of the ebb-shield will migrate faster than the inner part because it is more exposed to waves and alongshore tidal currents. Over time, the ebb-shield will likely slowly lose its shape, which is largely determined by ebb flows, and be reworked by waves. Modelled transport pathways suggest that sediment will be transported away from the ebb-shield along the ebb-delta front. However, these modelled pathways do not include transport which occurs through morphologic change such as the migration of bars or shoals. Examples such as the Bornrif Strandhaak (Elias et al., 2019) and the Noorderhaaks in the Texel inlet (Elias, 2006) show that a shoal can maintain itself as it migrates across an ebb-delta platform. Sediment from the second ebb-shield and the nourishment is expected to migrate across the central part of the Bornrif in a similar way to the Bornrif Strandhaak. It may take decades before the sediment from the ebb-shield reaches the Ameland coast. With the previous switch from the Akkepollegat to a more westward main ebb-channel, the Akkepollegat was abandoned around 1958 and a shoal (Bornrif Strandhaak) formed near the northwest coast of Ameland between 1970 and 1986, finally attaching in 1986. If this is indeed how the second ebb-shield develops, it may attach close to the Borndiep as the Bornrif Strandhaak did.

Sediment is also accumulating on the southern tip of the Bornrif. A similar shoal is visible in the 1958 bathymetry (Elias et al., 2019). Although the lack of detail in the depth contours does not allow tracking of further development, the shoal is expected to have contributed to the formation of the Bornrif Strandhaak prior to its attachment. The new shoal on the southern tip of the Bornrif visible in the 2020 bathymetry can be expected to interact with the shoal which forms from the ebb-shield in a similar way.

7.4 Novelty

The contribution to the existing pool of knowledge on sediment bypassing processes at Ameland is twofold, firstly in adding to that understanding and secondly in applying a new approach (SedTRAILS).

The understanding of sediment bypassing processes at Ameland inlet has been improved by extending the existing analysis synthesised in Elias et al. (2020) with the most recent bathymetric data. In the same way, more recent data have enabled an elaboration of the analysis of the development of the pilot nourishment by Van Rhijn (2019) to include not only the first response but also expectations for longer term behaviour. Additional detail on the behaviour of individual features such as the ebb-shields and the channels was also added. Combined with the process-based links between subsequent bathymetries provided by SedTRAILS, this formed the basis for setting up a series of conceptual models to describe sediment bypassing behaviour at different stages in the sediment bypassing cycle.

Prior to this thesis, SedTRAILS had not yet been applied to consecutive bathymetries, allowing for the process based linking of observed behaviour. This modelling exercise has given insights into how to distribute sources, desired simulation time, selection of the appropriate morphological tide, the possible effect of a velocity gap on residual transports and other details involved in the process. To facilitate many runs, the scripts have been adjusted so that they are compatible with Linux and can be run on an external cluster, which is both faster and frees up local computational power for post-processing. Post-processing approaches which can be applied to gain useful insights from the initially chaotic SedTRAILS results include isolation of particles originating in or traversing a certain polygon, schematising the results with lines of divergence and major transport pathways and superimposing tide only and coupled tide-wave simulations.

The underlying objective for improving the understanding of sediment bypassing processes is to better understand the potential of a nourishment on the ebb-tidal delta and thereby

improve the coastal management strategy. In this respect, the first results are positive as the nourishment is shown to contribute both to the sediment stored on the ebb-tidal delta and to the coast of Ameland, thereby contributing to the coastal foundation. This was also a successful proof of concept for SedTRAILS as a tool in coastal management. This will help to make choices between beach, foreshore and system nourishments in future.

7.5 Recommendations

This study gives insights into the development of the ebb-tidal delta and the sediment bypassing processes involved under average conditions. This and the insights into the behaviour of the nourishment contribute to the objectives of the Kustgenese 2.0 project, but also give rise to ideas for future research.

The amount of data and the frequency of the bathymetric surveys available at Ameland inlet is unique. This has made it possible to study processes that are part of the sediment bypassing cycle in a lot of detail. A next step would be to generalise these findings and compare them to studies performed at other tidal inlets or more general conceptual models (Bruun & Gerritsen, 1959; FitzGerald, 1982; Herrling & Winter, 2018).

Both the morphologic change observed in the bathymetries and the transport pathways suggest that the influence of the pilot nourishment on sediment bypassing is limited. However, the morphostatic runs performed to visualise transport give no indications of the volumes following different paths. To verify whether the nourishment indeed has a limited effect on behaviour, a morphodynamic simulation with and without the nourishment is needed in which changes can be quantified in terms of volume.

The current model includes one uniform sediment fraction (200µm), which means that any continuous transport pathways for other fractions which do not result in bed level changes in subsequent bathymetries will not come forward in this study. Results from Herrling & Winter (2018) show a strong dependency of the sediment bypassing mechanism on sediment grain-size fractions. For this reason, it is recommended to include multiple sediment fractions in future modelling studies on sediment bypassing.

Recent studies suggest that the sediment bypassing cycle is initiated by local instabilities on the Kofmansplaat, which develop into a dynamic ebb-chute and shield system. Although the results describe how an area that is favourable for these instabilities is created, they do not show what the trigger for these instabilities is. This is because this study describes deterministic behaviour, predictable behaviour based on average conditions. To find the trigger a different approach is necessary. Possible causes for these instabilities are storms of flow instabilities, which will have to be modelled in more detail to better understand the role they play.

During the period of study, the connecting transport pathways between individual features such as the ebb-shields and distinct areas on the ebb-tidal delta such as the Kofmansplaat, the Bornrif, the Borndiep and the tidal basin are continuously evolving. Visualising this using SedTRAILS can result in very complex patterns which are sometimes difficult to interpret. Schematising such patterns in a network using the concept of connectivity (Pearson et al., 2020) may make results easier to interpret and help to compare the changing transport connections between different years. A description of connectivity and how it is applied along with several trials are included in Appendix C.

Another way to visualise the transport patterns would be to look at areas where transport pathways converge and diverge. This has been done manually for a number of the SedTRAILS results, where convergent pathways and zones of divergence are indicated.

Divergence can also be calculated based on a transport vector field. Another possibility is to investigate whether it is possible to apply the concept of Lagrangian coherent structures to transport fields, a concept that is generally applied to flow fields (Kuitenbrouwer et al., 2018; Peacock & Haller, 2013; Samelson, 2013).

With the constantly changing morphology, it is difficult to be consistent with the definition of different morphological features throughout the period of study. This means that the naming of channels and shoals needs to be regularly updated to reflect these changes.

There is no universal definition for which channel is the main ebb channel. In many morphologic configurations, the main ebb-channel is apparent from the bathymetry. The high frequency surveys at Ameland inlet have illustrated that there is a period of about two years (2017-2018) when the main ebb-channel is not so clear. In this study, the depth of the channel has been used to define which is the main ebb-channel. In future, it would be interesting to see whether discharges and sediment transport though the channels show same trend. Because the channels shift, it is not sufficient to compare discharges across a single transect, and a more complex approach will have to be used to extract reliable discharge from model results which can be compared with different years.

There are many different methods to determine a morphological tide and the choice will have implications for the SedTRAILS results. For this reason, it is important to consider the selection method used for any future studies applying SedTRAILS. For this study, the morphological tide was selected based on a statistical comparison of transport across a number of cross-sections in the model area. Other options include a visual comparison of the transport vector fields or a mathematical comparison of the direction and magnitude of the transport vectors.

For analysis of the bathymetries, many different polygons were used which were defined manually based on bed levels and sedimentation-erosion patterns. For future analysis, reliability of the results would improve if an objective polygon definition is developed.

8 Conclusions

The objective of this research is to improve the understanding of sediment bypassing across the Ameland ebb-tidal delta first under natural circumstances and then under the influence of a nourishment. This is done by answering a series of research questions proposed in section 1.3.

8.1 Natural sediment bypassing processes

The first set of sub-questions concerns the natural sediment bypassing processes.

Which morphological processes are wave-, tide- or wind-driven?
In general, inlet tidal currents dominate transport on the central part of the ebb-delta platform and waves dominate mainly on the margins. Transports by flood-dominated shore-parallel tidal currents are greatest on the western side of the ebb-tidal delta and less so on the Bornrif platform due to their interaction with inlet tidal currents (Sha, 1989). Waves also amplify tidally driven transports through increased stirring up of sediment, which is indicated by the longer transport pathways. Furthermore, the depth of a morphological feature also plays an important role, with wave-breaking driven transports becoming important as the feature becomes shallower. The role of wind-driven circulation (van Weerdenburg, 2019) has not been considered in this investigation.

Seaward growth of the ebb-shields and of the ebb-delta front is driven by ebb currents. Ebb-currents passing through the main ebb-channel supply large volumes of sediment to the seaward margin of the ebb-delta, and via the ebb-chutes to the outer edges of the ebb-shields. Upon passing over the edge of the ebb-shields, flow diverges and the sediment is deposited. After 2016, the ebb-delta front no longer grows seaward because the Akkepollegat no longer supplies enough sediment. This is because the channel has migrated too far east and is no longer the main ebb-channel.

Rotation of the ebb-shields is largely wave-driven although shore-parallel tidal currents also contribute. The dominant wave direction is from the northwest, resulting in transports towards the east across the shallower eastern side of the ebb-shields. The shallower depths of the ebb-shields cause wave breaking which increases transport. This wave-driven clockwise rotation of the ebb-shields is also the primary driver for the migration of the Akkepollegat, which is constricted by the migrating sediment.

A similarly shallow area where wave-driven transports dominate is the outer margin of the Bornrif platform. Wave-breaking on the ebb-delta platform induces transport towards the southeast with sediment piling up to form the Bornrif Bankje. Waves eventually push this shoal all the way to the Ameland coast in 2017.

Which of the three modes of sediment bypassing as defined by Herrling & Winter (2018) occur on the Ameland ebb-tidal delta? These are flow bypassing and bar welding, sediment recirculation and ebb-delta periphery bypassing.
Of the three modes of sediment bypassing, flow bypassing and bar welding is the most apparent. Depending on the stage in the sediment bypassing cycle, flood-driven currents transport sediment coming in from the west either onto the Kofmansplaat or into the Borndiep. Sediment on the Kofmansplaat forms ebb-shields which eventually link to the major transport pathway along the ebb-delta front. The Akkepollegat which is linked to the Borndiep directly transports sediment to the ebb-delta front. Waves drive sediment towards Ameland

either through shoal attachments which originate on the ebb-delta front or through the migration of bars slightly offshore of the main ebb-delta platform.

Sediment recirculation occurs, though at a smaller scale than illustrated by Herrling & Winter (2018). Sediment on the southern tip of the Bornrif is transported seaward by ebb currents until halfway across the Bornrif platform, rather than to the outer edge of the ebb-tidal delta as described by Herrling & Winter (2018). On the Bornrif platform, waves drive the sediment towards the southeast where the sediment follows the seaward bank of the eastern flood channel back to the southern tip of the Bornrif. Similar transport patterns are visible in all bathymetries and result in the formation of a shoal in 2020. This could be the origin of a new shoal attachment.

For ebb-delta periphery bypassing, there is no clear evidence in either the bathymetries or the model results. Where sedimentation-erosion patterns and model results clearly indicate transport towards Ameland along the northern and eastern margins of the ebb-tidal delta this is not the case for the western side. This could be because during the period of investigation the region between the Kofmansplaat and the coast of Terschelling is relatively deep, interrupting any possible wave-driven transport along the margin of the ebb-tidal delta. Also only the dominant grainsize (200µm) is considered, while Herrling & Winter (2018) observe different patterns for different fractions. Their results show that ebb-delta periphery bypassing is the dominant sediment bypassing mechanism for very fine to fine sand (125µm), a fraction which is not modelled in this study.

8.2 Sediment bypassing under the influence of a nourishment

The second set of sub-questions concerns the influence of the nourishment on sediment bypassing processes.

How is the pilot nourishment developing?
Two years after the construction of the pilot nourishment, it continues eroding with roughly 62% of the original sediment volume remaining at the original nourishment location. There are two main pathways transporting sediment away from the nourishment. The first passes from nourishment directly along the outer edge of the second ebb-shield and is driven by a combination of waves and shore-parallel tidal currents. The second is driven by shore-parallel tides and moves sediment east into the second ebb chute, where tidal inlet currents transport the sediment to the outer edge of ebb-shield to re-join the first transport pathway.

In the initial response waves dominate, forcing more sediment to follow the path along the outer edge of the ebb-shield. This smoothens the nourishment along the outer edge of the second ebb-shield, bringing it increasingly into equilibrium with its surroundings. After about a year, waves become less important and the shore-parallel tidal currents take over in a second response. Sediment is transported to the east, partly into the ebb chute and partly along the outer edge of the ebb-shield. This second response is expected to continue in the long-term.

Is the morphological response of the nourishment dominated by storms or day-to-day processes?
The largest morphological changes to the nourishment occur during the stormy winter season, with 72% of the 1.83 million m^3 sediment volume loss from the original nourishment site occurring during the 2019 and 2020 winter season. The changes under calm conditions are much smaller. This matches the earlier conclusion by Van Rhijn (2019). Although individual storms are not considered in this research, surveys of the pilot nourishment are of sufficient frequency to distinguish between changes during the storm season and during the calmer spring and summer months. The transects analysed clearly show increased erosion of

the outer edge of the nourishment resulting in gentling of the outer slope, and faster migration of sand bars during the winter months. These changes are likely not only due to storms but also because the nourishment is constructed far out of equilibrium with its surroundings.

How does the pilot nourishment affect the naturally occurring sediment transport mechanisms on the ebb-tidal delta at the scale of channel and shoals?
The interaction of the pilot nourishment with natural features on the ebb-tidal delta is limited to the second ebb-shield. In the initial response, wave-driven transports along the outer edge of the second ebb-shield increase. Also, due to the extra volume of sediment, the nourishment reinforces tide-driven circulation through the second ebb-chute. In both cases, this does not visibly change the existing transport patterns but only increases the amount of sediment following each path. The initial strong response to storm events leads to increased outbuilding of the ebb-shield directly following the completion of the nourishment in February 2019. This response is temporary, with no more outbuilding after June 2020.

How are sediment bypassing processes influenced by the pilot nourishment on an ebb-tidal delta scale, either actively by directly influencing the process of shoal attachments, or passively by increasing sediment volume?
On ebb-tidal delta scale the effects of the nourishment on sediment bypassing processes are limited. The contribution of the pilot nourishment is passive, as it increases the sediment volumes following the existing transport pathways but does not actively change these pathways. Sediment from the nourishment passes either directly along the outer edge of the second ebb-shield or via the ebb-chute. In both cases, the sediment then joins the major transport pathway along the outer edge of the ebb-tidal delta meaning that the general pathway sediment follows towards Ameland is unchanged. The same is true for the sediment naturally present in the vicinity of the nourishment which continues to follow the major transport pathways through the ebb-chutes and along the outer edges of the ebb-shield towards the major transport pathway along the ebb-delta front. The limited influence of the nourishment is in part because the nourishment volume (~5.5 million m^3) is small compared to the dynamic volume present on the ebb-tidal (115-135 million m^3 between 2005 and 2020). A large part of this dynamic volume is stored in the ebb shoals which dominate morphological behaviour on the ebb-tidal delta.

How is sediment from the nourishment linked to other areas in the Ameland inlet?
The pilot nourishment is largely erosive and dominated by transport towards the east. There is only limited tide-driven transport onto the nourishment from the west. Sediment from the nourishment first interacts with the second ebb-shield, passing either along the outer edge or through the ebb-chute. From here the transport pathways link to the major transport pathway along the ebb-delta front.

Sediment from the nourishment location will eventually reach the Ameland coast via the outer edge of the ebb-tidal delta. Particle trajectories starting on the nourishment do not reach the coast in the chosen runtime but they do reach the bar complexes on the northeat side of the ebb-tidal delta which are known to migrate towards Ameland (Elias et al., 2019). The modelled transport pathways suggest that it is unlikely that sediment from the nourishment will feed the Terschelling coast or the tidal basin.

How can the location of a nourishment be optimised based on a specific goal?
Current results can be used to show whether a set of pathways exists linking a nourishment location to the coast or another target area. If a proposed nourishment location is expected to contribute passively to sediment bypassing (without changing the existing transport patterns) as this pilot nourishment has done, then sediment from the nourishment can be expected to follow the existing pathways. However, this gives no indication of the time needed for sediment from the nourishment to have effect. Using the lines of divergence found based on

the SedTRAILS results, areas can be defined which would potentially feed different target zones such as the Boschplaat, the tidal basin or the Ameland coast.

If the nourishment is to be designed to have an active effect on sediment bypassing, then the improved understanding of the natural sediment bypassing processes should be applied. For wave-dominated transports, the depth of the nourishment is a key feature. As is the case for the ebb-shields, transport driven by wave breaking only occurs when the nourishment is shallow enough. For tide-dominated transport it would be interesting to see whether shoal formation either on the southern tip of the Bornrif or along the ebb-delta front can be triggered. Morphodynamic modelling will be necessary to test such a design.

9 References

3e Kustnota: Traditie, Trends en Toekomst. (2000).

Bak, J. (2017). *Nourishment strategies for Ameland Inlet*.

Battjes, J., & Janssen, J. P. F. M. (1978). Energy loss and set-up due to breaking of random waves. *Proceedings of the 16th International Conf. on Coastal Engineering*, 569–587.

Beets, D. J., & Van Der Spek, A. J. F. (2000). The Holocene evolution of the barrier and the back-barrier basins of Belgium and the Netherlands as a function of late Weichselian morphology, relative sea-level rise and sediment supply. *Geologie En Mijnbouw/Netherlands Journal of Geosciences*, *79*(1), 3–16. https://doi.org/10.1017/S0016774600021533

Beets, D. J., Van der Spek, A. J. F., & van der valk, L. (1994). *Holocene ontwikkeling van de Nederlandse kust (RGD rapport 40.016 - Projekt Kustgenese)*.

Bruun, P., & Gerritsen, F. (1959). Natural by-passing of sand at coastal inlets. *Journal of the Waterways and Harbors, Harbor Division*, *85*(4), 75–107.

Cowell, P. J., Stive, M. J. F., Niedoroda, A. W., De Vriend, H. J., Swift, D. J. P., Kaminsky, G. M., & Capobianco, M. (2003). The Coastal-Tract (Part 1): A Conceptual Approach to Aggregated Modeling of Low-Order Coastal Change. *Journal of Coastal Research*, *19*(4), 812–827.

Davis, R. A., & Hayes, M. O. (1984). What is a Wave-Dominated Coast? *Marine Geology*, *39*(C), 313–329. https://doi.org/10.1016/S0070-4571(08)70152-3

de Fockert, A. (2008). Impact of Relative Sea Level Rise on the Amelander Inlet Morphology. In *MSc thesis*.

de Graaff, R. F. (2009). *SBW Wadden Sea, water level modelling; Calibration hydrodynamic model. Technical report*.

De Kruif, A. C. (2001). *Bodemdieptegegevens van het Nederlandse Kustsysteem; Beschikbare digitale data en een overzicht van aanvullende analoge data*.

De Swart, H. E., & Zimmerman, J. T. F. (2009). Morphodynamics of tidal inlet systems. *Annual Review of Fluid Mechanics*, *41*, 203–229. https://doi.org/10.1146/annurev.fluid.010908.165159

de Vriend, H. J., van Koningsveld, M., & Aarninkhof, S. G. J. (2014). “Building with nature”: The new Dutch approach to coastal and river works. *Proceedings of the Institution of Civil Engineers: Civil Engineering*, 18–24.

Dean, R. G., & Walton, T. L. (1975). *Sediment transport processes in the vicinity of inlets with special reference to sand trapping* (Volume 2). Academic Press.

Deltares. (2014a). Delft3D-FLOW User manual. In *Delft3D*. Deltares. https://doi.org/10.1016/j.csr.2014.01.025

Deltares. (2014b). Delft3D-WAVE User Manual. In *Delft3D* (pp. 1–226). Deltares.

Dillingh, D. (1990). *Frequentie en dichtheid van kust- en vaklodingen*.

Elias, E. P. L. (2006). *Morphodynamics of Texel Inlet*.

Elias, E. P. L. (2017). *Understanding the present-day morphodynamics of Ameland inlet. Deltares Report 1220339-006-ZKS-0007*.

Elias, E. P. L. (2018a). *Bench-mark morphodynamic model Ameland Inlet - Kustgenese 2.0 (ZG-C2)*.

Elias, E. P. L. (2018b). Understanding the present- day morphodynamics of Ameland inlet. In *Deltares report 1220339-006*.

Elias, E. P. L. (2019). *Een actuele sedimentbalans van de Waddenzee*.

Elias, E. P. L. (2021). *De morfologische ontwikkeling van de Boschplaat - Terschelling*.

Elias, E. P. L., & Bruens, A. (2013). *Beheerbibliotheek Ameland*.

Elias, E. P. L., Cleveringa, J., Buijsman, M. C., Roelvink, D. J. A., & Stive, M. J. F. (2006). Field and model data analysis of sand transport patterns in Texel Tidal inlet (the Netherlands). *Coastal Engineering*, *53*(5–6), 505–529. https://doi.org/10.1016/j.coastaleng.2005.11.006

Elias, E. P. L., Gelfenbaum, G. R., van Ormondt, M., & Moritz, H. R. (2011). Predicting

sediment transport patterns at the Mouth of the Columbia River. *The Proceedings of the Coastal Sediments 2011*, 588–601.
Elias, E. P. L., & Pearson, S. G. (2020). *SedTRAILS - Sediment TRAnsport visualization & Lagrangian Simulator*.
Elias, E. P. L., Pearson, S. G., & Van der Spek, A. J. F. (2020). *Understanding the morphological processes at Ameland Inlet*.
Elias, E. P. L., Roelvink, F., & Pearson, S. G. (2020). *Kustfundamentsuppleties op Eilandkoppen; Uitwerking suppletievarianten Texel en Ameland*.
Elias, E. P. L., Van der Spek, A. J. F., Pearson, S. G., & Cleveringa, J. (2019). Understanding sediment bypassing processes through analysis of high-frequency observations of Ameland Inlet, the Netherlands. *Marine Geology*, *415*, 105956. https://doi.org/10.1016/j.margeo.2019.06.001
Elias, E. P. L., Van der Spek, A. J. F., Wang, Z. B., & De Ronde, J. (2012). Morphodynamic development and sediment budget of the Dutch Wadden Sea over the last century. *Geologie En Mijnbouw/Netherlands Journal of Geosciences*, *91*(3), 293–310. https://doi.org/10.1017/S0016774600000457
FitzGerald, D. M. (1982). Sediment Bypassing At Mixed Energy Tidal Inlets. *Proceedings of the Coastal Engineering Conference*, *2*, 1094–1118. https://doi.org/10.9753/icce.v18.68
FitzGerald, D. M. (1984). Interactions between the ebb-tidal delta and landward shoreline: Price Inlet, South Carolina. *Journal of Sedimentary Petrology*, *54*(4), 1303–1318. https://doi.org/10.1306/212F85C6-2B24-11D7-8648000102C1865D
Hayes, M. O. (1979). Barrier island morphology as a function of tidal and wave regime. *Marine Geology*, *387*(January), 74–84. https://doi.org/10.1016/j.margeo.2017.02.016
Hayes, M. O., & FitzGerald, D. M. (2013). Origin, Evolution, and Classification of Tidal Inlets. *Journal of Coastal Research*, *69*, 14–33. https://doi.org/10.2112/SI
Herrling, G., & Winter, C. (2018). Tidal inlet sediment bypassing at mixed-energy barrier islands. *Coastal Engineering*, *140*, 342–354. https://doi.org/10.1016/j.coastaleng.2018.08.008
Israel, C. G., & Dunsbergen, D. W. (1999). Cyclic morphological development of the Ameland Inlet, The Netherlands. *Proceedings of Symposium on River, Coastal and Estuarine Morphodynamics*, 705–714.
Kuitenbrouwer, D., Reniers, A., MacMahan, J., & Roth, M. K. (2018). Coastal protection by a small scale river plume against oil spills in the Northern Gulf of Mexico. *Continental Shelf Research*, *163*(April), 1–11. https://doi.org/10.1016/j.csr.2018.05.002
Kustverdediging na 1990, Beleidskeuze voor de Kustlijnzorg. (1990). In *Kamerstuk 21.136 nr 5 (2e kamer) vergaderjaar 98-90*.
Laan, S. C. (2019). *Understanding coastal dynamics at an ebb-tidal delta in the Wadden Sea.* TU Delft.
Lesser, G. R. (2009). *An Approach to Medium-term Coastal Morphological Modelling* [TU Delft]. http://www.narcis.nl/publication/RecordID/oai:tudelft.nl:uuid:62caa573-4fc0-428e-8768-0aa47ab612a9
Lintsen, H. (2002). Two Centuries of Central Water Management in the Netherlands. *Technology and Culture*, *43*(3), 549–568. https://doi.org/10.1353/tech.2002.0126
Nederhoff, C. M., Schrijvershof, R., Tonnon, P. K., & van der Werf, J. (2019). *The Coastal Genesis II Terschelling - Ameland inlet (CGII-TA) model. Model setup, calibration and validation of a hydrodynamic-wave model. Report 1220339-008-ZKS-0004*.
Oost, A. (1995). Dynamics and sedimentary developments of the Dutch Wadden Sea with a special emphasis on the Frisian Inlet : a study of the barrier islands, ebb-tidal deltas, inlets and drainage basins. In *Geologica Ultraiectina* (Vol. 126).
Peacock, T., & Haller, G. (2013). Lagrangian coherent structures: The hidden skeleton of fluid flows. *Physics Today*, *66*(2), 41–47. https://doi.org/10.1063/PT.3.1886
Pearson, S. G., van Prooijen, B., Elias, E. P. L., Vitousek, S., & Wang, Z. B. (2020). Sediment Connectivity: A Framework for Analyzing Coastal Sediment Transport Pathways. *Earth and Space Science Open Archive*. https://doi.org/10.1002/essoar.10502451.1
Rijkswaterstaat. (2021). *Kustgenese 2.0: kennis voor een veilige kust*.
Rubinov, M., & Sporns, O. (2010). Complex network measures of brain connectivity: Uses and interpretations. *NeuroImage*, *52*(3), 1059–1069.

https://doi.org/10.1016/j.neuroimage.2009.10.003
Samelson, R. M. (2013). Lagrangian motion, coherent structures, and lines of persistent material strain. *Annual Review of Marine Science*, *5*, 137–163. https://doi.org/10.1146/annurev-marine-120710-100819
Sha, L. P. (1989). Variation in ebb-delta morphologies along the West and East Frisian Islands, The Netherlands and Germany. *Marine Geology*, *89*(1–2), 11–28. https://doi.org/10.1016/0025-3227(89)90025-X
Son, C. S., Flemming, B. W., & Bartholomä, A. (2011). Evidence for sediment recirculation on an ebb-tidal delta of the East Frisian barrier-island system, southern North Sea. *Geo-Marine Letters*, *31*(2), 87–100. https://doi.org/10.1007/s00367-010-0217-8
Stevens, A. W., Elias, E. P. L., Pearson, S. G., Kaminsky, G. M., Ruggiero, P. R., Weiner, H. M., & Gelfenbaum, G. R. (2020). Observations of coastal change and numerical modeling of sediment-transport pathways at the mouth of the Columbia River and its adjacent littoral cell. *Open-File Report*. https://doi.org/10.3133/ofr20201045
Stive, M. J. F., Roelvink, D. J. A., & de Vriend, H. J. (1990). Large-scale coastal evolution concept. *The Dutch Coast; Report of a Session on the 22nd International Conference on Coastal Engineering*, *Paper 9*, 1962–1974.
Stive, M. J. F., & Wang, Z. B. (2003). Morphodynamic modeling of tidal basins and coastal inlets. In *Advances in Coastal Modelling* (pp. 367–392). Elsevier Oceanography Series.
Teske, R. (2013). Tidal inlet channel stability in long term process based modelling. In *MSc thesis* (Issue July).
Van Der Brugge, R., Rotmans, J., & Loorbach, D. (2005). The transition in Dutch water management. *Regional Environmental Change*, *5*(4), 164–176. https://doi.org/10.1007/s10113-004-0086-7
Van der Spek, A. J. F. (1995). Reconstruction of tidal inlet and channel dimensions in the Frisian Middelzee, a former tidal basin in the Dutch Wadden Sea. *International Association of Sedimentologists, Special Publication*, *24*, 239–258.
van Prooijen, B., Tissier, M., de Wit, F., Pearson, S. G., Brakenhoff, L., van Maarseveen, M., van der Vegt, M., Mol, J.-W., Kok, F., Holzhauer, H., van der Werf, J., Vermaas, T., Gawehn, M., Grasmeijer, B., Elias, E. P. L., Tonnon, P. K., Reniers, A., Wang, Z. B., den Heijer, C., … de Looff, H. (2020). Measurements of Hydrodynamics, Sediment, Morphology and Benthos on Ameland Ebb-Tidal Delta and Lower Shoreface. *Earth System Science Data Discussions*, *February*, 1–18. https://doi.org/10.5194/essd-2020-13
Van Rhijn, M. W. (2019). *Sediment transport during the execution of the pilot nourishment Ameland Inlet*. TU Delft.
van Rijn, L. C. (1993). *Principles of Sediment Transport in Rivers, Estuaries and Coastal Seas*. Aqua Publications.
van Rijn, L. C. (2007a). Unified View of Sediment Transport by Currents and Waves. I: Initiation of Motion, Bed Roughness, and Bed-Load Transport. *Journal of Hydraulic Engineering*, *133*(6), 649–667. https://doi.org/10.1061/(ASCE)0733-9429(2007)133:6(649)
van Rijn, L. C. (2007b). Unified View of Sediment Transport by Currents and Waves. II: Suspended Transport. *Journal of Hydraulic Engineering*, *133*(6), 668–689. https://doi.org/10.1061/(ASCE)0733-9429(2007)133:6(668)
van Rijn, L. C. (2007c). Unified View of Sediment Transport by Currents and Waves. III: Graded Beds. *Journal of Hydraulic Engineering*, *133*(7), 761–775. https://doi.org/10.1061/(ASCE)0733-9429(2007)133:7(761)
van Soest, M. (2021). *Wave nonlinearity parameterization for modelling the Ameland inlet*. Universiteit Utrecht.
van Weerdenburg, R. (2019). *Exploring the relative importance of wind for exchange processes around a tidal inlet system : the case of Ameland Inlet*. 78.
Wang, Z. B., Elias, E. P. L., Van Der Spek, A. J. F., & Lodder, Q. J. (2018). Sediment budget and morphological development of the Dutch Wadden Sea: Impact of accelerated sea-level rise and subsidence until 2100. *Geologie En Mijnbouw/Netherlands Journal of Geosciences*, *97*(3), 183–214. https://doi.org/10.1017/njg.2018.8
Wiegmann, E. B., Perluka, R., Oude Elberink, S., & Vogelzang, J. (2005). *Vaklodingen: De*

inwintechnieken en hun combinaties. Report AGI-2005-GSMH-012 (in Dutch).
Zijderveld, A., & Peters, H. (2009). Measurement programme Dutch Wadden Sea. *31st International Conference on Coastal Engineering*, 404–410.
Zijl, F., Verlaan, M., & Gerritsen, H. (2013). Improved water-level forecasting for the Northwest European Shelf and North Sea through direct modelling of tide, surge and non-linear interaction. *Ocean Dynamics*, *63*, 823–847. https://doi.org/https://doi.org/10.1007/s10236-013-0624-2

A Bathymetries

This appendix includes the bathymetric data for the ebb-tidal delta and the pilot nourishment during the period of study, and the sedimentation erosion patterns between consecutive bathymetries.

A.1 Ebb-tidal delta

The bathymetric data for the development of the Ameland ebb-tidal delta between 2005 and 2020 is included below. Incomplete bathymetries have been made complete with data from neighbouring years where necessary.

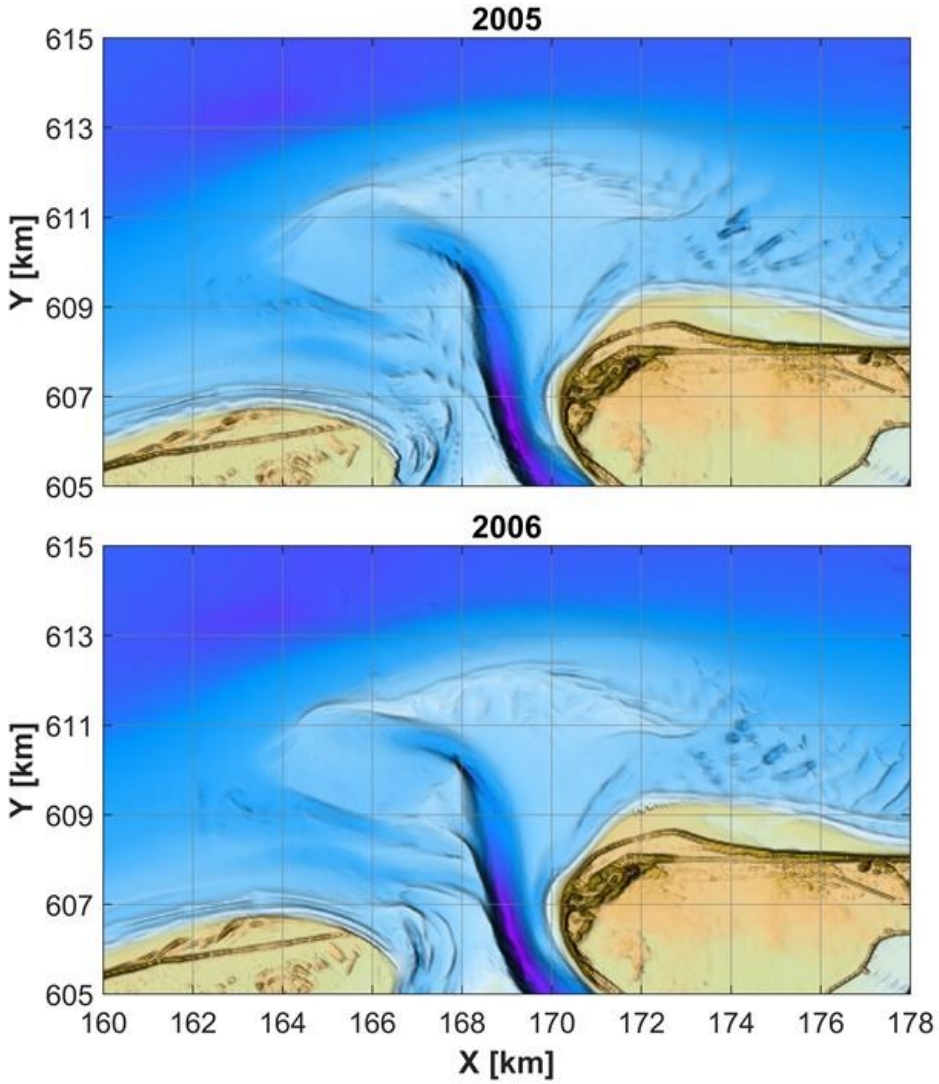

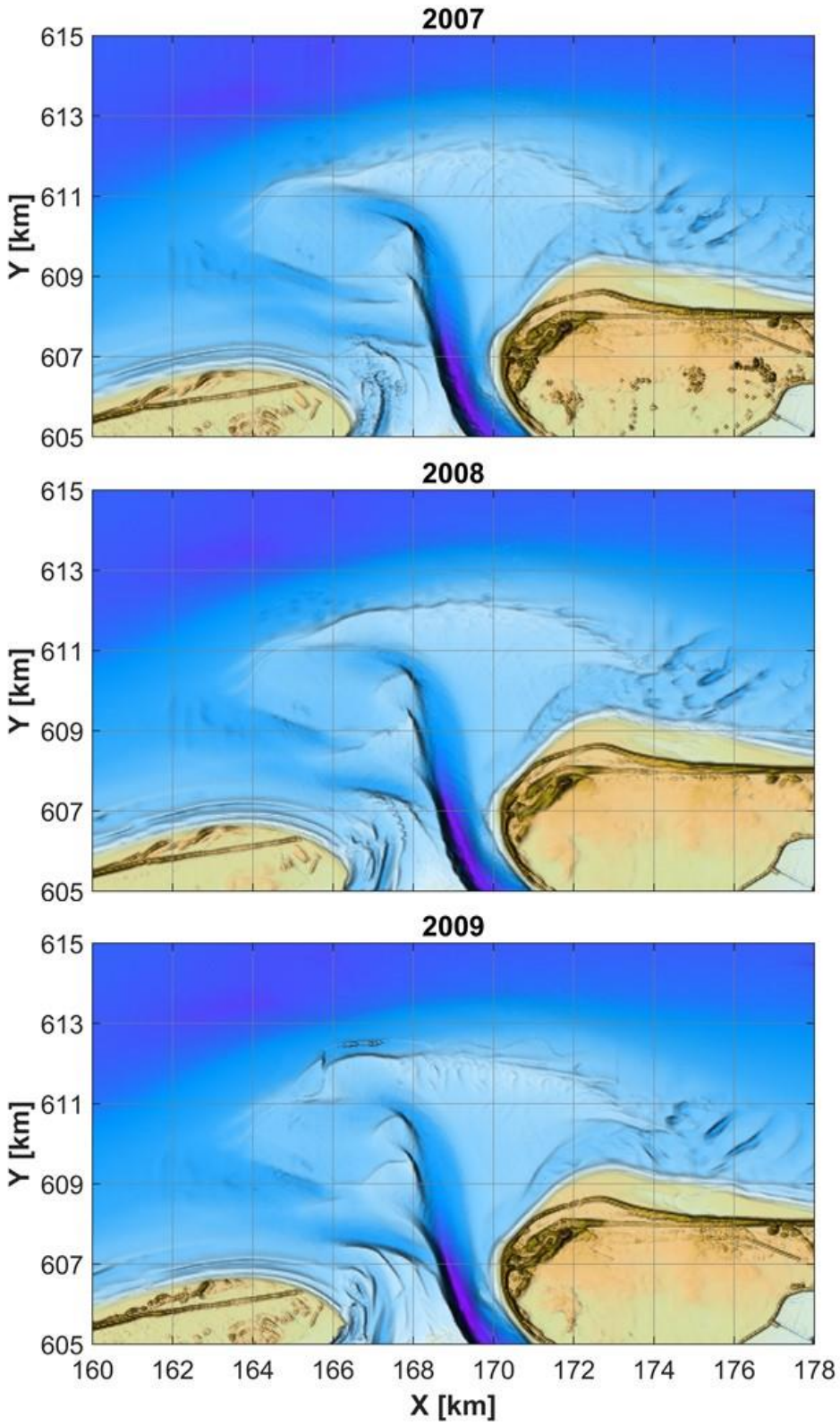
2007
2008
2009
Y [km]
615
613
611
609
607
605
160
162
164
166
168
170
172
174
176
178
X [km]

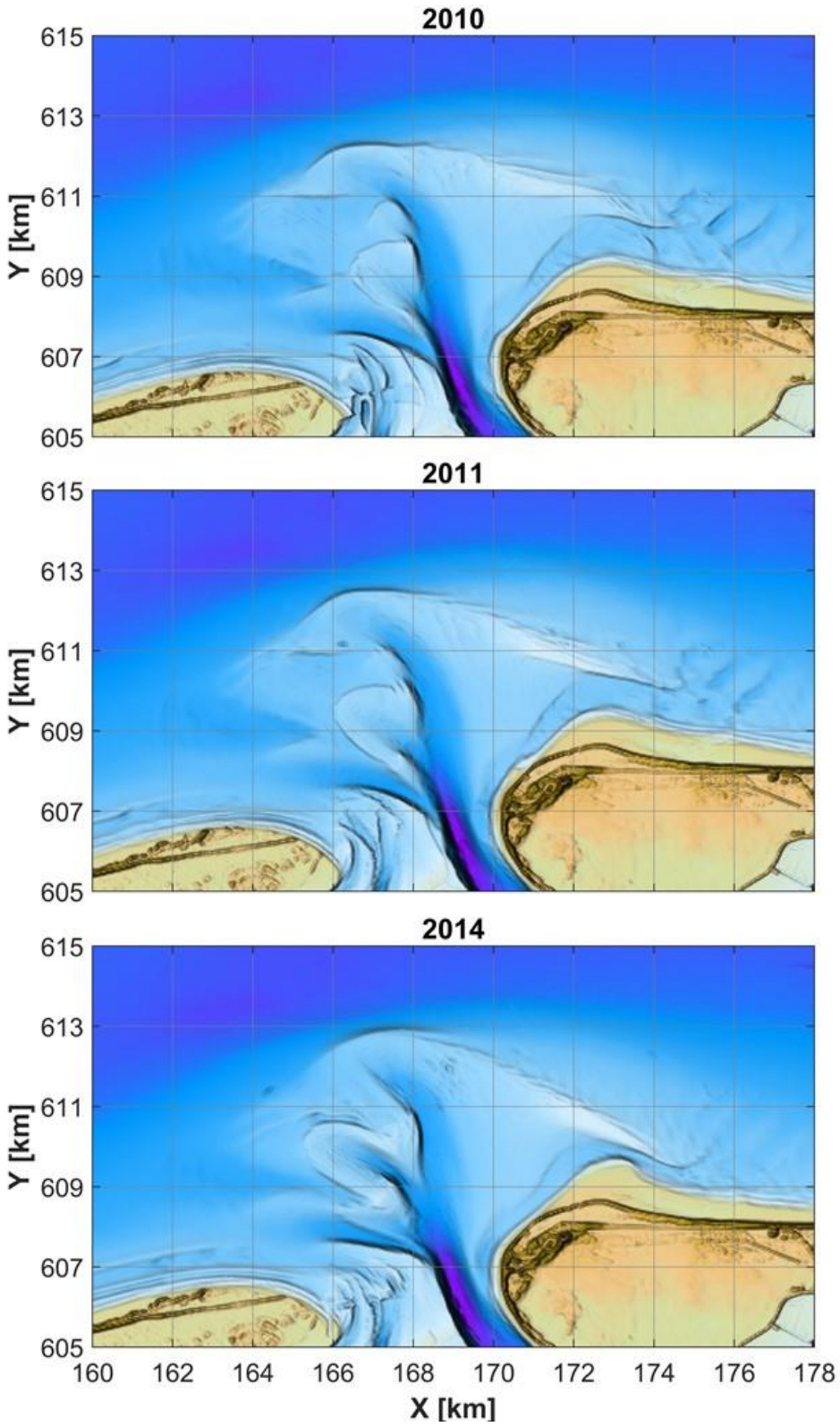
2010
2011
2014
Y [km]
615
613
611
609
607
605
160
162
164
166
168
170
172
174
176
178
X [km]

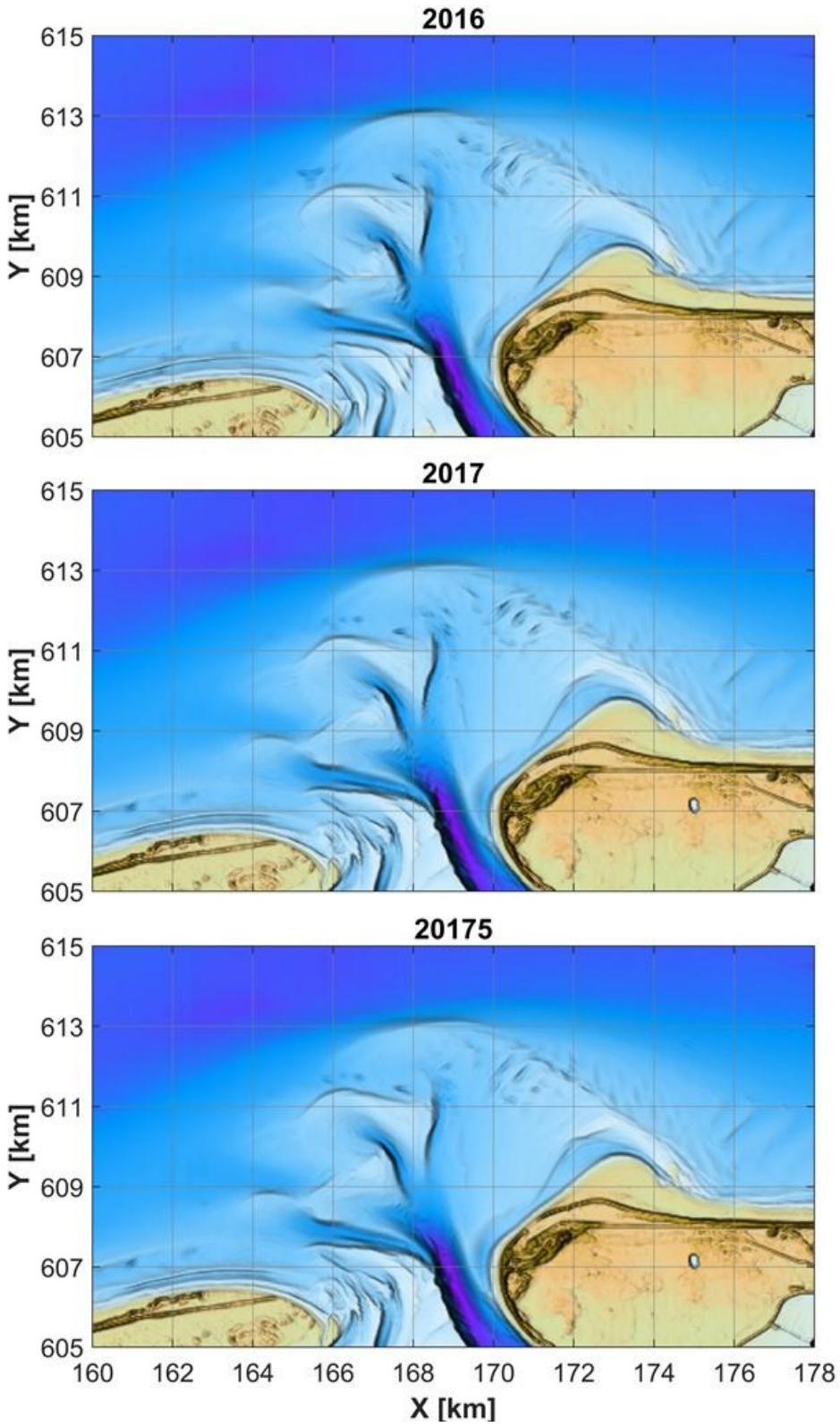
2016
2017
20175
Y [km]
X [km]
615
613
611
609
607
605
160
162
164
166
168
170
172
174
176
178

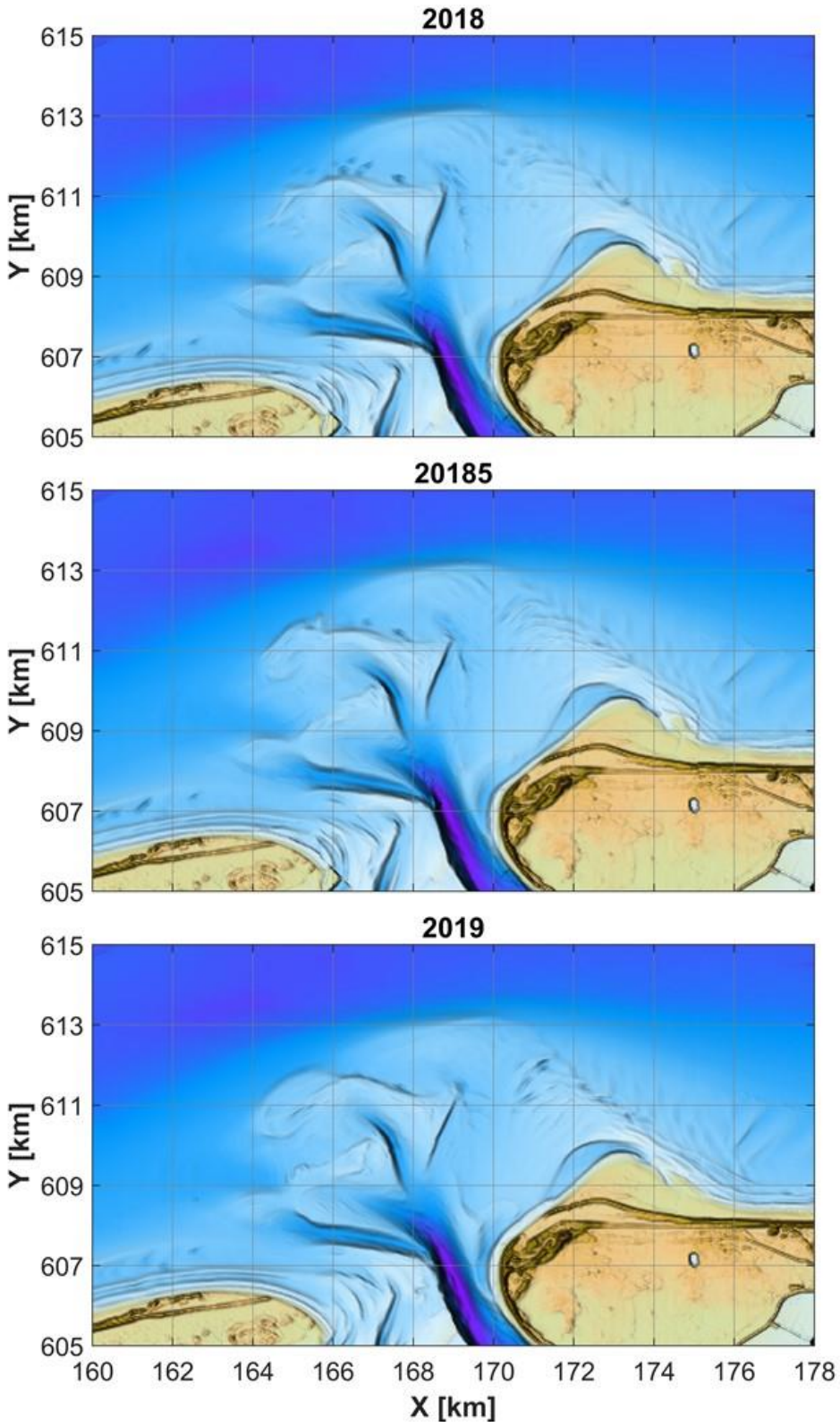
2018
20185
2019
Y [km]
615
613
611
609
607
605
160
162
164
166
168
170
172
174
176
178
X [km]

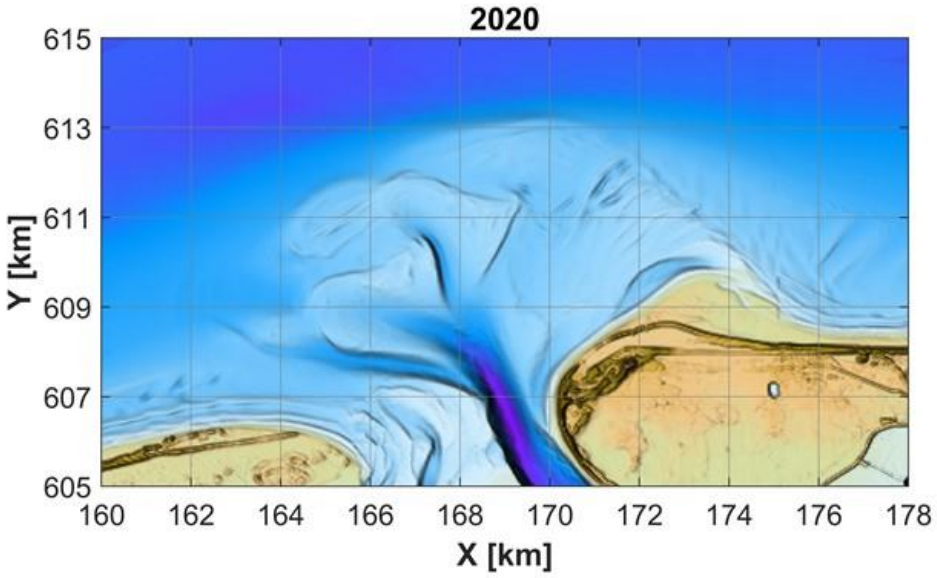
2020
615
613
611
609
607
605
Y [km]
160
162
164
166
168
170
172
174
176
178
X [km]

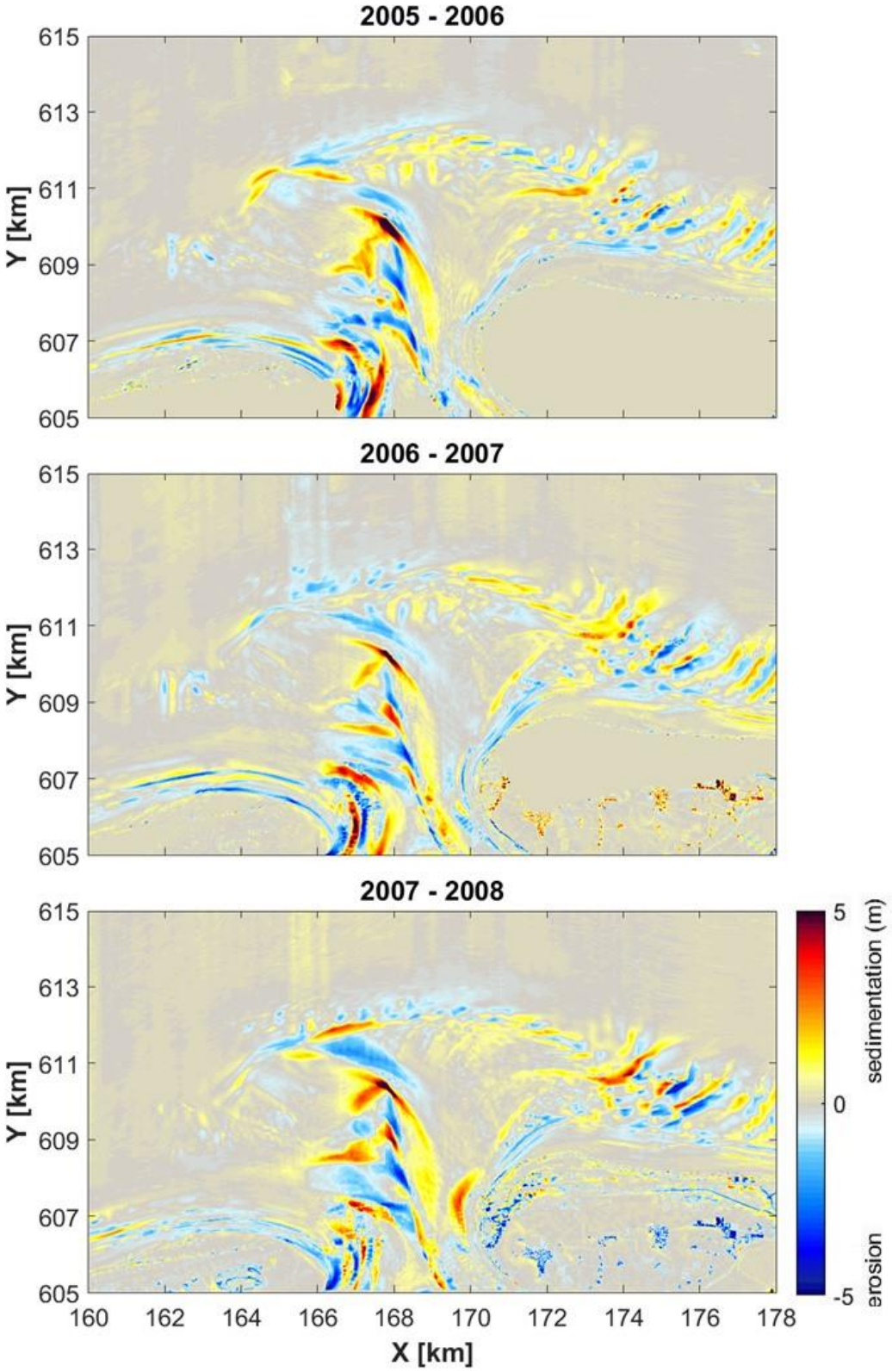
2005 - 2006
2006 - 2007
2007 - 2008
Y [km]
X [km]
615
613
611
609
607
605
160
162
164
166
168
170
172
174
176
178
5
0
-5
sedimentation (m)
erosion

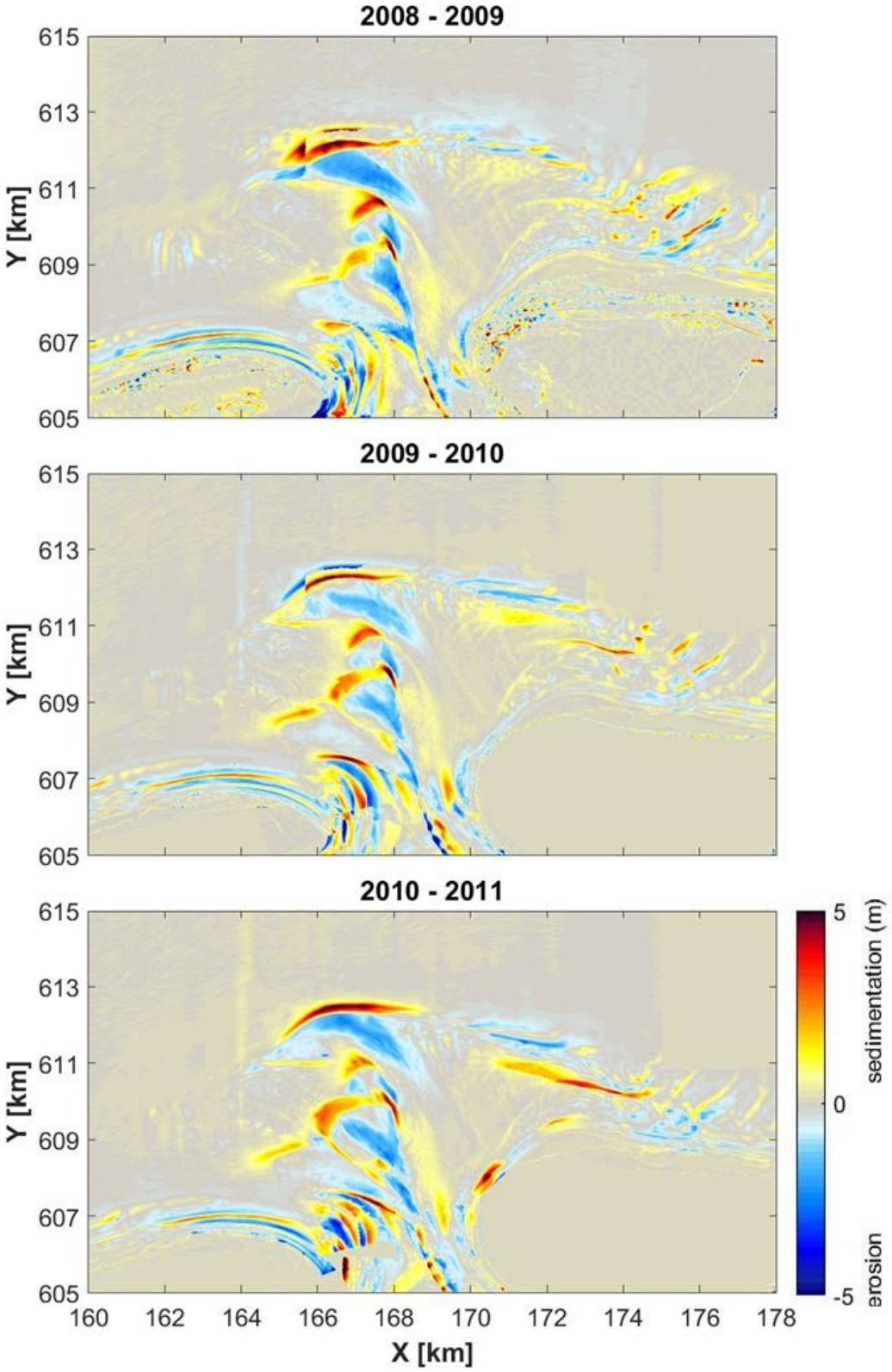
2008 - 2009
2009 - 2010
2010 - 2011
Y [km]
X [km]
615
613
611
609
607
605
160
162
164
166
168
170
172
174
176
178
5
0
-5
sedimentation (m)
erosion

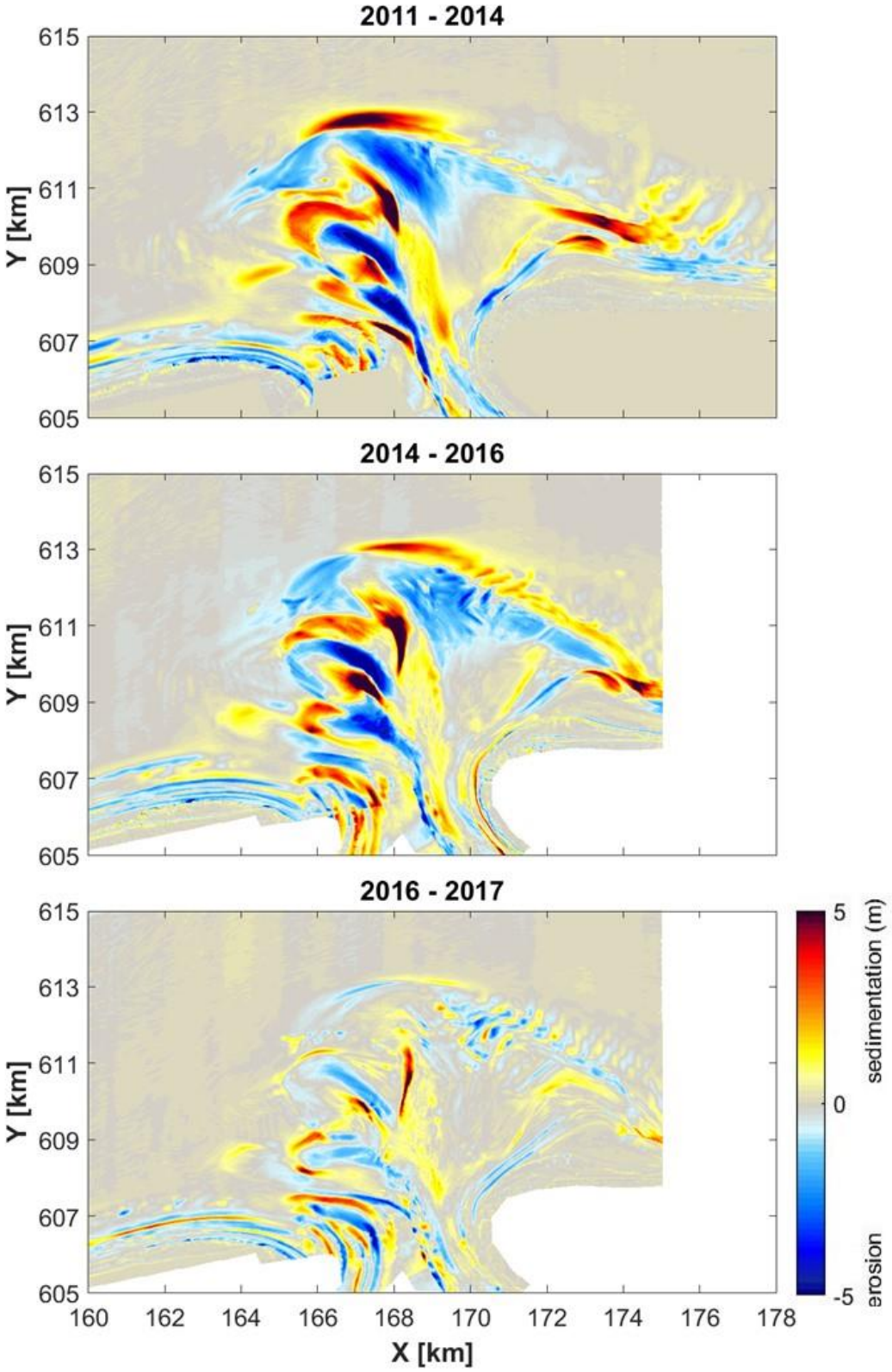
2011 - 2014
2014 - 2016
2016 - 2017
Y [km]
X [km]
615
613
611
609
607
605
160
162
164
166
168
170
172
174
176
178
5
0
-5
sedimentation (m)
erosion

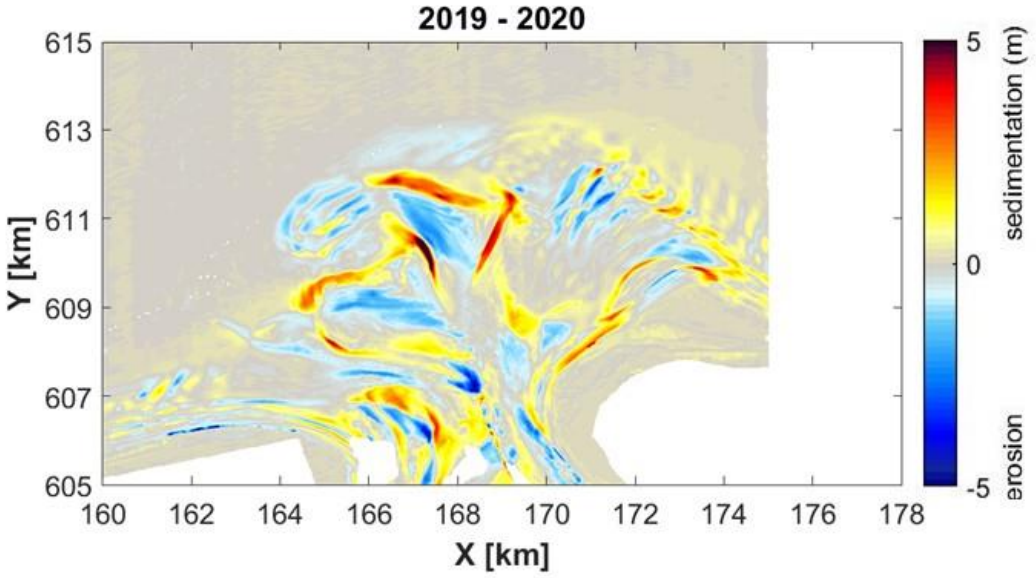
2019 - 2020
615
613
611
609
607
605
Y [km]
160
162
164
166
168
170
172
174
176
178
X [km]
5
0
-5
sedimentation (m)
erosion

A.2 Nourishment

Here is an overview of the nourishment surveys performed as part of the Kustgenese 2.0 campaign and the sedimentation-erosion patterns between consecutive surveys. Construction of the nourishment was completed in February 2019.

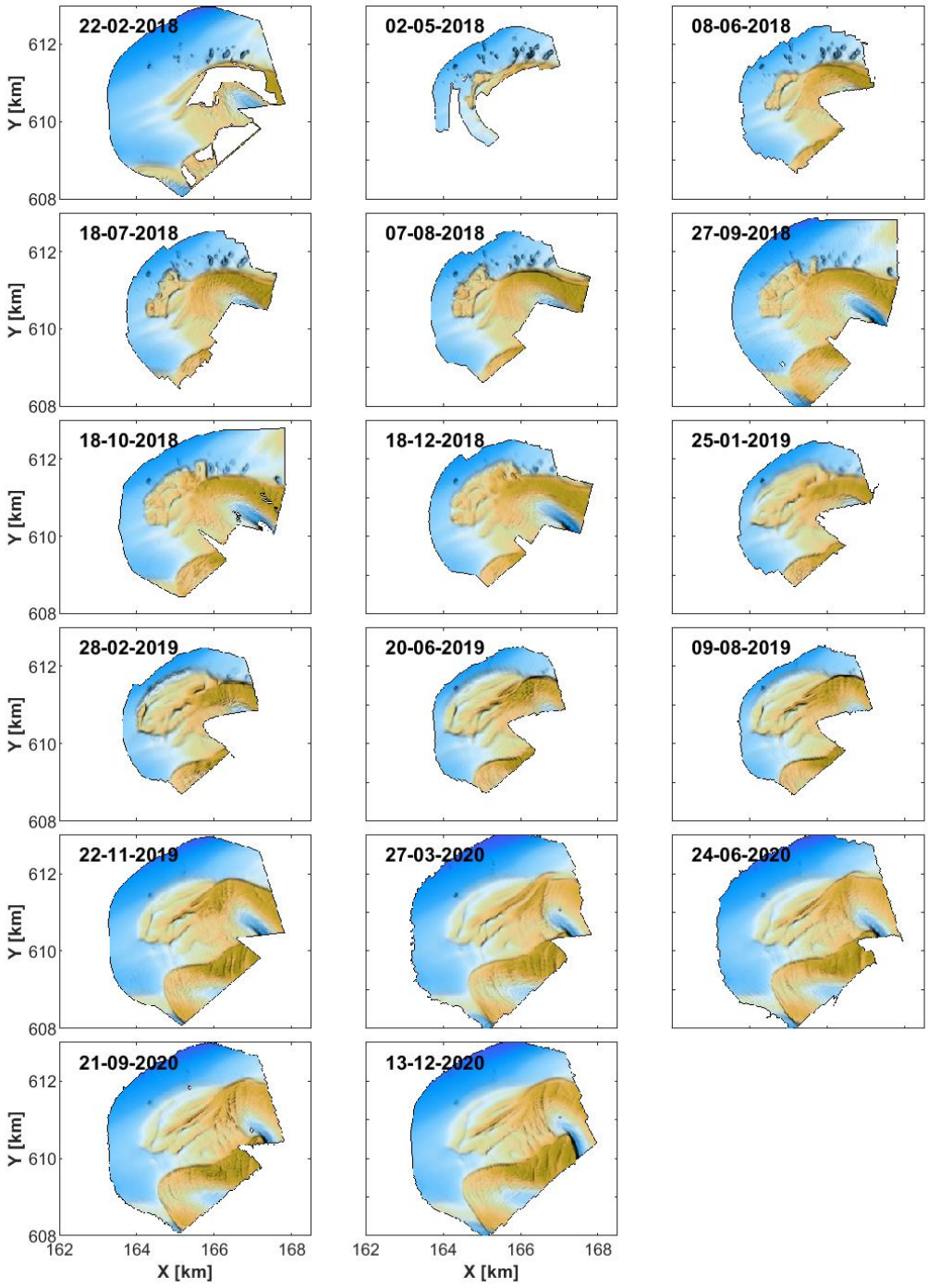

Figure 9.1 - Overview of the measured bathymetries obtained from detailed mapping of the ebb-delta nourishment between 22-02-2018 and 13-12-2019.

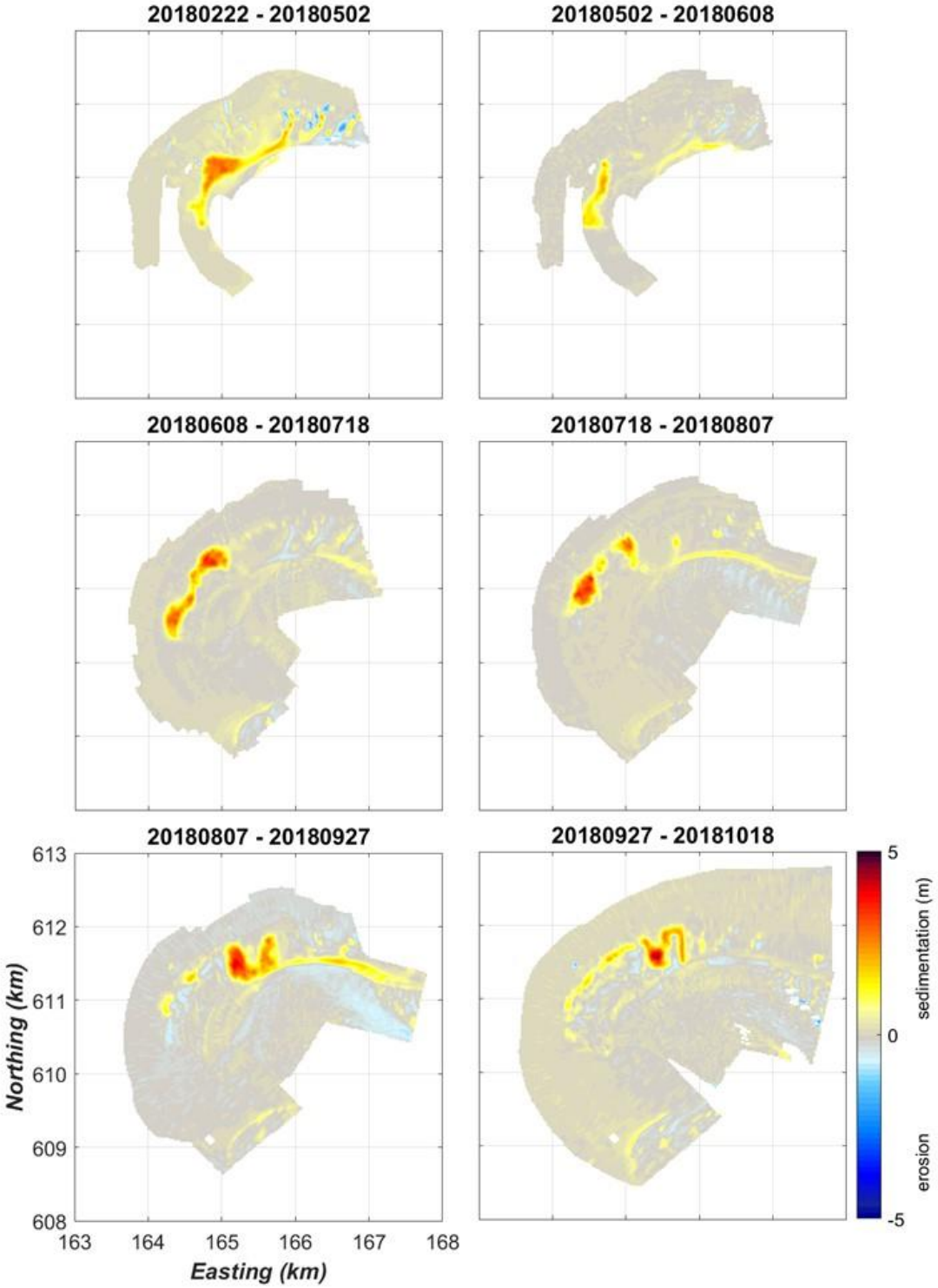

Figure 9.2 – Sedimentation-erosion patterns for consecutive surveys (part 1/3).

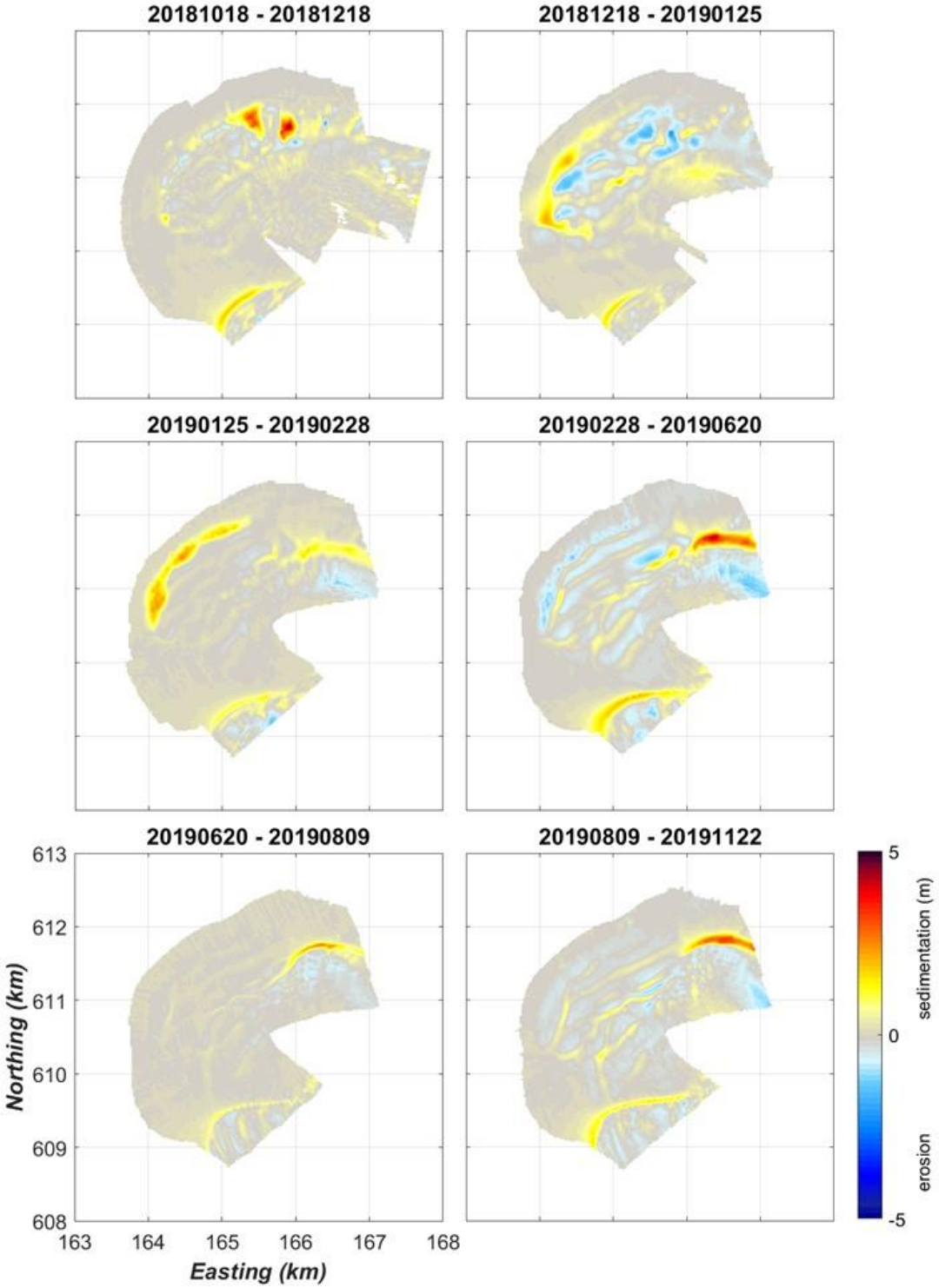

Figure 9.3 – Sedimentation-erosion patterns for consecutive surveys (part 2/3).

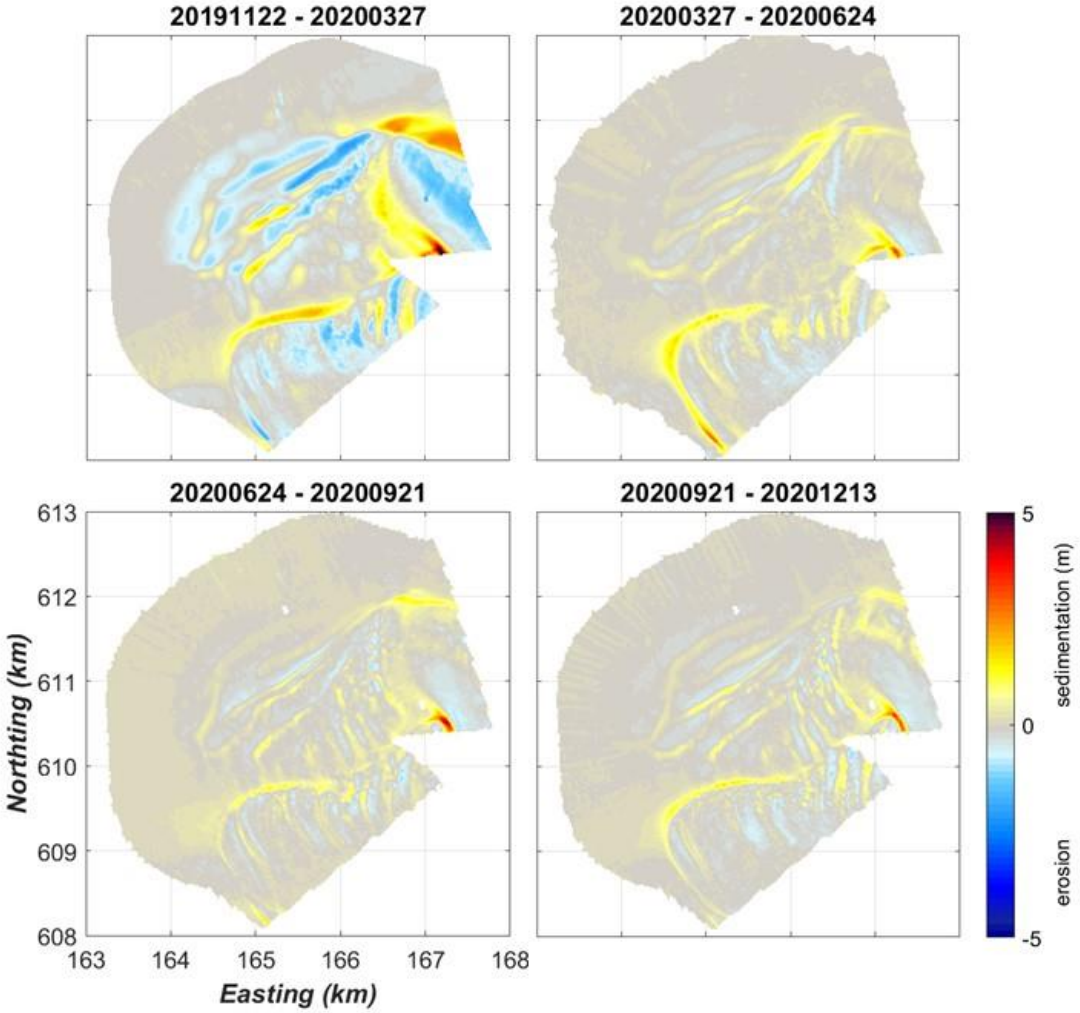

Figure 9.4 – Sedimentation-erosion patterns for consecutive surveys (part 3/3).

B Additional modelling results

B.1 Wave-driven transport along the Bornrif

As can be seen in Figure 9.5, the Bornrif is dominated by wave-driven transports. In the tide-only simulation, almost no transport occurs on the Bornrif, while in the coupled tide-wave simulation particle trajectories traverse the Bornrif from west to east.

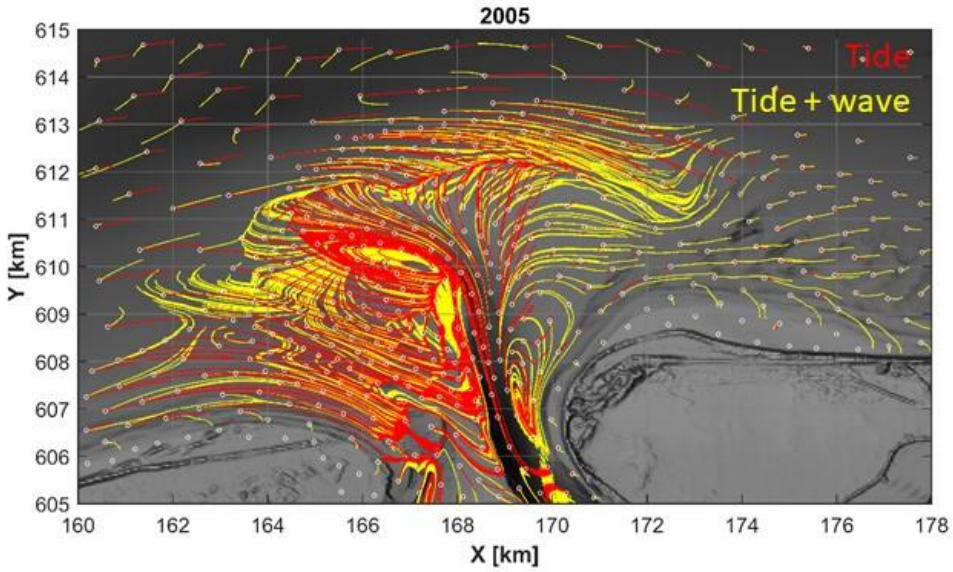

Figure 9.5 – The SedTRAILS results for a tide-only (red) and a couple tide-wave simulation for the 2005 bathymetry.

B.2 Discharge through the Westgat

Figure 9.6 shows an increase in discharge through the Westgat until it peaks in 2011, after which the discharge decreases slightly and stabilises.

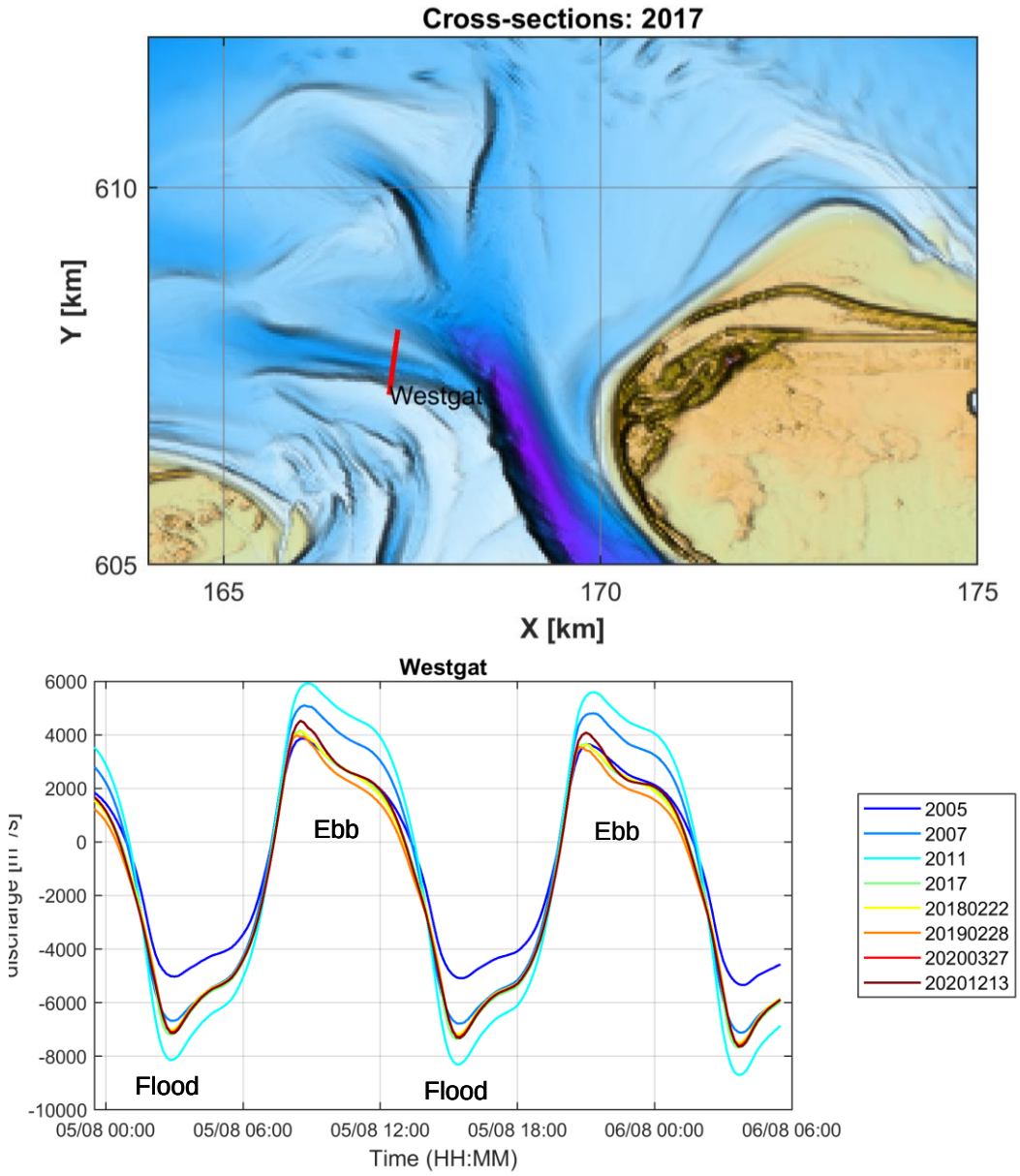

Figure 9.6 – Discharge through the Westgat is approximated across the cross-section shown in the top panel from the tide-only simulations for different years.

C Connectivity

The particle trajectories output by SedTRAILS are often chaotic and thus difficult to interpret. Connectivity provides a framework for analysing these sediment pathways, with the system split into a series of cells with sediment pathways between these cells acting as links. This can be tabulated in an adjacency matrix where you keep track of particles moving from a given source to different receptors.

Here I apply Stuart Pearson's work on connectivity to the 2011 bathymetry (coupled tide-wave) to show how it works and give an idea of the range of possibilities. For sediment transport we are mainly interested in functional connectivity rather than structural connectivity. Functional connectivity is related to the sediment fluxes between different cells whereas structural connectivity is related to their geographic position with respect to each other (i.e. are they neighbours?)

C.1 Working principles

Before running SedTRAILS, geomorphic cells are defined by clustering the area of interest into 500 cells weighted by XY-position and bed elevations. The centroids of these cells are used as source points. Connectivity requires a seamless coverage of the model domain (which the original clusters do not provide) so Voronoi polygons are defined around the source nodes (Figure 9.7). This partitions the model domain based on the nearest node. The Voronoi polygons are the source and receptor cells used for the connectivity analysis.

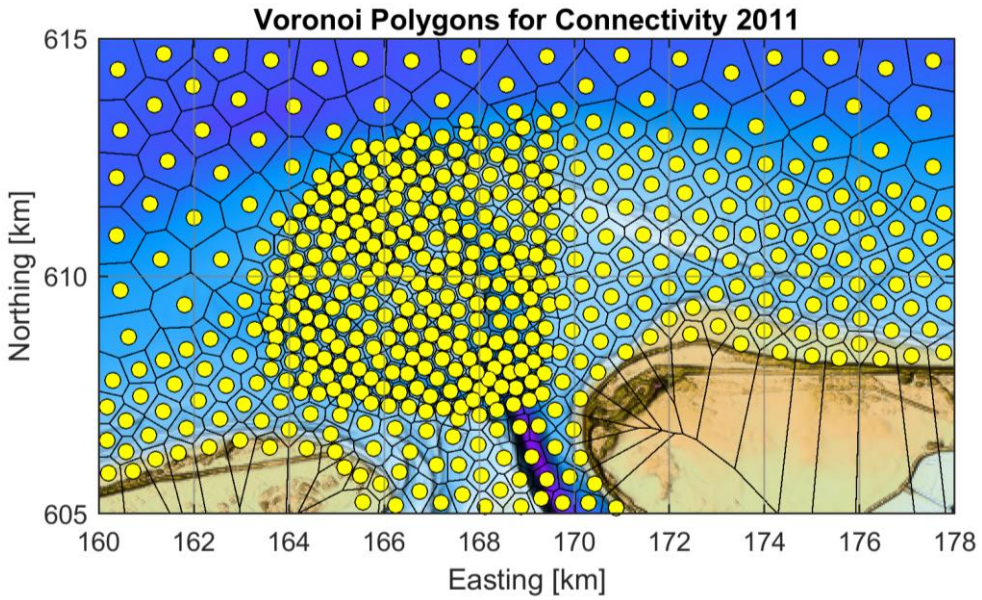

Figure 9.7 – Voronoi polygons for 500 source points for the 2011 bathymetry.

A single particle is released at each source, and the position of every particle is recorded at each time step. A particle can pass through several receptor cells during the simulation time and the time it spends there is effectively the residence time. The connectivity for a given source and a given receptor is then proportional to the number of time steps the particle from that source spends in the receptor in question (normalized with the total time). For each source and receptor combination, this is tabulated in an adjacency matrix (Figure 9.8). An

example is shown for source 91, which is received by one other cell. The diagonal represents self-self interactions and these are disregarded for most applications.

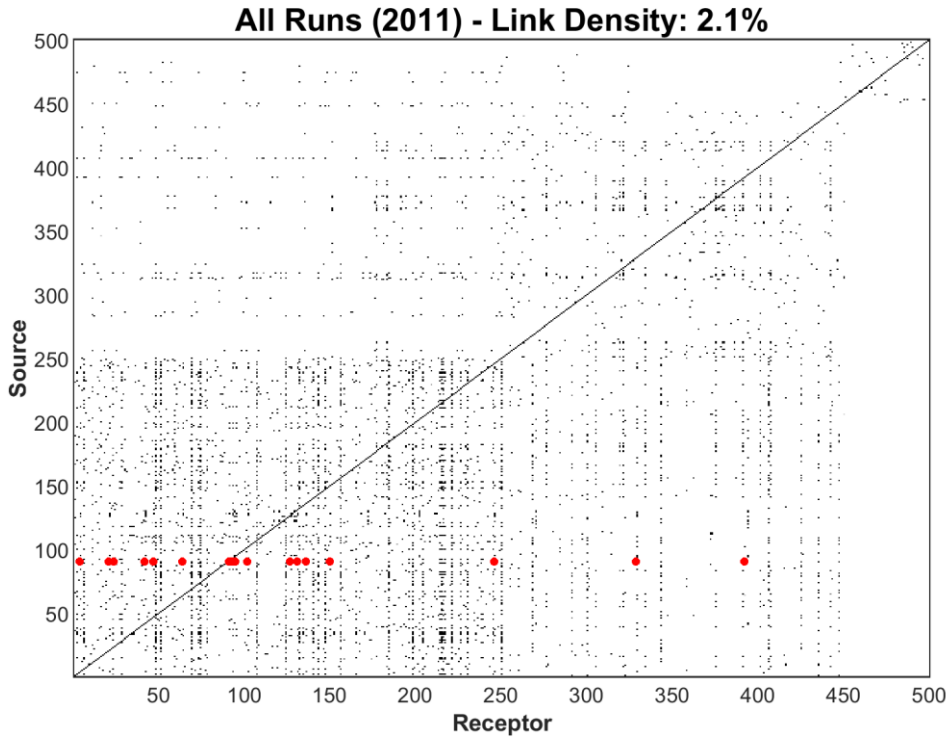

Figure 9.8 – Adjacency matrix for a total time of 500 days for the 2011 scenario. Each point on the plot represents a connection from source I to receptor j. The connections from source 91 are highlighted in red.

This is an example of a weighted directional network. Links are weighted by the residence time in receptor cells. The asymmetry in the matrix means that particles travelling from cell A to B do not necessarily also travel from B to A. This means that individual connections correspond to gross transports.

The matrix can also be represented as a network diagram where sources and receptors are points on the map connected to one another by links (Figure 9.9). Here the nodes are bound to their geographical location. Another option is to visualise the network in topological space (Figure 9.10), focusing on the connections between nodes rather than their position within the geographical structure.

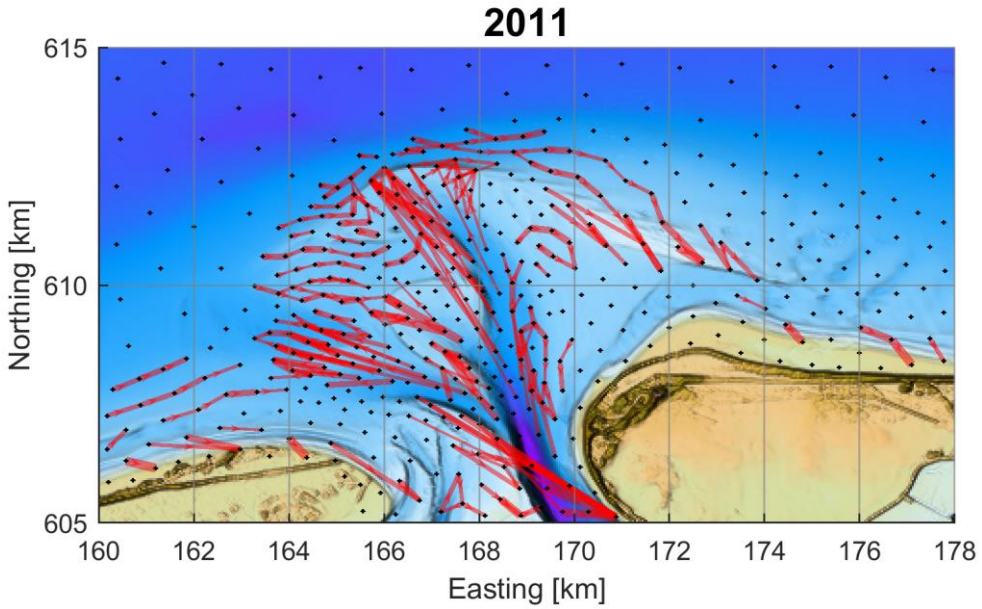

Figure 9.9 - Network diagram for the top 0.1% strongest connections for a 100 day simulation. Red lines indicate the connection between two nodes, with thickness representing the strength of the connections, and the arrow the direction.

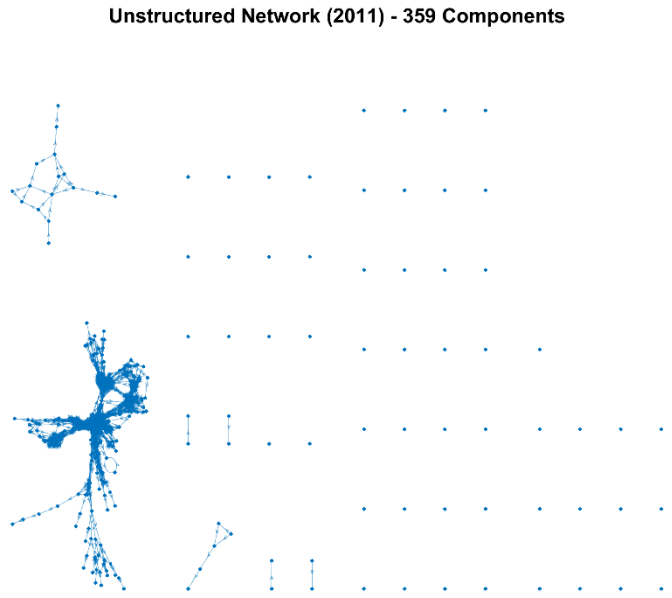

Figure 9.10 – Unstructured network where blue lines indicate connections between nodes, and the arrows their direction.

C.2 Connectivity analysis

Once you have the adjacency matrix and the network, there are a wide range of statistical techniques available to analyse the network. Until now, I have only done individual node analysis and not looked the statistics for the system as a whole. Here some of the characteristics than can be explored:

Degree: This is the number of nodes that a given node is connected to, irrespective of how many particles are passing between the two nodes (Figure 9.11a). This gives an indication of the diversity and mixing intensity of the sediment.

Strength: This corresponds to the number of particles passing in and out of a given receptor, in other words, the sediment flux (Figure 9.11b)

Betweenness centrality: This is a measure of which nodes lie on the greatest number of shortest paths (i.e. which nodes are the cross roads that most particles must use) (Figure 9.11c). For this metric, the question is whether this reveals something or whether this is simply a result of the points being in the middle of the domain.

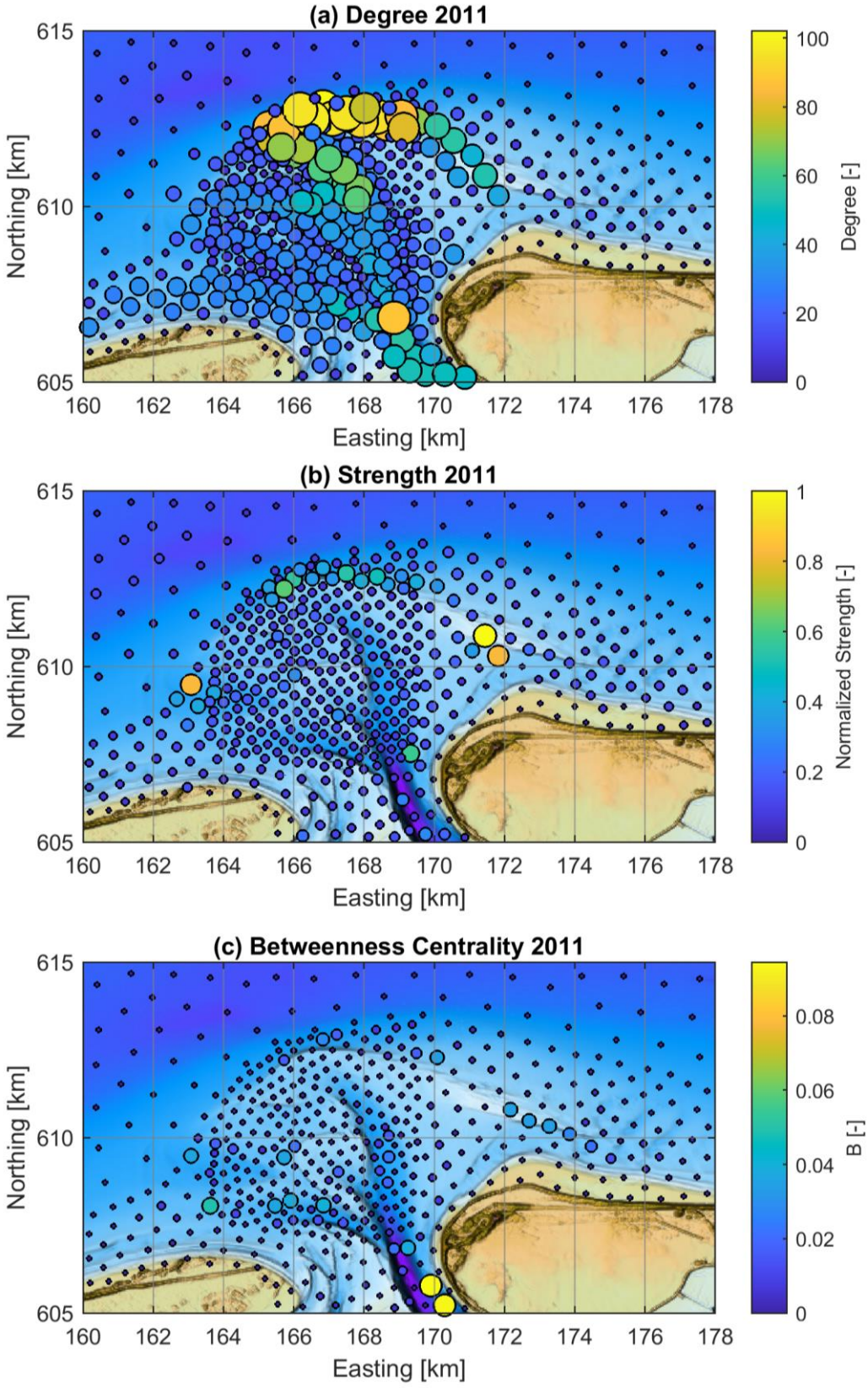

Figure 9.11 – Individual node characteristics of each node in the network. (a) Degree of each node. Lighter colours and larger dots indicate that a node is connected to more other nodes. (b) Strength of each node. Lighter colours and larger dots indicate that more particles are passing in or out of that node. (c) Betweenness centrality of each node.

C.2.1 Shortest transport pathways

Network theory can also be used to calculate the shortest transport pathway between two nodes that are not necessarily connected by a single transport path from SedTRAILS. The distance between two nodes is considered to be the inverse of its weight (a higher weight indicates a larger flux and stronger connection so the distance is shorter). From this a matrix can be derived with the shortest pathway between any two nodes. This matrix can be queried for pathways between any two nodes which are part of the same component, for example for points on the west and east side of the ebb-tidal delta (Figure 9.12).

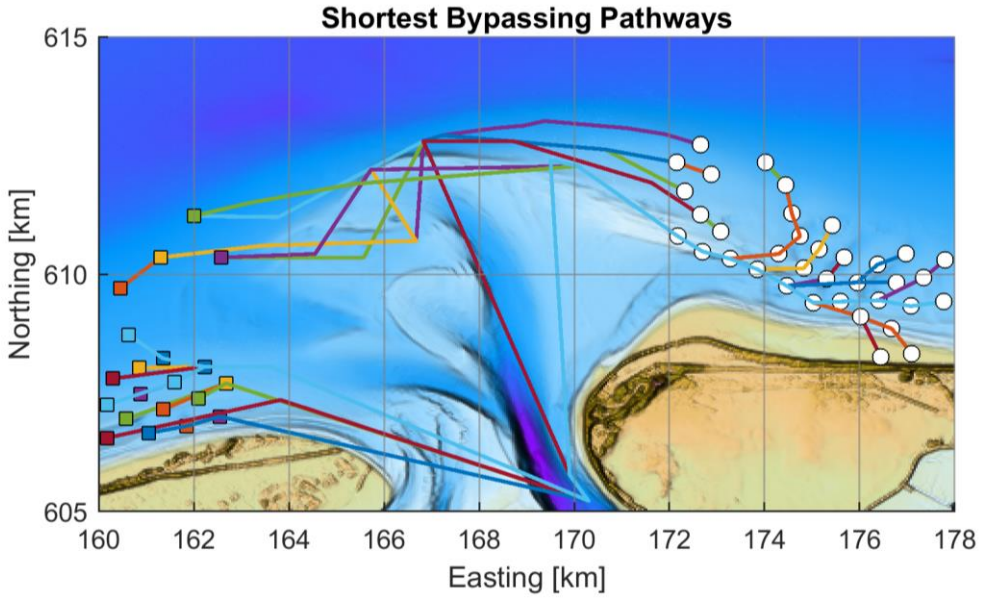

Figure 9.12 – Shortest bypassing pathways from the west to the east side of the ebb-tidal delta for the 2011 bathymetry.

C.2.2 Modularity

A network showing modularity can be grouped into communities that are highly connected internally but have limited interaction with nodes outside the community. These communities can be identified using optimisation techniques such as the Louvain Community Detection algorithm (Rubinov & Sporns, 2010). Clusters for the different communities are created by reordering the adjacency matrix (Figure 9.13). The same colour scheme is used to show the cells that are included in each of the sediment-communities (Figure 9.14).

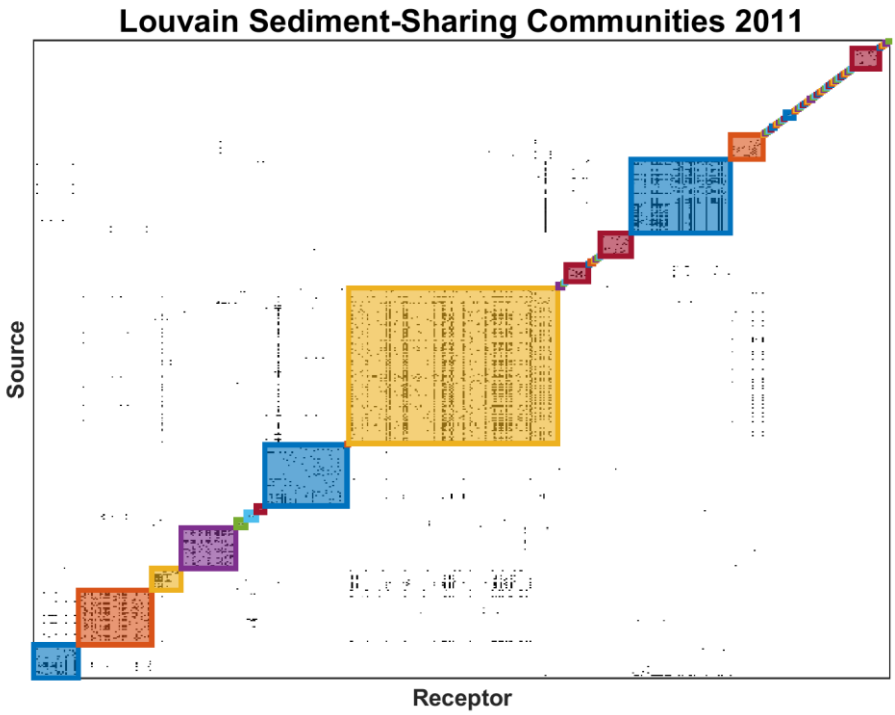

Figure 9.13 – Adjacency matrix reordered using the Louvain Community Detection algorithm. Each coloured square corresponds to a sediment-sharing community with strong internal connections and week connections to nodes outside the community.

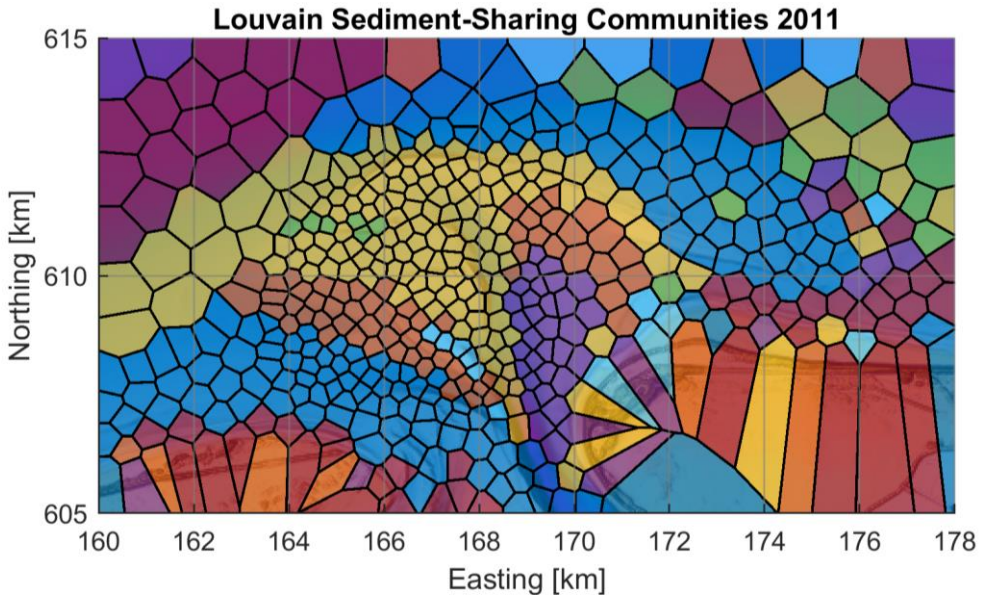

Figure 9.14 – Networks cells shaded according to the sediment-sharing community to which they belong as determined using the Louvain Community Detection algorithm.

C.3 A reflection on the current approach to connectivity

Connectivity as described here is a tool that offers many new insights into the sediment transport patterns on the ebb-tidal delta. I do think however that it is important to reflect on what we are actually seeing.

Connections and more importantly the weight they are given is based on residence time in a receiving cell. Connectivity for a given source (i) and a given receptor (j) is then calculated as $c_{ij} = \frac{t_{r,j}}{t_{total}}$, where both the residence time and the total time are counted in the number of time steps. This gives an advantage to slower particles as they will spend longer in a receiving cell, and with this approach this corresponds to a higher connectivity. On the other hand, a particle which travels further within the same simulation time will spend fewer time steps in each of the receptor cells it passes through, resulting in a lower connectivity for the individual connections. It also makes it likely that sediment sinks (where the sediment arrives but never leaves) will come forward. Using residence time as weighting will mainly affect the thickness of the connections in the network, the strength plot and the shortest pathway calculations. In the strength plot (Figure 9.11b), a point on the tip of the ebb shield has a far greater strength than all the other nodes, which I think is an indication that this is a sediment sink.

For the sediment pathways, a greater weight is said to correspond to a greater flux. Based on this motivation, the “distance” between two points is approximated as the inverse of the weight. However, if weight is based on residence time an advantage is given to more slowly travelling particles, as they will be in a particular cell for longer and thus have a greater weight. In that case a greater weight does not correspond to a stronger flux. I think you need to find a metric that can be better linked to flux. For example, the number of particles using that connection (might require longer SedTRAILS simulations or more source points to reach significant numbers) or how fast they move from one cell to the next (take middle time step within that cell as reference time step, or maybe use the relative velocity work by Floortje). I will need to look in more detail at what the mathematical formulations for the different options would be.

Another point to be aware of is that connections are tabulated with respect to the original source cell and not with respect to the last cell they were in. I think that this choice will mainly distort the betweenness centrality statistics, because for particles travelling further, a direct connection to the later receptor is shown even though the particle has passed through other cells on the way there. For this metric, I think it would be valuable to tabulate connections with respect to the last cell the particle was in rather than with respect to the original source.

Some of these ideas will be expanded on in the following section.

C.4 Experimenting with connectivity

In this section I experiment with connectivity using the 2006 tide-only simulation.

C.4.1 Using sediment communities as units for connectivity

In the work with connectivity networks I have seen done until now I see two main issues:

- Including all individual source points in a connectivity analysis results in a cluttered and difficult to interpret network.
- Defining geomorphic units on the ebb-tidal delta can be highly subjective.

I wanted to find a way to define units on the ebb-tidal delta that could be used to map connectivity, and preferably with units that were define in an objective way. Here we introduce the concept of modularity (from Stuart’s work). A network with high modularity can

be grouped into communities that are highly connected internally but have limited interaction with nodes outside that community. These communities can be identified using optimisation techniques such as the Louvain Community Detection algorithm (Rubinov & Sporns, 2010). An example of these sediment-sharing communities as found using the default calibration parameters is shown in Figure 9.15.

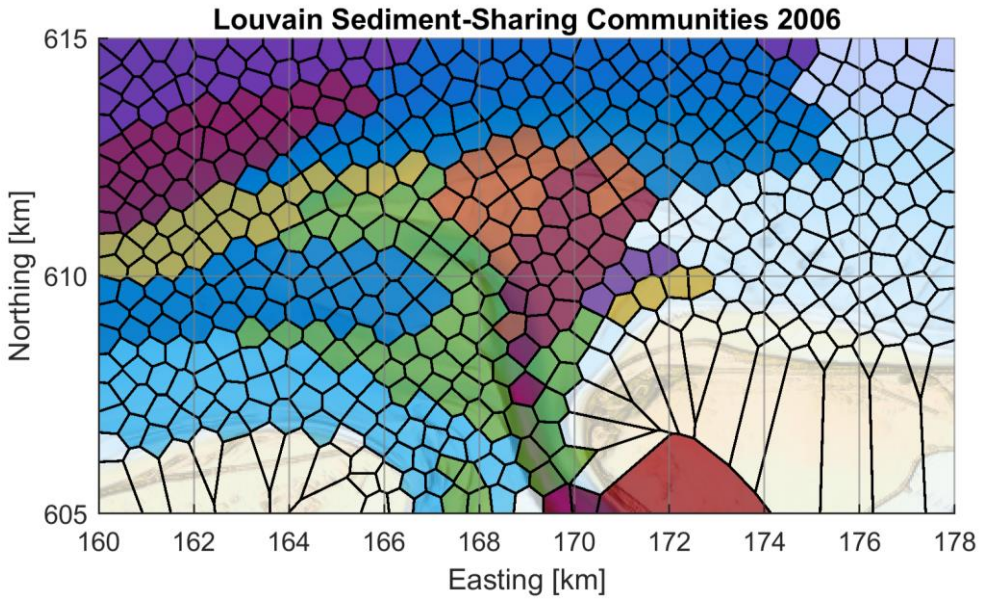

Figure 9.15 - Louvain sediment sharing communities using default calibration parameters for the 2006 bathymetry for 500 source points and 100-day runtime. Any polygons that form a community only with themselves are shaded white.

Using these communities makes the definition of units for connectivity less subjective, and because they are by definition less connected with each other, reduces the number of connections between units, making interpretation easier. The interaction between communities should be limited so then only more meaningful connections will come forward. Using the polygons for the different sediment communities, an adjacency matrix can be set up in a similar way to for the source/receptor polygons, counting the number of timesteps a particle from a source community spends in the receiving community. The resulting network is shown in Figure 9.16.

This network can also be plotted as an unstructured network (Figure 9.17), nicely separating the different elements of the ebb-tidal delta. The main channel and its ebb-shields play a central role in the connectivity network. Moreover, looking at the most important connections (printed in bold), highlights two distinct sub-networks. One of these passes seaward of the ebb-tidal delta from west to east, and the other passes directly through the ebb-tidal delta, culminating in the main channel and shield module. I think that networks such as this one definitely show potential in deciphering the ebb-tidal delta scale dynamics.

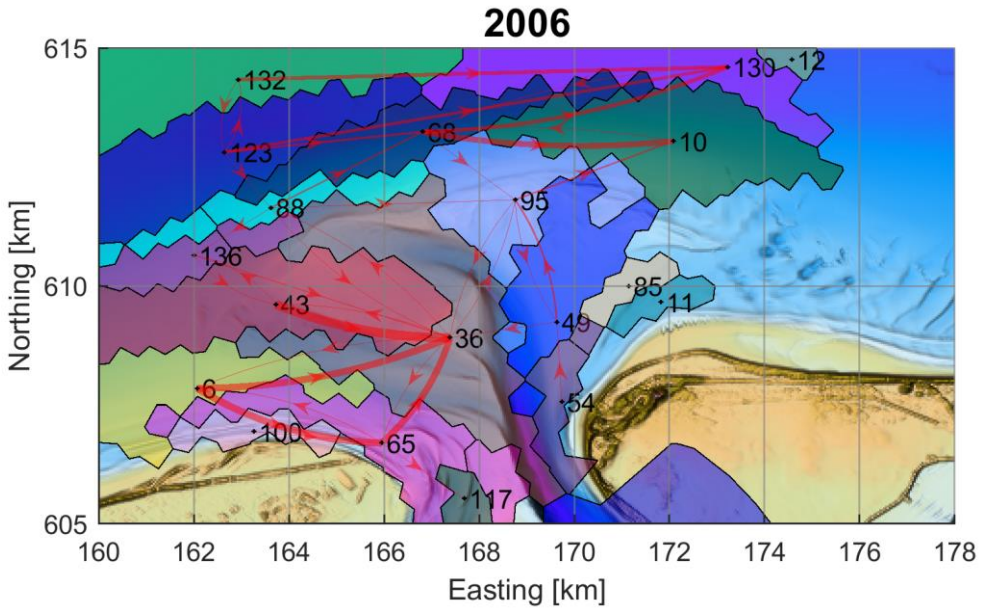

Figure 9.16 – Network between the sediment communities as defined by the Louvain algorithm for the 2006 bathymetry. The numbers are labels for the community polygons and have no further meaning.

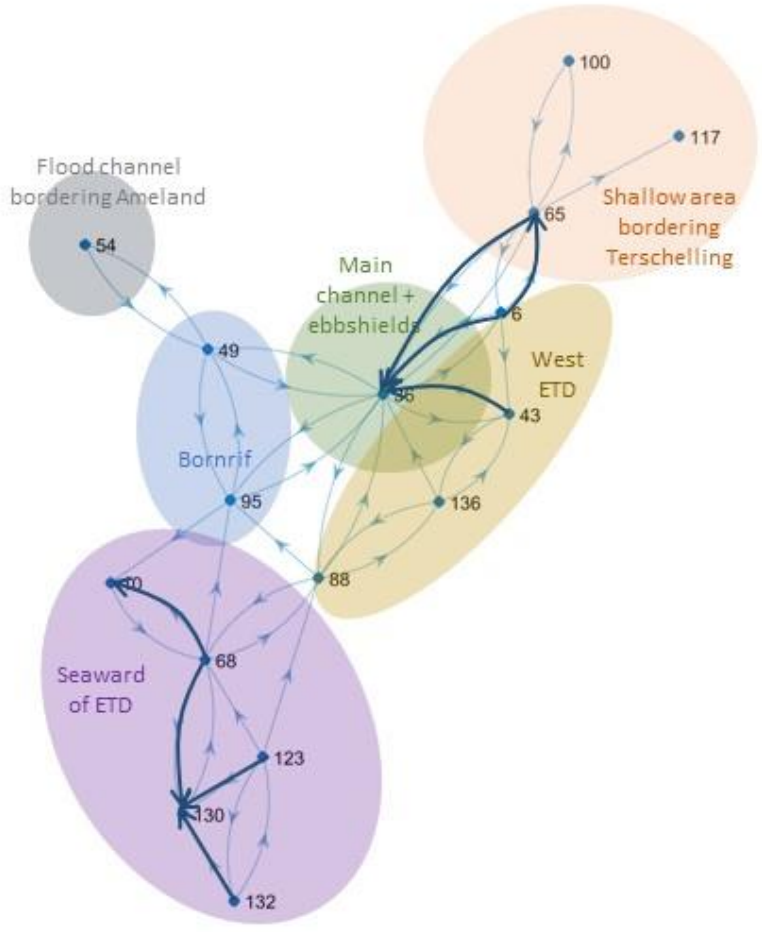

Figure 9.17 – Unstructured network for the 2006 bathymetry. Nodes are labelled with the morphological feature to which they correspond. The numbers can be used to match the nodes with the sediment communities in the previous figure. Stronger connections as seen in the structured network are printed in bold.

C.4.2 The role of residence time in connectivity

What we are essentially trying to do with connectivity is to map the results of a Lagrangian model onto a coarser matrix. There are multiple possibilities for doing this discretisation and basing this on residence time is just one of them. To get some more insight into what this means, I have plotted the residence time for each cell and the number of times it acts as a source or a receiver.

Figure 9.18 shows the residence time particles spend in a given cell as a percentage of the total time particles spend outside their source cells. This is tabulated by counting the number of time steps particles spend in receiving cells. This plot appears the same as the strength plot shown earlier (Figure 9.11b). In my eyes this is useful as a first indicator of where sediment sinks might be, but it also means that we need to find a different approach for weighting connections which will allow them to correspond roughly to sediment fluxes.

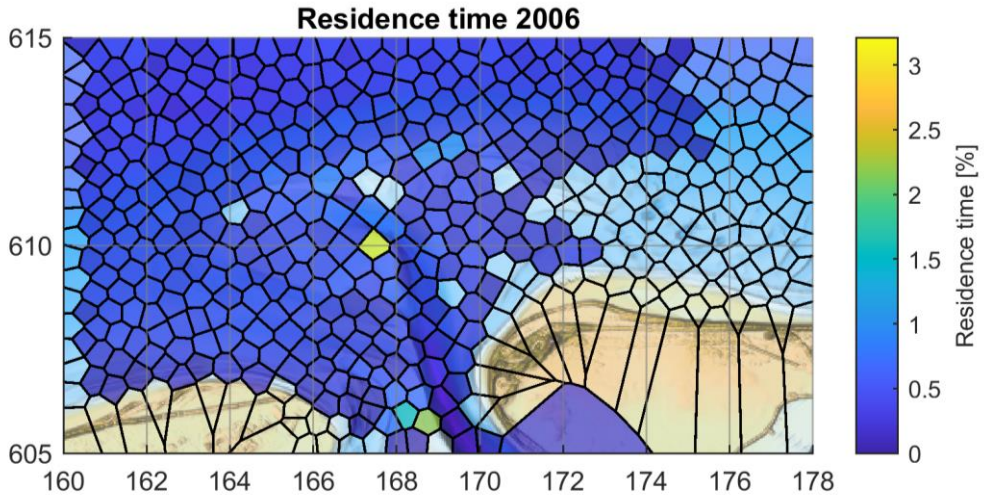

Figure 9.18 – The time that a particle spends in a receiving cell as a percentage of the total time that all particles spend somewhere other than their source cell. Cells which never receive a particle are shown in white. Self-self interactions have been removed.

C.4.3 Connectivity based on transitions between polygons

Following discussions with Stuart on the residence-based connectivity approach, we came up with an alternative, namely counting transitions between cells rather than time steps in a cell. In Figure 9.19 this is done with the transitions counted with respect to the last cell the particle was in rather than the original source. This gives a very different network.

To get an idea of what these transitions mean I have mapped the number of times each cell acts as a source and as a receiver (Figure 9.20). For a cell to be considered a source, the particle must actually leave that cell. As you can see, only cells near the Boschgat and the ebb-shield forming act as a source or receiver more than once or twice. The adjacency matrix then becomes a transition matrix indicating the probability of a particle going from a given cell to another in the course of the simulation. Perhaps, with a little more work we will be able to ask the question: if a particle starts at location A, where is it most likely to end up? Marchov chains could be a tool to do this.

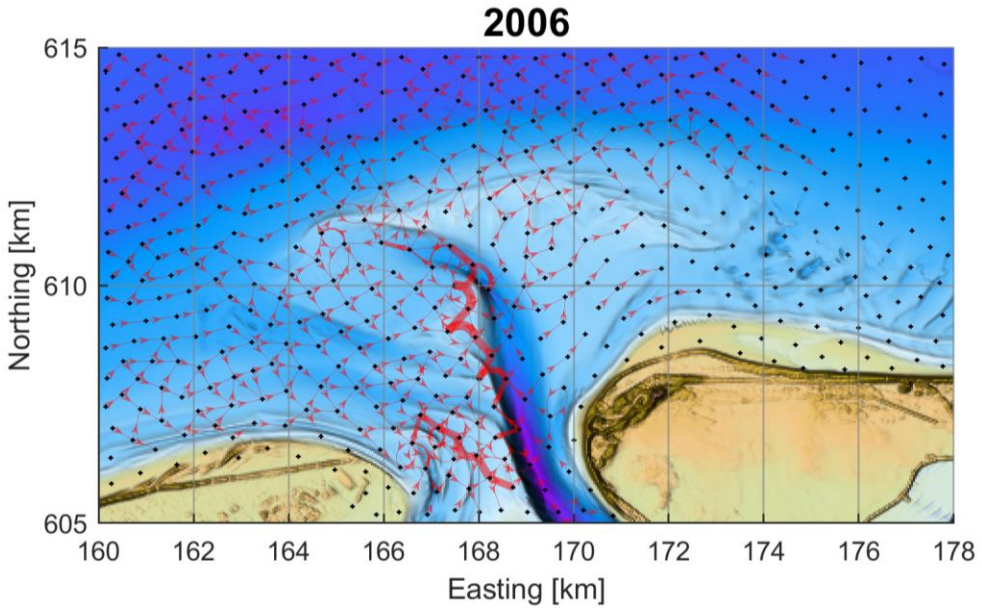

Figure 9.19 – Connectivity based on the number of transitions between cells with respect to the last cell the particle was in rather than with respect to the original source.

For the transition approach to be used effectively in further applications (e.g. mapping strength or shortest paths), we need to find a way to increase the number of transitions. Most connections are now based on a single transition. Perhaps this can be achieved by increasing the runtime or by working with receptors larger than a single cell.

Another approach to connectivity (also briefly mentioned in section C.3) could be to try and quantify the travel time from one cell to the next as a way of approximating flux. Ideas for determining travel time are:

- Working from the middle time step within a cell to middle time step within the next cell. You would have to take care in how you define travel time for the first and last transitions.
- Determine the time step where the particle is closest to the node within that cell. Define the travel times between these time steps in the different cells.

Perhaps you could divide the total travel time (in time steps) by the number of particles making that transition. This would be away to avoid needing a large number of particles to pass from one cell to the next.

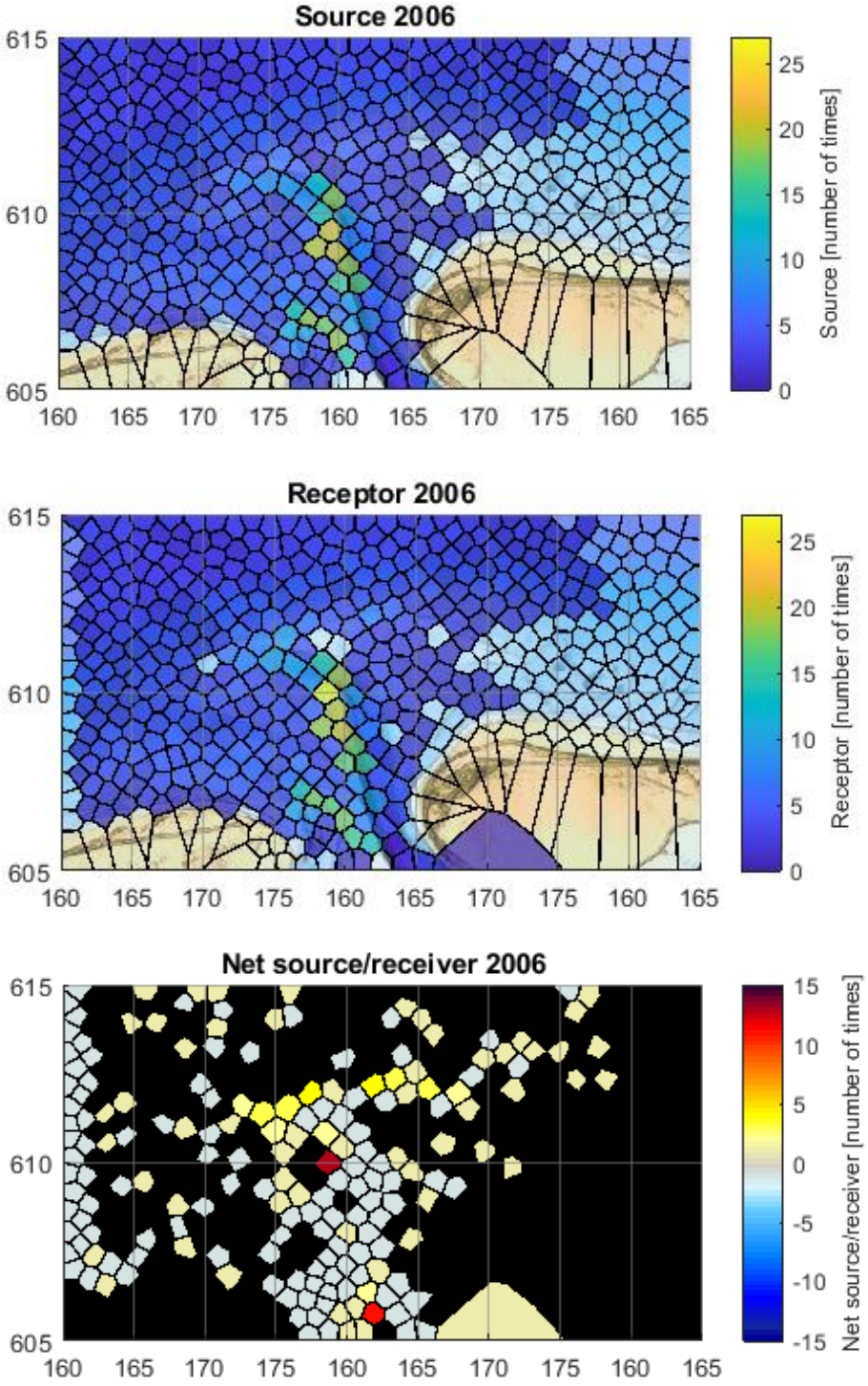

Figure 9.20 – The number of times a cell acts as a source (top), and as a receptor (middle). The bottom plot shows whether the cell is a net receiver (positive) or a net source (negative). If the cell is not a net source or receiver (netto count: zero) or does not interact with other cells then it is printed in black.

Deltares is an independent institute for applied research in the field of water and subsurface. Throughout the world, we work on smart solutions for people, environment and society.

Deltares

www.deltares.nl